OCT ANGIOGRAPHY ASSESSMENT OF CENTRAL RETINAL VEIN OCCLUSION

TABLE OF CONTENTS

LIST OF TABLES

LIST OF FIGURES

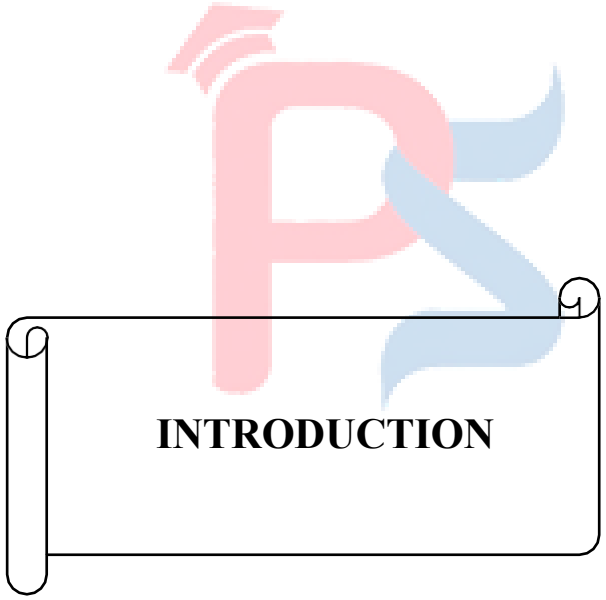

INTRODUCTION

INTRODUCTION

A Our eyes are susceptible to ageing, trauma, and stress just like any other organ in our body. Therefore, without adequate maintenance, it may not reach its full potential. Even vision loss and blurriness may occur later on. High blood sugar levels are a symptom of the condition known as diabetes. Both of these disorders have the potential to harm the kidney, nerves, feet, eyes, and other body parts if left untreated. The retina and iris are the two areas of the eye where diabetes may be shown to have an impact (1). Type I diabetes, or diabetic insipidus, and Type II diabetes, or diabetic mellitus, are the two major forms of the disease. Insufficient insulin production by the pancreas is known as type I diabetes insipidus. When insulin is not used by the body as it should, it results in type II diabetes mellitus. healthy vision is a critical component in promoting human happiness and overall well-being. Actually, our eyes are the most essential sense organs. The retina is a thin layer that is placed close to the optic nerve. It is responsible for converting light into neural signals, which are then sent to the brain for the purpose of visual recognition. Therefore, visual insight is the result of damage to the retina that is caused by factors such as an increase in blood pressure, hyperglycemia, deterioration of blood vessels, macular degeneration, and other factors. The signs of retinal damage, such as blurry or dim vision, black spots or blind spots, and impaired peripheral vision, can be used to forecast the severity of the damage (2).

After diabetic retinopathy, a retinal vascular condition known as retinal vein occlusion (RVO) may lead to significant vision loss. This illness has a high prevalence rate (3). Depending on the locations of the venous blockage, retinal vein occlusion (RVO) may be divided into two distinct categories: central retinal vein occlusion (CRVO) and branch retinal vein occlusion (BRVO). RVO is characterized by an increase in venous pressure, which causes capillaries to leak out of their normal spaces and the development of macular the disease, which ultimately leads to a loss of vision. Furthermore, the severity of retinal ischemia is a determining factor in the outcome of RVO, which resulted from neovascularization of the retina and iris (4).

In order to detect and monitor eye diseases, optical coherence tomography (OCT) is a transparent examination of three-dimensional images that allows for extremely rapid and exact measurements of the macula. The quantity of fluid deposit in the macula layer, the volume of vitreous deposited in the retinal layer, the extent of the sub retinal fluid, and the

detachment of the retinal pigment epithelium (RPE) may all be determined with the use of this OCT apparatus in the case of CSCR. It has been shown that a high-speed three-dimensional OCT equipment may help explain pathophysiologic abnormalities in CSCR (5).

In ophthalmology clinics, the most common applications of retinal imaging are for the diagnosis of diabetic retinopathy, age-related macular degeneration, glaucoma, retinal neoplasms, and other similar conditions. An important clinical indicator for a wide range of systemic disorders, such as diabetes mellitus, hypertension, cardiovascular diseases, and cerebrovascular diseases, has been discovered by researchers in the course of their research (7). The demand for creating computational techniques and algorithms to quantify medical images has grown significantly as imaging technologies have advanced. It would be simpler to analyze medical pictures if robots could comprehend and interpret them. Experts can diagnose illnesses earlier and treat patients more quickly and easily using automated image analysis (8). High resolution cross-sectional pictures of live tissues may be obtained using optical coherence tomography, a non-invasive and non-contact imaging technique. Although it operates similarly to an ultrasound scanner, light waves are utilized as opposed to sound waves. It is predicated on the idea of light interference. Using the time delay information, the OCT system creates a depth profile of the sample from the light waves reflected back from various depths within the sample. Three-dimensional images are produced by moving the beam laterally over the sample structure.

Diagnostic and detection procedures for a variety of eye-related conditions rely heavily on retinal images. The ability to observe local and temporal information of the retina is facilitated by the retinal image, which is stored in the image at all times. The human retina is made up of several layers and components, some of which are visible and may provide important information concerning pathological conditions, such as the optic disc, macula, fovea, etc. OCT and intravenous fluorescein angiography are two of the most heavily utilized imaging techniques for retinal imaging fundus. This is due to the wealth of information they provide regarding the morphology and anatomy of the retina (6).

OBJECTIVES

OBJECTIVES

1. To evaluate and measure changes in retinal blood flow parameters in patients with central retinal vein blockage that's 50 years of age or older using OCT angiography.

2. To investigate the relationship between vascular changes identified by OCT angiography and functional changes, including altered visual acuity.

3. To evaluate the diagnostic accuracy of OCT angiography with respect to the detection and characterization of central retinal vein occlusion.

BACKGROUND AND REVIEW OF LITERATURE

BACKGROUND AND REVIEW OF LITERATURE

The eye is one of the most essential sense organs in human vision because of the high quality and accuracy of the messages that it records, as well as the fact that the loss of the eye has a negative impact on the quality of life. It was believed that the eye is responsible for capturing seventy percent of the sensory information that would be understood by humans. The light is able to be captured by it, and then it is converted into electric impulses in the retina, which are then sent to the human brain for interpretation. As a result of its lenses, which refract and concentrate the light that is coming in via the sensory area, its operation is comparable to that of traditional picture capturing systems.

Developmental biologists have been interested in the genetics of the human eye for many decades. This issue has been of particular interest to them. In vertebrates, the determination of the so-called eye field takes place in the midst of the partition of the anterior neural plate into domains, which marks the beginning of the retina's development. This area is the site where the bilateral optic vesicles, which are part of the eye anlage, are ultimately created. The retina is located in the posterior wall of the optic cup, which is generated from the optic vesicle by its invagination with the optic vesicle (9).

ANATOMY OF HUMAN EYE

Vision, which many consider to be the most vital of our senses, is provided by our eyes, despite their diminutive size. In this particular design, there are eleven parts that are similar to one another. These sections include the cornea, the posterior chamber (PC), the anterior chamber (AC), the iris, the lens, the vitreous humor (VH), the trabecular meshwork (TM), the ciliary body (CB) , the sclera, the retina, and the choroid. Horizontally, the eyeball measures 24.22 millimeters, and then vertically, it measures 23.1 millimeters. There are 0.54 millimeters of thickness in the cornea.

HUMAN EYE STRUCTURE

The ability to see what we are looking at is provided by the light-sensitive tissue that is the human eye. It makes sense to compare the human sight to a camera. The crystalline lens in the retina and the cornea in the human eye are essentially identical. Consider them as

camera lenses. Through a process that is analogous to that of the diaphragm of a camera, the iris of the eye is responsible for regulating the quantity of light that is able to reach the retina by altering the size of the pupil. The light that travels via the cornea, the pupil, and the lens eventually reaches the retina, it is positioned behind the eye and contains photoreceptors that are sensitive to light. The picture that is produced on the retina is converted into electrical impulses and then sent into the brain via the optic nerves. It is in the brain that the signals are processed and where visual experiences are produced.

The macula is the name given to the dark yellowish center region of the retina, which is around 5.5 millimeters in diameter. Macula and its core area, known as the fovea, are responsible for providing acute center vision. At the very least, a healthy macula could provide normal vision, which is defined as 20/20. A small number of trichromatic photoreceptors, also known as "cone" photoreceptors, are found in the fovea, which is related with human color vision. When it comes to the fovea, there are no 'rod' photoreceptors that can supply information about brightness. In contrast to the rod cells, which do not offer color data in the manner shown in Figure (1), the lens, macula, and sclera cone cells are sensitive to long, medium, and short-wavelength ranges in the visible portion of the electromagnetic spectrum (i.e., 380 nm – 780 nm) (10).

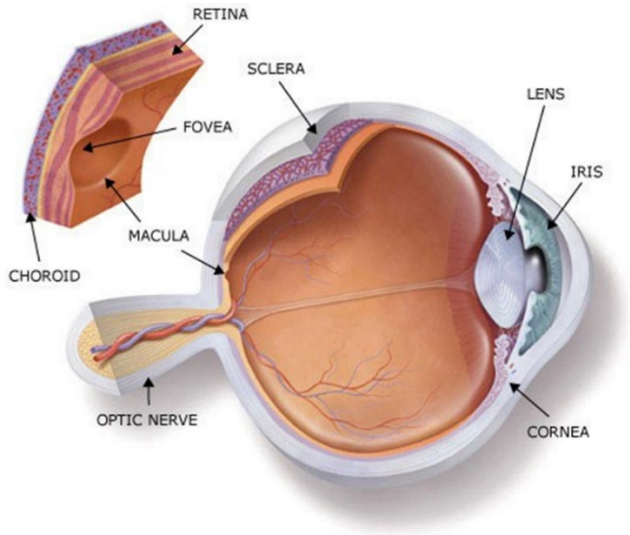

Figure: 1 Structure of the human eye

There are three separate fluids present inside the eye, as well as three compartments and three the coatings or layers present.

The human eye undergoes changes as a person ages. When a person gets older, the lens of their eye becomes larger. As people become older, both the breadth and the thickness of the lens will rise. A consequence of this is that as one gets older, the depth of the AC and the distance between the lens and the cornea both are reduced (11).

Between the “aqueous humor” (AH) and the “vitreous humor” (VH), the human eye has stuffed with fluid areas. The dynamics of the stuffed with fluid areas, particularly the AH,

are an essential sign of the health of the eye. Glaucoma and other eye illnesses are diseases that are caused by a deviation from the normal flow of AH.

The terms vitreous body, vitreous, and virtues may all refer to the vitreous humor (VH). The VH fills up around 80% of the eye's volume with a colorless, fragile, translucent gel. Its axial length is around 16 mm, and its capacity is approximately 4.5 ml. It has a pH of 7.5, a specific gravity between 1.0050 and 1.0089, and a refractive index of 1.3341, which is somewhat lower than the watery humor. The viscosity of vitreous humor is about twice that of water, and its osmotic pressure is similar to that of AH. Its osmolality varies from 288 to 323 mOsm/kg. It is the toughest structure in the eye, almost spherical in shape and including the patellar fossa, which curves behind the lens on the anterior surface. VH is primarily made of 0.9% salts and 99.9% water. Low-molecular-weight solutes and ions represent the remaining 0.1% of the solid material, which also includes protein and polysaccharide components.

LENS

The lens is a component in the eye that is curved and capable of bending light and focusing it for the retina, which enables the retina to view images more clearly. In order to improve the capacity to see things at varied distances, the crystalline lens, which is a transparent disc located below the iris, is flexible and can change form. Damage or deterioration of the lens may occur with increasing age. In this context, the capsule of the lens is taken into consideration. It is an essential component in the organ's capacity to receive inputs from the outside world and serves as a barrier. The capsule of the lens is composed of three distinct components: the cortex of the lens, the nucleus of the lens, and the lens capsule itself. The diameter of the nucleus was 2.1 millimeters, while the thickness of the capsule was calculated to be 0.5 millimeters (12).

The cornea and the lens both have a translucent appearance. The water medium is the only source of sustenance for this avascular their bodies. Molecular components, such as proteins, are unable to enter or exit the capsule because it is made of a thick, elastic material. Over the course of one's lifetime, the lens continues to develop. The lens germinal epithelium, which is situated near the lens equator, is responsible for the production of new lens fibres, which originate from the When the lens matures, it eventually moves inward toward the nucleus from the subcapsular area. The lens is composed of 36% proteins and 65% water. As

a lens ages, its water content decreases and the depth increases, making the lens less flexible. The structure that suspends the lens from its ciliary body is the zonule, which emerges from the ciliary body and inserts into its capsule at the equator. The anatomy of the lens mage is given below figure (4).

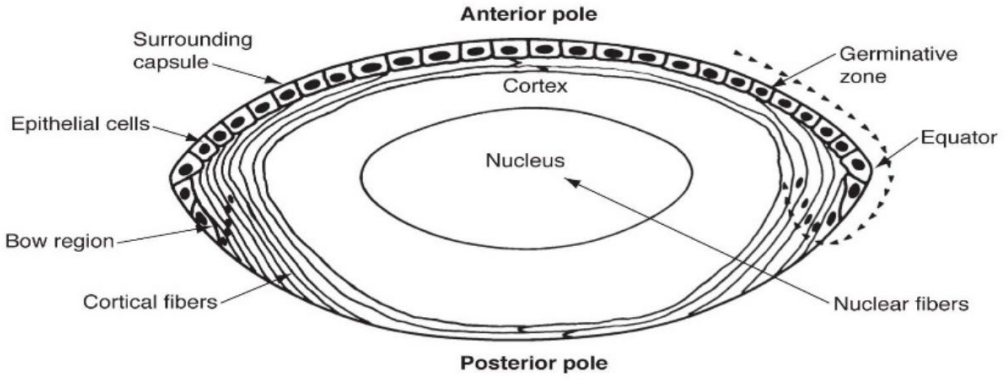

Figure: 4 Leans anatomy

AQUEOUS HUMOR

An assault to the optic nerve that was caused by an elevated intraocular pressure (IOP). The accumulation of aqueous humor (AH) fluid in the cornea causes a rise in IOP in the eye. Figure (5) illustrate the structure of aqueous humor pathway. The AH fluid is produced in the ciliary body of the eye and then passes via the canal that joins the iris and lens to reach the front chamber of the retina. Avascular tissue, the lens, and the cornea get nutrition from AH fluid, which also eliminates waste products from the metabolic process. As an additional function, AH fluid is responsible for the management of ocular tissue homeostasis, the stabilization of ocular structure, and the transportation of neurotransmitters. Trabecular meshwork and Schlemm's canal are the pathways by which AH fluid is drained.

On the other hand, AH fluid can accumulate when the flow of fluid is blocked by the trabecular meshwork, Schlemm's canal, or by the iris and cornea together. Different eye illnesses, such as macular degeneration, retinitis pigmentosa, glaucoma, and diabetic retinopathy, could lead to vision loss in humans. Cataracts are another common cause of vision loss. Glaucoma is a condition that causes eyesight to deteriorate and, if left untreated, can contribute to visual loss. Glaucoma illness affects around four percent of the whole population that is between the ages of forty and eighty years old that are affected by it. Glaucoma is a condition that is caused by damage to the optic nerves associated with the

retina of the eye (13).

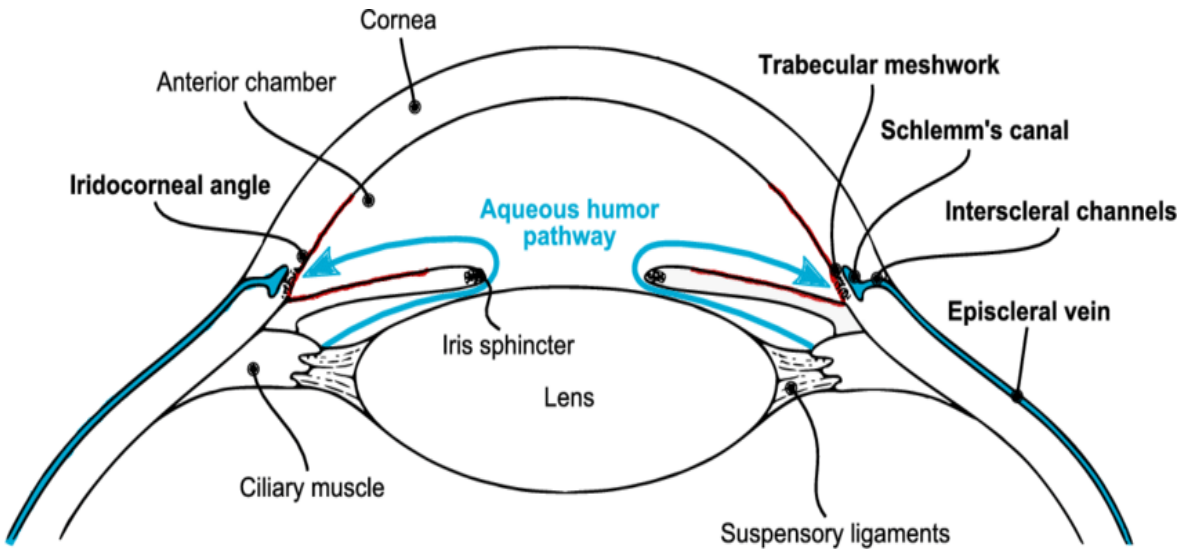

Figure: 5 Aqueous humor pathway

RETINA

The retina, which is a neuronal component of the eye, converts light into nerve impulses and sends them to the brain's visual centers. The retina is a component of the embryonic brain that is formed during the early stages of development. It is subsequently linked to the brain by a system of nerve fibres that is referred to as the optic nerve. In its most basic form, the retina of a mammalian eye is a layered sensorineural epithelial material that lines the eye. In addition to being an embryonic component of the central nervous system (CNS), this multi-layered structure exhibits a diverse range of neuronal types. The retina of a mammalian organism has around sixty different kinds of neurons, each of which plays a unique function in the processing of visual information. A three-tiered structure of the cell bodies is formed by these neurons, which are separated by two synaptic layers that are formed by the axons and dendrites of the respective neurons.

Both cones and rods that form up the hypersensitive layer, the outermost region of the retina, are only two types of neurons that have a direct sensitivity to light. This layer also contains the light receptors, also known as electroreceptors. Rods are responsible for dim eyesight and are typically more numerous than cones, which are responsible for responding to strong light. Cones are also involved in the sense of color (color perception). Throughout the retina, there is a discernible difference in the amounts of rods and cones that are present. The

macula, also known as the fovea centralis, is located in the middle of the retina and has a greater number of cones than the fovea, also known as the anatomic foveola. The fovea is a small place in the macula that is composed of solely tightly packed cones and is responsible for providing the retina with the finest vision.

CHOROID

In addition to the middle tunic of the eye, the choroid is comprised of the most posterior section of the uvea. The borders of the optic nerve are the beginning of the choroidal vasculature, which runs all the way in order to reach this plana. From a hist speaking, choroids are a kind of complicated framework that is made up of a variety of components. These components include resident immunocompetent cells, fibroblasts, blood vessels, melanocytes, and connective tissue that is both collagenous and elastic. The classification of this structure has ranged from three to five layers, depending on the assignment of the suprachoroidal region to the choroid and the belief that the larger choroidal arteries form two distinct layers. In addition, it has been divided into three layers, four layers, and five layers (14). Figure (6) provides an anatomy of the choroid.

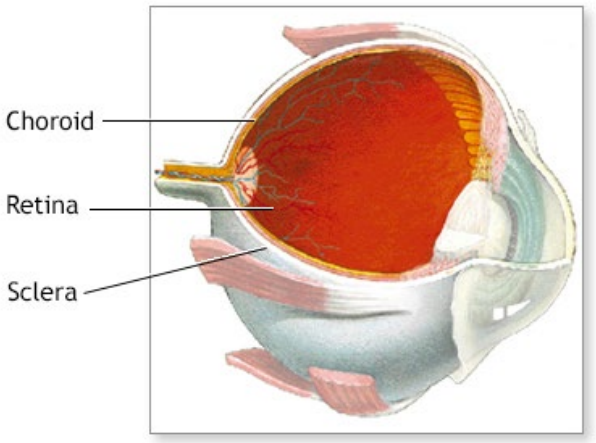

Figure: 6 Anatomy of the choroid

Despite the fact that it is a helpful method, it does have a few limitations. These drawbacks include the fact that it requires intravenous injection of indocyanine green angiography (ICG), that it does not have adequate transverse resolution to show choroidal microvasculature, and that it does not have depth-resolved differentiation. Given that it made it possible to get cross-sectional images of the choroid in live eyes, the development of the EDI

protocol for SD-OCT was a significant step forward in the field of imaging of the choroid. The Electronic Data Interchange (EDI) does, however, have certain limitations, which must be acknowledged. It does not allow for simultaneous optimum imaging of the vitreous, retina, and choroid, and the wavelength that is employed by SD-OCT is not large enough in certain circumstances to identify the choroidal-scleral border. In addition, it needs numerous scans to be averaged in order to produce good contrast and minimal speckle noise. In addition, the assessment of choroidal thickness (CT) using EDI on commercially available equipment requires manual segmentation, which restricts the measurements of thickness to a predetermined number of places (15).

1. BRUCHS MEMBRANE

Patients with DR do not experience any symptoms until the illness has progressed to a later stage, which potentially results in irreversible loss of vision or visual impairment. Patients who are at risk of developing this condition should undergo early screening and appropriate treatment, if any is necessary. Patients with diabetes are advised to have retinal examinations on a consistent and timely basis to permit the early detection and monitoring of DR.

The screening of the retina that was performed rec. A thin layer of fibrous tissue rich in ela1stic fibers and collagen is called the Bruch's border. Its existence and location ahead of the CC define it. The thickness of Bruch's membrane is typically between 2 and 4 micrometers, and it is traditionally composed of five sublayers (16).

According to some researchers believe that Bruch's membrane performs many roles. In addition, it act as hindrance to migration of cellular from the retinal. helps RPE cells adhere to one another, migrate, and differentiate. Additionally, it exercises control over the process of molecules moving back and forth between the CC and the RPE. Due to the fact that this section is entirely reliant on the framework of layer, the integrity of this physiological process may be altered if there are changes in the composition of the membrane that occur as a result of growing older or other pathological events.

2. CHORIOCAPILLARIS

Patients with DR do not experience any symptoms until the illness has progressed to a later stage, which potentially results in irreversible loss of vision or visual impairment. Patients

who are at risk of developing this condition should undergo early screening and appropriate treatment, if any is necessary. Patients with diabetes are advised to have retinal examinations on a consistent and timely basis in order to facilitate the early detection and monitoring of DR. The screening of the retina that was performed rec. The highly anastomosed network of capillaries known as the choriocapillaris is situated between the larger choroidal arteries and bruch's layer, isolating the innermost region of the choroid. It is also known as the choroid capillary network. The arterioles present in sattler's stage give rise to this thin layer of densely packed capillaries. These capillaries are organized into lobules, which are hexagon-shaped structures. The diameter of these lobules ranges from 200 to 350 μm at the posterior pole, and they gradually increase in size as they go towards the periphery. When fluorescein angiography is performed, the lobules of the choriocapillaris exhibit a pattern of lobular filling that is distinctive of the technique.

One very remarkable feature of the choriocapillaris is its meshwork. It consists of a thick network of minuscule capillaries spaced far apart by many tiny spaces between capillaries. Age (based on a energy) and disease (such myopia, hypertension, or age-related macular degeneration) may cause these gaps to enlarge. These interpapillary gaps enlarge and progressively lengthen as they approach the blind spot's edge due to a reduction in the choriocapillaris's diameter. Optical coherence tomography (OCT) angiography and other in real-time images have recently been used to record inter-capillary gaps. These spaces have the potential to serve as a quantitative biomarker of ageing and illness. This is because the increase in size of these spaces may be indicative of a decrease in the number or diameter of the capillary vessels (16).

BLOOD SUPPLY

Blood is supplied to everything that is through three arteries: the central retinal artery, the posterior ciliary artery, and the anterior ciliary artery. These arteries together are known as the ocular arteries and are derived from the inner carotid artery. The nerve that supplies the optics is the route that the main retinal artery follows to reach the inside of the eye. Following this, its branches spread out across the innermost layer of the retina, and blood vessels that break off from it supply the neuroretina, which is the inner half of the retina. At the base of the iris, the anterior choroid arteries penetrate the outermost layer after emerging from the recti muscles' insertion. They then go to an artery cycle from the ciliary body. The posterior ciliary

arteries are the tiny extensions of the ophthalmic arterial that enter the central region of the posterior pole of the eyelid. Some of these arteries supply the choroid, while two or more larger vessels originating from the anterior direction reach the arterial circle in the ciliary body. The bigger arteries are called the longer downstream ciliary arteries, whereas the arteries in the choroid space and peripapillary layer are called shorter posterior ciliary airways. Apart from the branches of the CRA, there is a vein that corresponds to every branch. The figure (8) provided an overview of the blood supply in human eye.

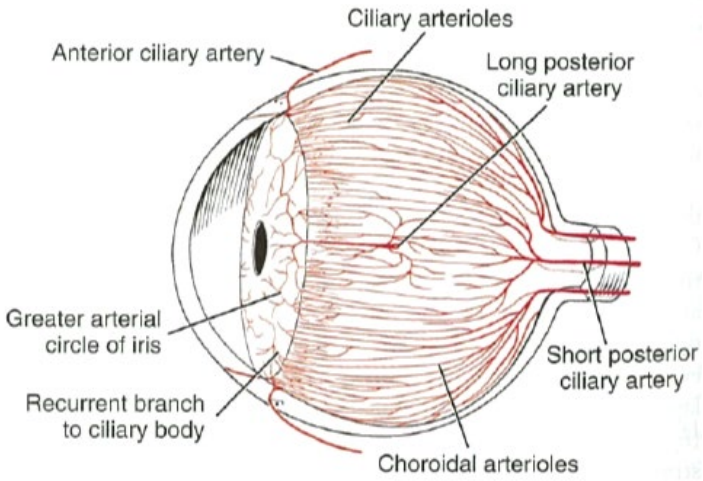

Figure: 8 The human eye blood supply

OPTIC NERVE

In order to reach the optic disc, the nerve fibers of the retina go via the deepest region of the retina. By closely observing how light passes off the retina's inner surface under a magnifying glass, one may use an ophthalmoscope to observe these nerve fibers. Furthermore, the retina's inner surface of the retina contains the arteries that comprise the retina. The optic nerve's connection to the side of the globe behind it is situated very little above the horizontal meridian and slightly nasal to the posterior pole. This specific area of the eye is called the optic disc, or optic nerve head for short. The optic disc does not include any cells that are sensitive to light, and as a result, light that falls on this portion of the fundus is not detected. This is something that relates to the blind spot that may be found in the range of vision of each individual.

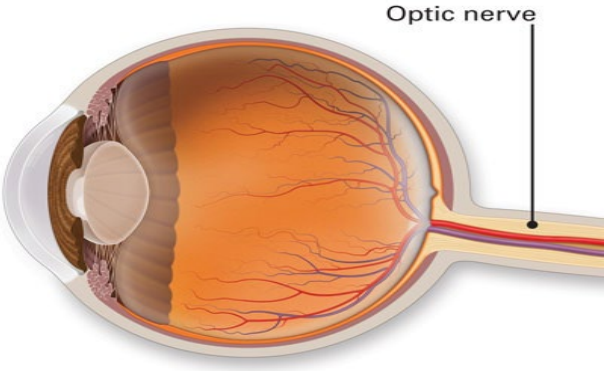

Figure: 9 Structure of the optical nerve

The coverings termed pia, head, and dura surround the nerve in the eye, allowing its fibers to pass in packages divided by fibrous tissue. Other types of cells that are responsible for maintaining the optic nerve include microglia, oligodendrocytes, and astrocytes. At the optic chiasma, around half of the fibers making up the optic nerve split off. The pretectal nucleus is one of the locations where a short range of nerve fibers terminate, although the lateral geniculate body is where most nerve fibers link with one another. The back pole of the earth's surface is perforated by many ciliary nerve endings, both short as well as long, along with that of the optic nerve. The flexor and muscles of the sphincter of the eye and the ciliary body (ciliary muscles) are supplied mainly by the parasympathetic, sympathetic, and sensory fibers that are contained within these. Patients may experience discomfort if inadequate local anesthesia is used while treating the iris. Furthermore, laser coagulation treatment of the chorioretinitis may cause discomfort to patients. This implies that the choroid and iris do indeed contain sensory fibers. The only sensory endings present are those that are in charge of pain, notwithstanding the cornea's extreme sensitivity (18).

EXTRAOCULAR MUSCLES

The two sides of the obliques, together with the medial, lateral, superior, and inferior recti, are the 6 outside muscles that, when combined, allow the pupils to move in various directions. All of these facial muscles are fed by the 3rd cranial nerve, except the lateral rectus, which is supplied by the sixth nerve, and the superior oblique, which is supplied by the fourth nerve. The annular region of Zinn, a fibrous ring that envelops the spinal cord at the orbital summit, is the source of all these muscles save the inferior oblique. A "muscle cone" is formed as the muscles spread out in the direction of the eye. In contrast, the oblique muscles attach

behind the equator, whereas all of the recti muscles attach to the eyeball anterior to the equator. The muscular cone contains the nerves that supply the extraocular muscles, the optic nerve, and the blood vessels that nourish the eye (save from the fourth nerve). There is a connection between the legator palpebrae superioris and the superior rectus. It travels over the orbital roof, stretching across the superior rectus and adhering to the skin of the above lid and the front of the tarsal plate of the above lid. It comes from directly above Zinn's disc. The tenon of the visual cullum is a layer of fibrous tissue that envelops the eye and is contiguous with the fascial layer of the muscle tissues (17). The anatomy of the extraocular muscles is shown in figure (7).

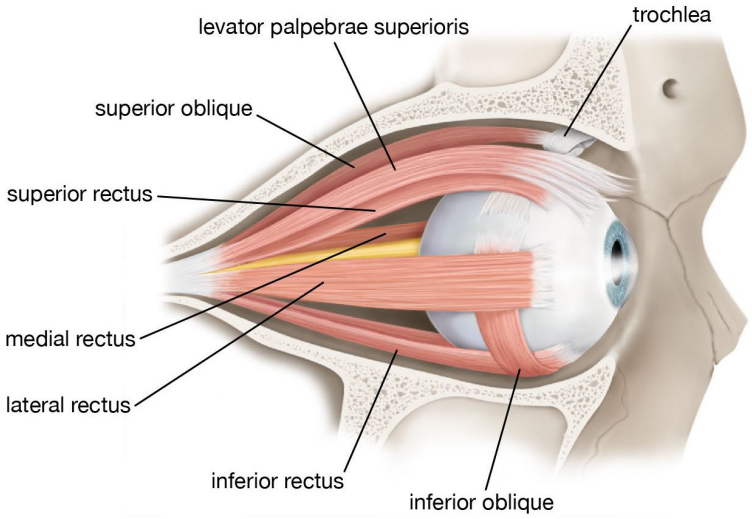

Figure: 7 Anatomy of the extraocular muscles

SCLERA

The sclera is a strong membrane that covers the whole eyeball. The front portion of the sclera is translucent, which allows light to enter the retinal. Not to mention because the membrane is made up of several layers, each of which has a distinct vein structure. In past research, these vessels were referred to as the conjunctival vasculature; however, they are now collectively referred to as the sclera vascular. When seen via an ocular picture, the sclera is the white portion that surrounds the iris, which is a somewhat dark-colored structure. In comparison to other places, the region in question has a greater degree of contrast. Due to the fact that the vascular pattern included inside the sclera is distinct and consistent to each eye of every person, it is feasible to recognise the sclera. Derakshani presented scleral recognition in 2006, however they referred to it as conjunctival vascular recognition. any as a standalone

biometric recognition modality or as a supplemental system in conjunction with other modalities, it may be used in any of these capacities. Reports on many benchmarking contests on sclera segmentation and identification were released between the years 2015 and 2020. These competitions were held in addition to the work done by a variety of research organizations. strategies that were based on rules were used in the majority of the early works; but, following that, strategies that were based on machine learning became more prevalent (19).

The sclera is the outermost fibrous layer of the eye, and it is responsible for providing the structural stability necessary for the housing of the intraocular constituents. Scleral thinning is a dangerous problem that develops with time and may eventually lead to perforation as well as a decline in visual functionality of the eye. The purpose of this study is to provide a concise summary of the anatomical considerations and causes of scleral thinning, as well as the diagnosis and the wide range of surgical methods that are available to treat scleral thinning. The white layer that covers the surface of the eye is called the sclera. The cornea, which is the transparent front portion of the eye, is the beginning of this tough, fibrous tissue, which runs all the way to the optic nerve, which is located at the rear of the eye. The sclera is responsible for the white color of the eyeball. A similar sort of collagen fibers is used in the construction of both the cornea and the sclera. The fibers in the cornea are structured in sheets and layers, which is what gives the cornea its transparent appearance. The sclera has fibers that are organized in a random pattern. Figure (10) demonstrates the anatomy of the sclera.

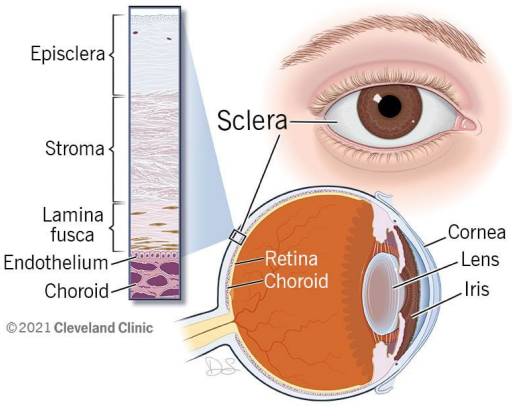

Figure: 10 Anatomy of the sclera

Sclera is a structure that develops from the mesoderm and is thicker in men than it is in females, according to embryology. From an ultrastructural viewpoint, the cornea may be divided into three separate sections: (1) scleral stroma, which makes up nearly all of the total

sclera and consists mainly of collagen, cells, proteins, and glycoproteins; (2) lama fusc, the lowest layer of sclera distinguished by richness of melanin cells; and (3) episcleral, the thin densely arterial layer of connective tissues surrounding sclera that is located below tenon's capsule. Towards the cornea, the human sclera progressively thickens, with the thickest portion being located close to the optic nerve and the thinnest portion being at the insertion of extraocular muscles. Therefore, the tissue of the sclera has a low metabolic requirement due to the slower turnover rates of collagen and other cell types. This may be attributed to the sclera's relative lack of blood vessels. Ciliary nerves provide a substantial amount of blood to the sclera. Compared to the front part, which is mostly controlled by both long ciliary nerves that emerge from the Nas ciliary nerve, the rear lens is irritated by the short choroid nerves that are formed from the ciliary ganglion. These nerves are susceptible to inflammation and discomfort, which may lead to episcleritis and scleritis if they are damaged in any way (20).

COMMON EYE DISEASES

Eye disorders such as diabetic macular edema, diabetic retinopathy, glaucoma, and cataracts are included in the category of retinal eye disease (RED). A patient's eyesight may be impaired as a result of the RED that was discussed before. According to the findings of a study conducted by the International Diabetes Federation (IDF), a significant numbers of people are afflicted with diabetes. Consequently, the rate has been steadily raised over the course of time. Due to the fact that diabetes is the fourth most deadly disease in the world, the clinical, social, and economic complications of diabetes have an impact on the health of individuals. The appearance of hard exudate (HE) in macula areas, the deployment of blood vessels in an unintended manner, and the existence of injured optic nerves are the starting points for severe retinopathy (21).

1. DIABETIC RETINOPATHY (DR)

Figure (11) illustrates how damage to the blood vessels in the retina, the light-sensitive tissue located at the back of the body, is one of the causes of diabetic retinopathy (DR). Actually, the receptor that receives light and transmits signals to the brain is the retina. The brain then decodes the information it has received in order to make observations. Early DR and advanced DR are two distinct phases of DR symptoms. When the blood vessel does not expand (proliferate) in the case of prior DR, a kind of DR known as non-proliferative DR (NPDR) develops.

The blood vessel walls inside the retina weaken in NPDR. Microaneurysms (MA), another name for narrower bulges, are projections that come from the surface of a thin artery and cause fluid to build up in the eyes. The NPDR moves from the normal stage to the severe stage when the greatest number of vessels are blocked. This happens when the retinal vessels start to significantly enlarge. Depending on how severe the problem is, the retina's nerve fibers swell.

Table: 1 Major risk factors for Diabetic retinopathy (124)

Non-Modifiable(Constitutional)	**Modifiable**
Hypertension	nephropathy
hyperglycemia	dyslipidemia
Gender	smoking
Age	higher body mass index

Prompt treatment is necessary since the macula, the central portion of the retina, has been damaged (ME). There are three classifications for NPDR: mild, moderate, and severe. Proliferative DR (PDR) is another term for advanced DR. At this point, weakened blood vessels start to drain the transparent jelly-like fluid that fills the vitreous, the center part of the eye, which eventually causes aberrant retinal growth. The pressure that has built up in the eyeball disrupts the capillaries and the normal flow of fluid.

Figure: 11 Diabetic retinopathy

1.1 VARIOUS STAGES OF DIABETIC RETINOPATHY

Diabetic retinopathy presents in six stages: Minimal, Mild, Moderate, Moderately Severe, Severe, and Proliferative. The trained model will be used to create a classifier that will employ the characteristics taken out of the retinal fundus pictures to categorize diabetic retinopathy (DR) into four groups or severity levels: mild, moderate, severe, and proliferative. The caption generator is meant to provide visual captions that explain the many symptoms in the retinal image and categorize diabetic retinopathy into four severity levels: mild, moderate, severe, and proliferative (22).

This is diabetic retinopathy's first stage. At this point, microaneurysms might manifest is shown in figure (12). Retinal microaneurysms might be brought on by arterial disease or any other kind of vascular illness. The most typical reason diabetes mellitus is the cause of diabetic retinopathy. In retinal imaging, microaneurysms are the first signs of diabetic retinopathy that are evident. These tiny aneurysms have the potential to burst and spill blood. A microscopic swelling known as a microaneurysm develops in the walls of tiny blood vessels tiny aneurysms vary in diameter from 25 to 100 µm.

Figure: 12 Mild diabetic retinopathy

MODERATE NONPROLIFERATIVE DIABETIC RETINOPATHY

This stage is believed to be less severe than severe NPDR in addition to microaneurysms. The Moderate NPDR is characterized by an increase in cotton-wool patches, hard exudates, microaneurysms, and intraperitoneal hemorrhages. Intraretinal microvascular abnormalities (IRMA) and a modest VB are also seen in severe NPDR. Figure (13) depicts the retinal fundus image with mild diabetic retinopathy.

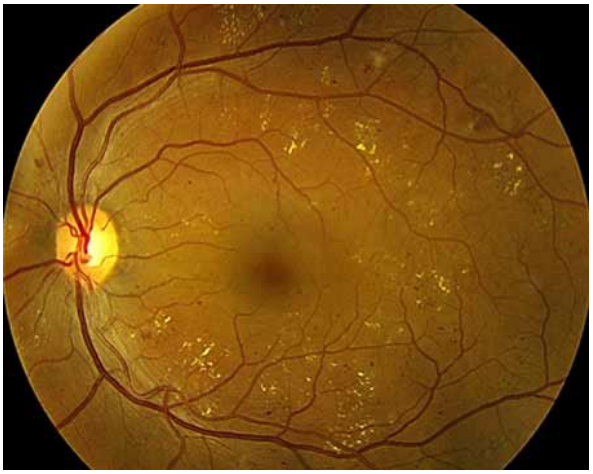

Figure: 13 Moderate diabetic retinopathy

NONPROLIFERATIVE RETINOPATHY

Hemorrhages, microaneurysms, or both in two or more quadrants, minor IRMA (less than or equal to 0.4mm2), or venous beading in one quadrant are all included in this degree of moderately severe DR. The retinal consider with moderately severe diabetic retinopathy is shown in Figure (14).

Figure: 14 Retinal fundus image with moderately severe diabetic retinopathy

SEVERE NONPROLIFERATIVE DIABETIC RETINOPATHY

Several parts of the retina lose their blood supply at this point due to the blockage of several more blood vessels. These retinal regions communicate with the brain to produce new blood vessels for nutrient uptake. the existence of venous beading (VB) in two or more quadrants and hemorrhages in all four quadrants The additional distinct symptoms for severe diabetic retinopathy include intraretinally distributed microvascular abnormalities (IRMA) in one or more quadrants.

1.1.5 PROLIFERATIVE DIABETIC RETINOPATHY

New blood vessels begin to form in the last stage when the retina sends signals for sustenance. These recently formed blood arteries are weak and unusual. They proliferate on the surface of the vitreous gel, which is transparent and fills the inside of the eye, as well as the retina. These blood vessels don't produce symptoms or visual loss on their own. But their walls are flimsy and brittle. They may cause serious vision loss or possibly blindness if they leak blood.

2. GLAUCOMA

This condition, which is classified as an ocular infection, affects the nerve that runs from the eye to the brain. An increase in intraocular pressure (IOP), or the fluid pressure within the eye, causes the optic nerve to deteriorate considerably, as seen in figure (17). High blood sugar levels increase the risk of developing glaucoma, which can result in blindness and loss of vision, if it is not identified in its early stages. Based on the size of the enlarged ONH or OD and the cup to disc ratio (CDR), glaucoma is classified into three groups.

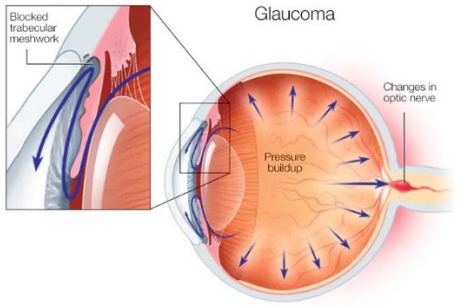

Figure: 17 Glaucoma

Glaucoma may pass through three stages: the normal, the medium, and the pathological. DME incidence is presented if the fluid develops in the middle portion of the retina (macula) because of the damage in blood vessel. As a result of fluid buildup, the macula becomes enlarged and thicker, which results in a decline in the quality of vision. The macula is responsible for crisp and direct vision.

3. EXUDATES

The leakage that happens in blood vessels is the cause of exudates, which are similar to

a fluid that is created from serum proteins, lipids, and protein. To be more specific, individuals who have been diagnosed with DR may later have exudates in their eyes, which are characterized by veins and arteries that exhibit leaking. Figure 18 shows a sample of the afflicted eye's exudates.

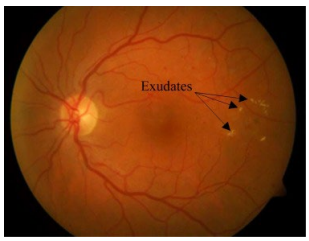

Figure: 18 exudates

The development of new blood vessels, bleeding, hard and soft exudates, microaneurysms, and hemorrhage are all consequences of diabetic retinopathy. These abnormalities result in a gradual loss of vision, which eventually leads to complete blindness from retinal detachment. Detection of hard exudates is crucial for the management of diabetic retinopathy, since these lesions, which may appear all over the eye and vary in size, are the first indications of the condition (24).

4. CATARACT

Diabetic individuals are more likely to experience the development of cataracts and clouded lenses at an earlier stage in comparison to those who do not have diabetes. In conclusion, the early prediction of RED is of the utmost significance in relation to the elimination of visual loss concerns. The time required for manual forecast of RED is greater. In addition, it is difficult for the specialists to forecast RED at an earlier stage based on the early symptoms. As a consequence of a high sugar level, it is characterized as a breakdown of lens protein, which leads to a hazy lens and ultimately impacts one's ability to see clearly. Most cataracts fall into one of four categories: non-cataractous, mild, moderate, or abnormal. These categories are used to categorize cataracts. Individuals who are diagnosed with diabetes have an increased risk of developing retinal eye disorders (RED). With cataracts accounting for half of all cases of blindness in middle-class and low-income countries, compared to only 5% in developed nations, cataracts are the primary cause of blindness in these regions. Furthermore, the World Health Organization predicts that an aging population and population expansion will

raise the possibility that more individuals can develop visual impairment. Since there are little resources available and a high disease burden, identifying risk factors is crucial to set methods in place that will slow the development of cataracts (25).

Age-related cataracts are the most frequent kind of cataract. They are classified into three categories according to the structure of the human lens: nuclear sclerotic, cortical, and posterior subcapsular.

NUCLEAR SCLEROTIC

Nuclear cataract refers to the development of nuclear sclerosis eyes, i.e., the lens growing older and foggier. Fetal nuclear cataract, also known as congenital nuclear cataract, is the term used to describe congenital cataract that is located close to the eye's nucleus. Increased spasticity combined with further dryness of the lens's cortical section and center results A cataract that is clouded from birth is referred to as congenital cataract. Molecular cataract is a term used to describe excessive central lens discoloration and reflection of light. in atomic old cataracts. Nucleus sclerosis causes the core, or center of the eye, to stiffen, become yellow, as well as become unclear. In addition to humans, dogs, cats, and horses can also develop nuclear sclerotic cataracts as a component of aging. Figure (20) shows the how nuclear sclerotic is affect the eye.

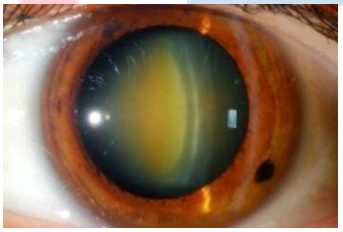

Figure: 20 Nuclear sclerotic

POSTERIOR SUBCAPSULAR

PSC stones develop directly ahead of the lens, in the rear chamber. Vacuoles are seen early in the age-related kind. Subsequently, epithelial cells move across the cornea's center to the forward pole in a posterior direction, where they undergo differentiation into Wedl's bladder or balloon cells. The dispersion of big particles is facilitated by the many organelles found in epithelial cells. An optical section approach is needed to classify a cataract as PSC, even though

PSC cataracts are best seen with a dilated pupil and fundus retro-illumination.

PSC cataracts usually appear around the age of 55, and they are identified as a side effect of systemic medications such oral corticosteroids. They are also linked to diabetes, ocular illnesses including retinitis pigmentosa and uveitis, and retinal trauma. Because PSC cataracts are often positioned near the center of the pupil, they might result in a significant decrease in vision when the pupil contracts. When seen via an undiluted pupil, these cataracts may be ignored because they blend in with the corneal and lens reflexes.

Table: 3 Major risk factors for cataract

Nonmodifiable	**Modifiable**
Genetic abnormalities	High cholesterol level
Family history	Increased sun exposure
Increasing age	Smoking
Gender	

4. MACULAR EDEMA

A disruption of the blood–retinal barrier (BRB) is the cause of diabetic retinopathy, which is a frequent complication of type 2 diabetes (T2D). The aberrant Vaso permeability causes the retinal vasculature wall to experience an irregular flow of molecules, including water, blood cells, fluids, and protein. This is a consequence of the phenomenon which is show in figure (21). The accumulation of these fluids in the macular area has a tendency to result in the formation of pigments such as exudates and me. This disruption causes an increase in vascular permeability, which in turn leads to diabetic macular edema to develop. When it comes to persons with type 2 diabetes, diabetic macular edema (DME) is the most prevalent cause of impaired vision in nations with high incomes, but in countries with low incomes, it is the most common cause of impaired vision overall. The macular region of the retina is located in the middle of the retina and is responsible for giving the highest possible level of vision. This condition, which is classified as an ocular infection, affects the nerve that runs from the eye to the brain. An increase in intraocular pressure (IOP), or the fluid pressure within the eye, causes the optic nerve to deteriorate considerably, as seen in figure (17). High blood sugar levels

increase the risk of developing glaucoma, which can result in blindness and loss of vision, if it is not identified in its early stages. Based on the size of the enlarged ONH or OD and the cup to disc ratio (CDR), glaucoma is classified into three groups.

An alteration that is thought to be the consequence of altered retinal blood flow is the accumulation of fluid in the inner to outer plexiform retinal layer, which is a characteristic of macular edema. Laser photocoagulation, vitrectomy, and the use of the steroid triamcinolone acetonide were the first therapies for diabetic macular edema (DME) (26).

Table: 4 Major risk factors for diabetic macular edema

Nonmodifiable	**Modifiable**
Genetic abnormalities	Smoking
Family history	Drinking
Increasing age	Total cholesterol
Gender	Proteinuria

5. AGE-RELATED MACULAR DEGENERATION (AMD)

Age-related macular degeneration (AMD), which is the primary cause of eye illnesses or the loss of vision, mostly affects persons who are older. An extra occurrence of drusen, which are yellow patches in the macular region, is a defining characteristic of age-related macular degeneration (AMD). Since adults over the age of 50 are more likely to develop drusen as a typical architecture of the retina, the minimal count of hard drusen is not regarded to be a marker of AMD. The aberrant growth of drusen, on the other hand, leads to the mutilation of the retinal pigment epithelium. Central blindness in developed countries is mostly caused by AMD, especially in people over 60. It is the third most common cause of severe permanent vision loss globally. According to prevalence estimates, 200 million or more individuals worldwide are thought to be afflicted by AMD now, and by 2040, this number is predicted to rise to around 300 million. Figure (22) shows the difference between the normal and macular degeneration affected eye.

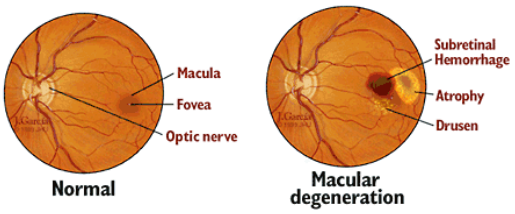

Figure: 22 Normal Vs Macular degeneration

AMD decreases central vision by causing pathologic changes to the adjacent capillaries and the deeper retinal layers of the center. A prominent clinical symptom in AMD (discussed below) is the buildup of retinal deposits, or drusen, which may be the first indication of the "dry" version of the illness. The most prevalent morphologic kind of AMD is called dry AMD. This might progress to "wet" or neovascular AMD (the national choroidal neovascular barriers, or CNV), it can result in emission and bleeding in the retina. They are formed by abnormal vascular spread, or angiogenesis, which releases a protein called vascular endothelial growth factor (VEGF). Intravitreal injections with anti-vascular endothelial growth factor (VEGF) therapy are the preferred treatment for these lesions and have completely changed the way progressive AMD is managed. The "dry" or nonexudative form of late AMD is another variation in which the macula develops atrophic scars or geographic atrophy. If the fovea is involved, these atrophic lesions have equally serious, irreversible impacts on visual function and do not respond to anti-VEGF medication (27).

The nerve that connects the eye to the brain is impacted by this illness, which is categorized as an ocular infection. Figure (17) illustrates how the optic nerve deteriorates significantly as intraocular pressure (IOP), or the fluid pressure within the eye, rises. If glaucoma is not detected in its early stages, it can cause blindness and loss of vision. High blood sugar levels raise this risk. Glaucoma is divided into three groups according to the cup to disc ratio (CDR) and the size of the enlarged ONH or OD.

Reduced vision may lead to despair, an increased risk of falls, and the need for long-term care if one is unable to do everyday tasks like eating, working, and dressing. With a constant yearly rise in the number of new cases, AMD's direct costs to the North American healthcare system exceeded 250 billion dollars in 2008. The population is becoming older, which suggests that these figures will keep rising at an exponential pace. The visual effects of AMD may have a major negative influence on quality of life and aggravate the elderly's already

difficult comorbidities and health-related issues. Comprehending the fundamental indications and manifestations of AMD aids in advising patients on when to see an ophthalmologist and stop more vision loss. Despite the fact that AMD cannot be cured, proactive and preventive care is essential.

By addressing some modifiable risk factors, such as diet, cardiovascular disease, and smoking, the course of the illness may be delayed. A particular vitamin supplement combination was developed for individuals with certain features of AMD in order to prevent the illness from progressing, according to the Age-Related Eye illness Study (AREDS). There are several AMD subtypes, and not all of them react to anti-VEGF medication or fit the requirements to be prescribed AREDS vitamins. Depending on the disease's stage, the prognosis varies. It is crucial to promptly send patients for ophthalmologic care in order to treat and avoid the long-term effects of AMD.

Table: 5 Major risk factors for Age-related macular degeneration (AMD)

Nonmodifiable	**Modifiable**
Genetic abnormalities	Diet
Family history	Cataract status
Increasing age	Smoking
Gender	Hypertension

6. REFRACTED ERRORS

A blurry image results from refractive errors, which indicate that your eye's condition isn't properly bending light. The four main types of refractive errors are astigmatism, presbyopia, hyperopia (farsightedness), and nearsightedness (myopia).

Symptoms

- Blurred vision

- Difficulty reading or seeing up close
- Crossing of the eye in children (esotropia)

MYOPIA

Things that are close are distinct, while those that are far away are blurry. Myopia, sometimes referred to as nearsightedness, is typically genetic and frequently identified in early infancy. During the adolescent years, when the body is expanding quickly, myopia often becomes stronger.

HYPEROPIA

Compared to distant things, close objects are more, blurry. Hyperopia, sometimes referred to as farsightedness, is inherited. Hyperopia is common in children and can get a lesser problem in adults. While close vision is blurry with moderate hyperopia, far vision is distinct. At all distances, vision may become blurry in the more serious forms of hyperopia.

PRESBYOPIA

The growing process of eye's lens. The eye lens becomes less flexible and more, hard beyond the age of 40. The eye loses its capacity for focused thought as a consequence, making close reading more challenging. Astigmatism, hyperopia, or myopia can occur with the biological aging process of the lens.

ASTIGMATISM

An unequal corneal curvature on the surface of the eye is the most frequent cause of astigmatism. Light may penetrate the cornea and concentrate equally on all planes, or directions, since the cornea is normally soft and similarly curved in all dimensions. The cornea's front surface is more flexed in one direction than the other as long as astigmatism is present. This anomaly might cause eyesight that resembles that of a warped, wavy mirror. Astigmatism often results in blurry vision at all viewing angles.

Side effects of refracted error of eye are,

- Obscured vision,

- Trouble reading or seeing very close and
- Intersection of the eyes in kids (esotropia)

CHORODIAL NEOVASCULARIZATION (CNV)

Neovascularization is the term for the development of new, aberrant blood vessels on the retina as a result of the blocked blood vessel caused by ischemia. This recently formed blood vessel can lead to wrinkles or retinal detachment, which would harm the retina. The investigation finds that glaucoma, a retinal condition that destroys the optic nerve, may be caused by neovascularization.

THE RETIAN STRUCTURE

The macula is a yellow patch that may be seen in the median region of the retina. The fovea is a concave depression located in the middle of the macula, which is responsible for the highest possible visual acuity. Photoreceptor cells in the retina are responsible for the detection of light and the generation of electrical impulses, which are then sent to the brain across the optic nerve. In the visual cortex of the brain, these impulses undergo further conversion, which results in the formation of visuals and optical sensations.

The human eye is a spherical organ that is responsible for our ability to see. It has a transverse diameter of 24 mm and a sagittal diameter that is approximately between 24 and 25 mm. The retina receives light that has been refracted by the lens. The rear lining of the eye is composed of a layer called the retina, which is shows in figure (23). Rods and cones are the two types of photoreceptor cells that are present. When there is a low amount of light, rods are able to detect motion. Cones are the parts of the eye that take care of color vision and function most effectively under bright light. A blind region on the retina is referred to as an optic disc, and it serves as the point of entry for the primary blood arteries that feed the retina with sustenance or blood. It is divided into two major sections:

Retinal pigment epithelium: This substance originates from the optic cup's outside layer. The cells that make up this structure are arranged in a single layer and are adhered to Bruch's membrane. There is a membrane called Bruch's membrane that divides the choroid from the outer retina (28).

Neuroretina: Each retinal layer derives from the innermost layer of the optic cup, which remains in place during embryogenesis.

ANATOMY OF THE RETINA

When looking at the retina from the middle of the eyeball outwards, the Retinal Pigment Epithelium, often known as RPE, is the retinal stratum that is the most external. The anatomy of the human eye retinal is represent in the figure (24). The retina is located between the vitreous body, which is transparent in the center, and the choroid. There is a transparent gel that fills the vitreous body. The content of this gel fluctuates in a concentric manner, with the most liquid phase being located in the center. As it gets closer to the retina, the gel progressively transforms into a fibrous network. The foot-like processes that extend from the matrix of structural cells that support the vascular and neurosensory parts of the retina proper are responsible for the formation of this limiting feature of the retina.

This blood retinal barrier, which is one of the numerous structures involved in the process, is responsible for ensuring that the homeostasis of the retina proper is preserved. The bulk of the lesions that are connected with early diabetic retinopathy, also known as mild to moderate instances, are situated between the structural cells that are adjacent to the vitreous, so constraining the retinal interiorly, and the "retinal pigment epithelium" (RPE) on the outside (8). Patients with diabetic retinopathy (DR) do not experience any symptoms until the illness has progressed to a later stage, which potentially results in irreversible loss of vision or visual impairment. Patients who are at risk of developing this condition should undergo early screening and appropriate treatment, if any is necessary. Patients with diabetes are advised to have retinal examinations on a consistent and timely basis in order to facilitate the early detection and monitoring of DR.

The screening of the retina that was performed rec. In order to detect diabetic retinopathy at an earlier stage, diabetic patients are advised to have retinal examinations on a consistent and timely basis. The screening of the retina that was performed recently with the assistance of a non-mydriatic digital retinal fundus camera is economical and does not involve any invasive procedures. In contrast to other methods, such as indirect ophthalmoscopy and slit-lamp fundus bio-microscopy, which need dilated pupils in addition to specialist knowledge for its operation, the operation of this camera just requires a fundamental level of training. Due to the many benefits that it offers, fundus imaging is the

method of choice for screening for DR. Having an awareness of the evolution of DR and a better grasp of the repercussions is essential for the management of the condition and for initiating therapy at an earlier stage (29).

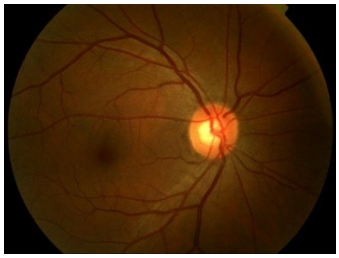

Figure: 24 Normal retinal anatomy

RETINAL BLOOD VESSELS

The retina receives its oxygen and nutrition from the retinal blood vessels and the choroid, which is located below the retinal shade epithelium (figure (25)). Arteries are the blood vessels that carry oxygen and nutrients within the retina itself. The primary one, the focal retinal tract, divides into the common (upper) and lower (lower) branches after entering the eye using the optic nerve. Then, comprising the segments of a tree, they keep spreading outward until they create a thin, delicate network of blood vessels.

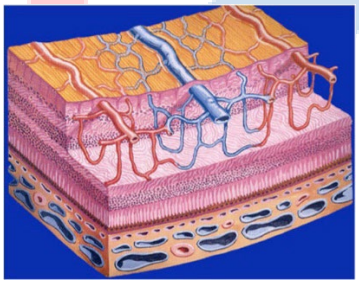

Figure: 25 Retinal blood vessel

It's important to remember that the retina has just one artery supplying it and one vein draining it. The majority of issues resulting from disorders affecting the retinal blood vessels achieve thus by obstructing or distorting the capillaries. Therefore, only the area of the retina fed by a blocked retinal vein or artery is affected, and therefore, only that area of the visual field. Retinal oxygen and nutrients are mostly taken in by the capillaries, where they are also removed from the retina along with carbon dioxide and waste products. Before entering the optic nerve and continuing to the heart, the essential retinal vein leaves the capillaries at the

optic nerve's exit point. Branch veins are formed when the capillaries connect together.

The whole area of perfused vasculature per unit area in a measuring zone is known as the vascular density (VD). Using built-in software, the VDs in the SCP (Superficial Capillary Plexus) and DCP (Deep Capillary Plexus) in the impacted sectors of the 3 x 3-mm foveal areas were measured at the 12-month visit. Vascular density and changes within it were compared between anatomical responders and non-responders, as identified by differences in CST (central subfield thickness).

VESSEL DENSITY MEASUREMENT

A 3-millimeter circular Late Therapy DR array positioned above the fovea was used to collect the vascular density data. The percentage of the measured area composed of the vessels at both the SCP and DCP levels was used to compute vascular density. Every sector's vessel density appeared on the grid. The center 1-mm sector of the grid served as the definition of the core area. The area that lies between the 3-mm border and its central 1-mm sector is known as the parafoveal zone. At the SCP and DCP levels, the vessel densities of the central, parafoveal, and total 3-mm area were measured.

Superficial Capillary Plexus (SCP)

The area between the outside edge of the ganglion cell layer and the vitreoretinal interface is referred to as the SCP. The segmentation was done at two different points: 2.6 µm below the internal limiting membrane and 15.6 µm below the inner plexiform layer (IPL).

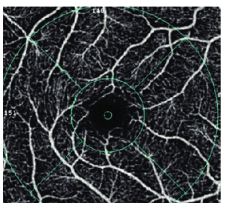

Figure: 27 Superficial capillary plexus (SCP)

Deep Capillary Plexus (DCP)

Segmenting the DCP automatically included dividing the region by the inside border of

the IPL and the outer margin of an outer plexiform layer. Under the IPL, the limitations were set at 70.2 µm & 15.6 µm, respectively (30).

Table: 6 Vessel density (%) (123)

		Vessel Density (%)
Scan Layer	**Sector**	**Healthy eyes**
SCP	Outer parafovea	50.2 (48.7,51.7)
DCP	Whole image	50.6 (48.9,52.4)
	Superior Hemifield	50.8 (49.1,52.5)

FOVEA

For a variety of reasons, including inconsistency in images obtained as samples and changes in the color of the fovea between individuals, the analysis of color retinal pictures is a challenging endeavor (31). In addition to being an essential component in the process of gathering pictures, it also gives the spectator the ability to feel as if they are a part of the surrounding world. With regard to the process of collecting distinct views, the fovea, which is located in the center area of the macula, is an important component. The location of fovea in the retina is shown in figure (29).When it comes to the process of grading diabetic maculopathy, the finding of the fovea and the distinction of the multiple structures that are included inside it become quite important.

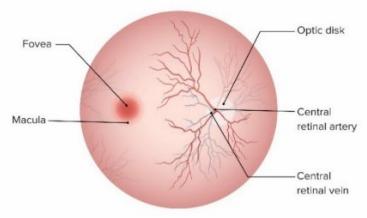

Figure: 29 Fovea location in the retina

FAZ

The foveal avascular zone (FAZ) is a specific region in the central macula that lacks capillaries and is next to the area where the density of cone photoreceptors is greatest and where

oxygen consumption is highest [4], This has unmatched importance. Variations in the FAZ's area may thus be related to how well one can see. More significantly, these alterations may have predictive as well as diagnostic relevance in a range of retinal conditions. It is crucial to first understand the variation in the FAZ area and the variables influencing FAZ in healthy persons in order to establish the association between variation in the FAZ region and retinal disorders. Many research on the FAZ have been published to date, but most of them intentionally picked just a limited number of programs, such as gender, axial length, retinal structure, and vascular characteristics, in order to identify variables impacting the FAZ area and probable relationships.

LAYERS OF RETINA

Each of the six distinct cell lines that make up the retina's 10 layers has a distinct function in the development and transmission of vision. More quickly than any other tissue in the human body, retinal tissue grows to become the most metabolically costly tissue. The following are the layers that go from the nearest to the front anterior of the head to the posterior of the head:

1. Inner limiting membrane
2. Nerve fiber layer (NFL)
3. Ganglion cell layer
4. Inner plexiform layer
5. Inner nuclear layer
6. Middle limiting membrane
7. Outer plexiform layer
8. Outer nuclear layer
9. External limiting membrane
10. Retinal Pigment Epithelium

These layers of the retina include a variety of cell types, each with a specialized function that aids in converting incoming photons into action potentials that the cortices of the brain process to produce three-dimensional vision. The retina's six distinct cell types are as follows:

1. Rods
2. Cones
3. Retinal Ganglion cells
4. Bipolar cells
5. Horizontal cells
6. Amacrine cells

The different types of cell in retina include the following:

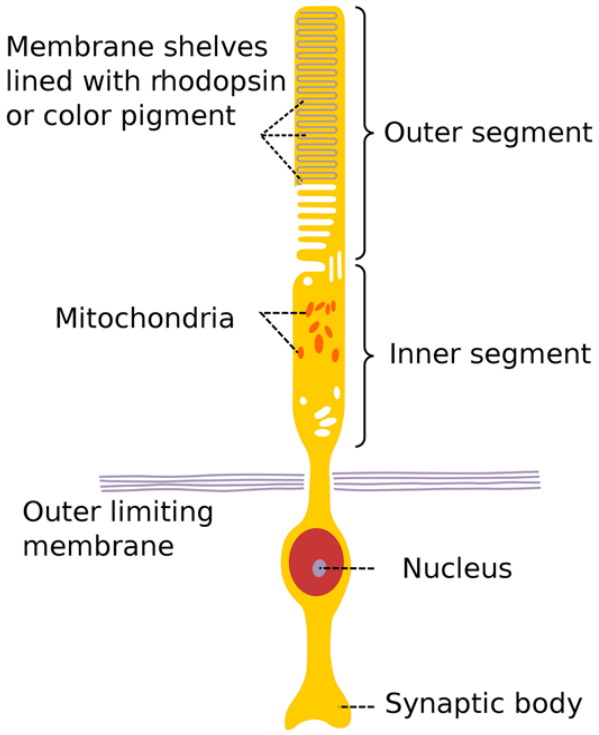

Figure: 31 Rods cells

1. RODS

Around 500 million years ago, a piscine ancestor created rods to complement the already-existing cones, which is when rod cells first appeared. This evolutionary shift is thought to have improved an organism's ability to survive in low light conditions. About 95% of the photoreceptors in the human retina are rods, which are very skilled at detecting low light levels and contributing to scotopic vision, which is characterized by black and white vision. There are no rods in the inner fovea and a concentration of rods in the outer retina that increases in density as one advances outward toward the retina's periphery. In many respects, rods are not the same as their color-sensing cone cousins. Cones have quick responses, great spatial acuity, and high contrast sensitivity; rods, on the other hand, respond slowly and have relatively poor spatial acuity and contrast sensitivity. Additionally, rods are "photo-bleached" throughout the day and need 20 minutes to recover. All of the rods may only come online and aid in scotopic vision 40 minutes after sunset or during immersion in darkness.

The rods provide extremely excellent off-axis visual quality, despite their apparent inferiority over cones in many aspects. When one stares slightly above or just below the targeted item in a dark situation, one may better appreciate this effect. It is crucial to realize that wiring, not any inherent weakness in the rod cell, is the cause of rods' low spatial acuity. This disparity in spatial acuity may be explained by the fact that more rods converge into a single retinal ganglion cell (RGC) whereas cones maintain a 1 to 1 ratio. Cones are more sensitive to certain light wavelengths (colors), whereas rods are more sensitive to individual photons of light. By concentrating many rods onto a single RGC and so minimizing background noise, the layout of rods within the retinal system enables them to make advantage of their specific sensitivity to photons and integrate the photon signal for longer. Rod cells synapse onto second-order bipolar cells in the outer plexiform layer, using glutamate as their neurotransmitter.

2. CONES

Although the human retina has between 6 and 7 million cones overall—roughly 5 percent of all retinal photoreceptors—our visual acuity depends on as little as 100,000 cones. Cones, in contrast to rods, are less sensitive to photons in general but more responsive to one of three distinct wavelengths of light (colors). Cone cells are specialized in detecting red light (64%), green light (32%), or blue light (2%), and they are mostly found in the macula, the center region of the retina that also houses the fovea. There are only 100% cones in the center fovea, which have an unhindered vision of the incoming light from the outer world, rather

than any rods or even synapses. Red and green specialized cone cells are found in the fovea in a 2 to 1 ratio, whereas blue light is detected by cones in the peripheral area around the macula.

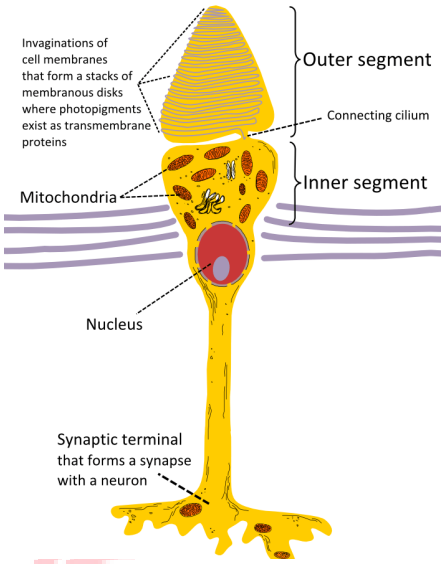

Figure: 32 Cone cells

Most of our daily interactions include color vision at different light levels, or photopic vision, which cone cells assist the brain in processing. The brain can distinguish between two points because of the large density of cones in the fovea, and while rods are more sensitive to light, cones generally allow for excellent spatial acuity. Moreover, each cone in the macula may contribute more visual information to the entire image the brain is attempting to interpret since cones have a 1 to 1 ratio of synaptic connections to retinal ganglion cells, compared to rods' 3 to 1. There are several ways in which cone cells are distinct from rod cells. For instance, unlike rods, cone cells are able to quickly adjust to light and do not get saturated with continuous light. Rods may take up to 20 minutes to regain their membrane current after photobleaching, although cones can do it in as little as 20 milliseconds. In the outer plexiform layer, cone cells discharge glutamate onto second-order bipolar cells (44).

3. RETINAL GANGLION CELLS

The retinal ganglion cells' somata are found in the GCL, yet some misplaced ganglion cells may also be seen at the inner border of the INL. These cells' dendrites propagate across the IPL's sublayers, ending in postsynapses that receive visual data from amacrine and bipolar cells. The graded potential changes in bipolar and amacrine cells translate visual information into

changes in the frequency of their action potentials, which are then translated by ganglion cells. At the inner surface of the retina, the ganglion cell axons run in the NFL and form nerve fiber bundles. These bundles come together at the optic nerve head, also known as the optic disc—the photoreceptor-free blank area of the retina—to create the optic nerve, which sends visual data from the retina to the brain. The dorsal lateral geniculate nucleus of the thalamus (image vision), the olivary pretectal nucleus of the midbrain (pupillary reflex), the superior colliculus (eye movements, saccades), and the suprachiasmatic nucleus (circadian rhythm) are among the visual centers of the brain to which different classes of ganglion cells project (45). Figure (33) illustrates the ganglion cells in retinal.

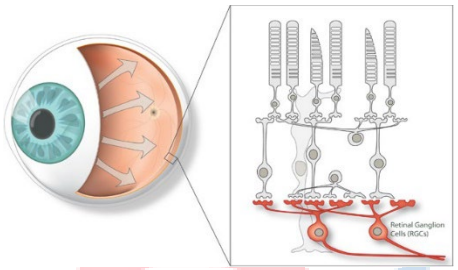

Figure: 33 Ganglion cells

4. BIPOLAR CELLS

The only neurons that link the inner and outer retinas are bipolar cells. Describe the primary routes that photoreceptors use to reach ganglion cells; they are the quickest and most direct routes that connect the retina's input and output of visual signals. They use a layer of processing that is 'additional' and not normally present in other sense organs. Differently, but not solely, in terms of chromatic preference, polarity (ON vs OFF), and kinetics (transient versus sustained responses), bipolar cells systematically alter the photoreceptor signal. Bipolar cells use a variety of processes, including various contact morphologies, receptor types, secondary messenger systems, and lateral inputs from horizontal cells, to initially create their unique response qualities at their dendrites. There is more room for signal modification in the axonal terminal system, where lateral inputs from amacrine cells and local ionic currents help shape the final output that a bipolar cell sends to its postsynaptic partners. It is theoretically possible for individual bipolar cells to provide distinct input to several postsynaptic circuits. Different kinds of bipolar cell inputs may be combined by postsynaptic circuits to inherit extremely particular signaling features (46).

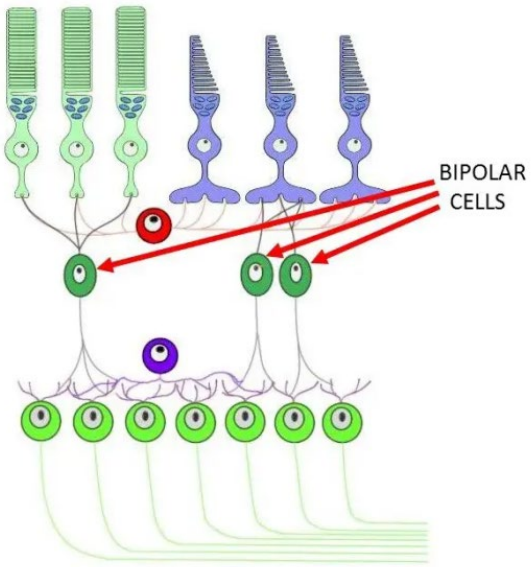

Figure: 34 Bipolar cells

5. HORIZONTAL CELLS

Important interneurons of the retina's first synaptic layer are called horizontal cells, or HCs. They start spatial and spectral opponency for receptive field structure of second- and third-order retinal neurons via lateral inhibition, feedback, and feed-forward connections to photoreceptors and bipolar cells. There are two different kinds of horizontal cells in the outer plexiform layer: those with a short axon and those without, which are referred to as "amacrine" cells (47). The structure of horizontal cell is shown in the figure (35).

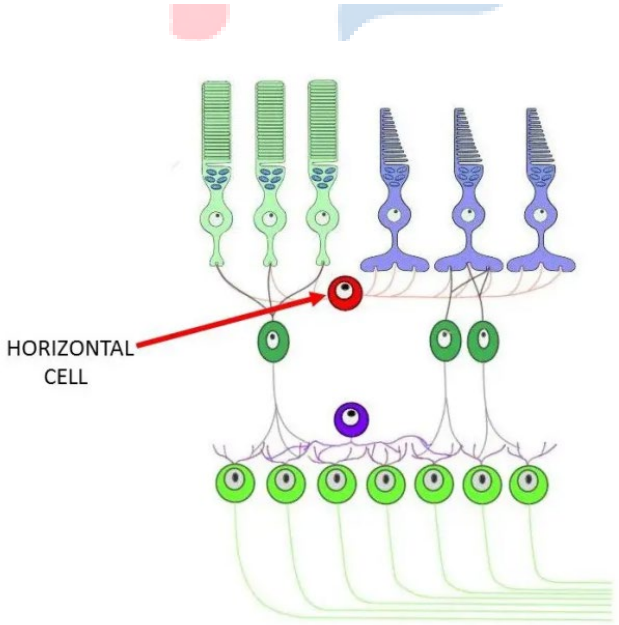

Figure: 35 Horizontal cells

6. AMACRINE CELLS

Interneurons that connect at the second synaptic level of the vertically directed pathways that comprise the photoreceptor-bipolar-ganglion cell chain are known as amacrine cells of the retinaThey function to integrate, modify, and interpose a temporal domain to the visual information supplied to the ganglion cell. They are synaptically active in the inner plexiform layer (IPL). The reason amacrine cells get their name is because they are believed to be nerve cells without axons. most likely perform the same role as real axons in that they are the cell's output fibers (see a later section on dopaminergic amacrine cells). Unlike ganglion cell axons, these amacrine axons stay within the retina and do not exit it inside the optic nerve (48).

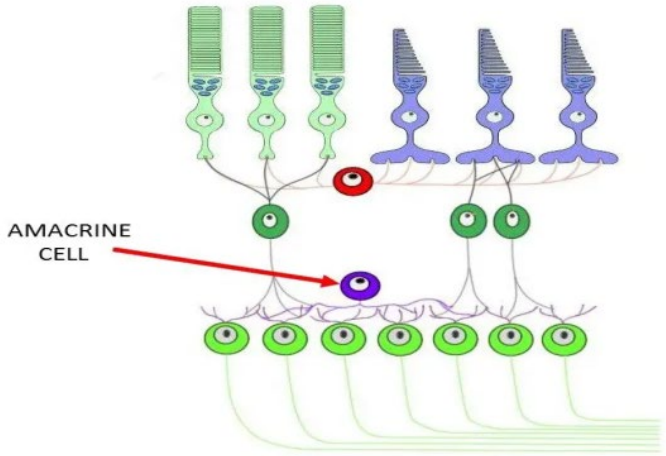

Figure: 36 Amacrine cells

RETINA BASED DISEASES

Since a healthy retina is necessary for central vision, the early diagnosis of retinal disorders is a difficult endeavor. There are many retinal illnesses that may damage the eye, such as,

- Retinal tear
- Retinal detachment
- Glaucoma
- Diabetic Retinopathy
- Macular hole

- Macular degeneration

RETINAL TEAR

The separation of the retina from the body's outer layers results in a retinal tear. If a retinal tear is not detected in early stages, it might result in retinal detachment, a condition that can cause complete blindness. A typical individual's eyesight and that of a person with a retinal tear are shown in Figure (37).

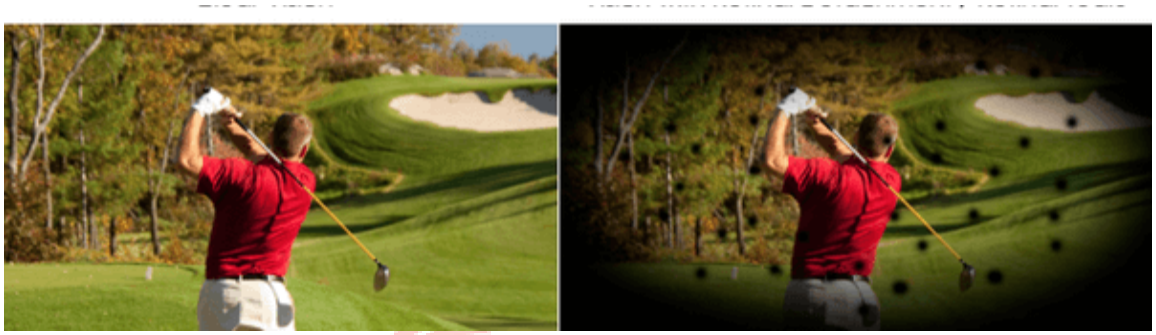

Figure: 37 Normal Vs. Retinal tear vision

The symptoms of a retinal tear are:

- A sharp rise in area and the presence of floaters can indicate retinal tearing.
- The sudden appearance of sparks could be the first sign of a retinal tear.
- Shadow hosting occurs in the shadows of the way we view things.

GLAUCOMA

A group of eye conditions called glaucoma can lead to optic nerve damage. Normally, the extra fluid, or aqueous, causes the optic nerve to be damaged and our pupil to weigh more. When a person reaches the age of 60, glaucoma can become a significant factor in visual loss. Due to the lack of symptoms and lack of discomfort until vision loss occurs. One common term for glaucoma is "silent thief of sight." The eyes of a healthy individual and a person with glaucoma are shown in Figure (38).

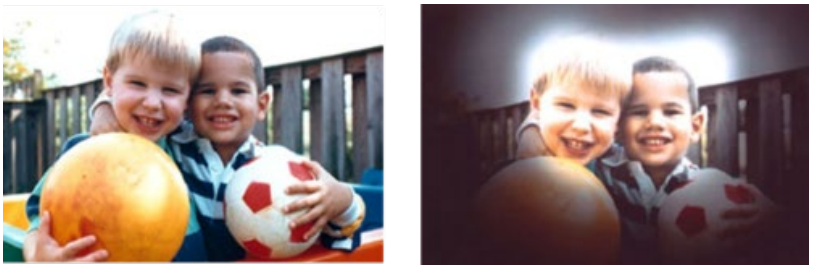

Figure: 38 Normal vision Vs. Glaucoma

DIABETIC RETINOPATHY

A disorder that may afflict patients with diabetes is called diabetic cataracts. The veins in the retina are now subject to low, darker levels of sugar. The blood arteries have the ability to dilate and spill. Additionally, it has the ability to sealed blocking blood from frequently flowing through unusually produced new blood vessels in the retina. A loss of eyesight might arise from any of these. Figure (39) depicts the eyes of a healthy person and a person with diabetic retinopathy.

Figure: 39 Normal Vs. Diabetic retinopathy vision

The common retinopathy sign include:

- Floating pupils and marks
- Twofold vision
- Eye ache

PROGRESSION OF DIABETIC RETINAL PATHOLOGY

A decrease in or complete loss of visual acuity may result from changes to the structure

and function of the micro- and macrovascular system. Each person's experience with the blood-retina barrier breakdown varies in terms of its course, effects, and appearance. An intact diabetic retina has the potential to develop any, some, or all of the lesions that are characteristic of early retinopathy. In early DR, lesions like MA, which are thought to be crucial to the development of DR, may be present, absent, or imperceptible. The language used to characterize the condition and phases of DR, however, is linear; it begins with a normal or healthy retina and concludes with a phase of severe scarring and retinal tissue loss. This is true despite these variations.

The tiny, local lesions mentioned in the DR aetiology are the first signs of diabetic retinal disease. Mild NPDR is often associated with lesions such as microanuerysms, minor intra-retinal hemorrhages, and calibre deformities known as intra-retinal microvascular abnormalities, or IRMA. Figure 1.9 shows the location of these lesions. Greater regions of cheamic retina may result from capillary dropout and blockage. Axoplasmic fluid builds up in focal regions of non-perfusion or infarcts, resulting in soft exudation. These stains are widespread and white or gray, also known as cotton wool patches.

MACULAR HOLE

The retina, or the surface of the tag at the back of our eye, may have a narrow, geographical range that is known as the macula. Spotless, blurry areas might get settled in a macula gap, spinning our focusing vision. The retina, which is composed of light-touched tissues, is located in the center of the eyes due to a macular gap that somewhat smoothest the macula. The macula provides focused, crisp vision that aids with movement reading and the identification of very minute details. Focal vision may become smeared or blurry as a consequence of a macular difference. The vitreous fluid in the eye gradually recedes and pulls away from the retina as an individual ages. On occasion, the vitreous fluid may also cause a macular gap to form in the retina. Figure (40) is an example picture that compares the eyesight of a person without a macular hole to that of a person with one.

Figure: 40 Normal vision Vs. Macular hole vision

In some instances, the fluid that fills the hole that has been cleared for the vitreous gel may flow across that distance and into the macula, causing it to move and blur.

- Extreme short-sightedness
- Epiretinal membranes that advance the macular wrinkle stage
- Retinal separation
- Diabetic retinopathy
- Eye harm alternately trauma

MACULAR DEGENERATION

Macular degeneration refers to the degeneration that utilizes the optic nerve to process and convey visual information from the eye to the brain, spiraling downward into the focal portion of the retina and the pupil inside the rear surface of the eye. The macula, an important component of the eye, is in charge of preserving the visibility of the mark in the center of the eye as well as regulating our capacity to read, operate a vehicle, distinguish between various colors, and see questions closely clustered next to several areas of interest. A normal individual's eyesight and that of a person with macular degeneration are shown in Figure (41).

Figure: 41 Normal Vs. macular degeneration

The most important risk factor for macular degeneration is becoming older. As the age of the individual grows, the probability of experiencing pain and danger increases as well (33).

Other signs and symptoms include of:

- In the center of our eyesight are dark, fuzzy regions.
- We can adjust color recognition in some rare situations.

DIFFERENT RETINAL IMAGING TECHNIQUES

In regards to the diagnosis and treatment of retinal inflammations, precise imaging of retinal cells and brain tissue is crucial. The guidelines for the ophthalmoscope were created in 1823 for retinal examination. Numerous imaging techniques were used to visualize the retina's anatomical structure without causing damage. Fundus photography (FP), among many other prediction approaches, is intended to be effective to early detection of three major causes of vision loss, such as MD, glaucoma, and DR. Secondly, the main fundus camera's 2D depiction of the retina is not capable of capturing depth, which leads to an imperfect analysis of retinal diseases such as cotton wool spot. These types of problems have been resolved with the use of computed tomography (CT). OCT, or optical coherence tomography, is a useful tool for creating 3D retinal representations. The various imaging modalities used in retinal disease analysis are shown in Figure (42) (49).

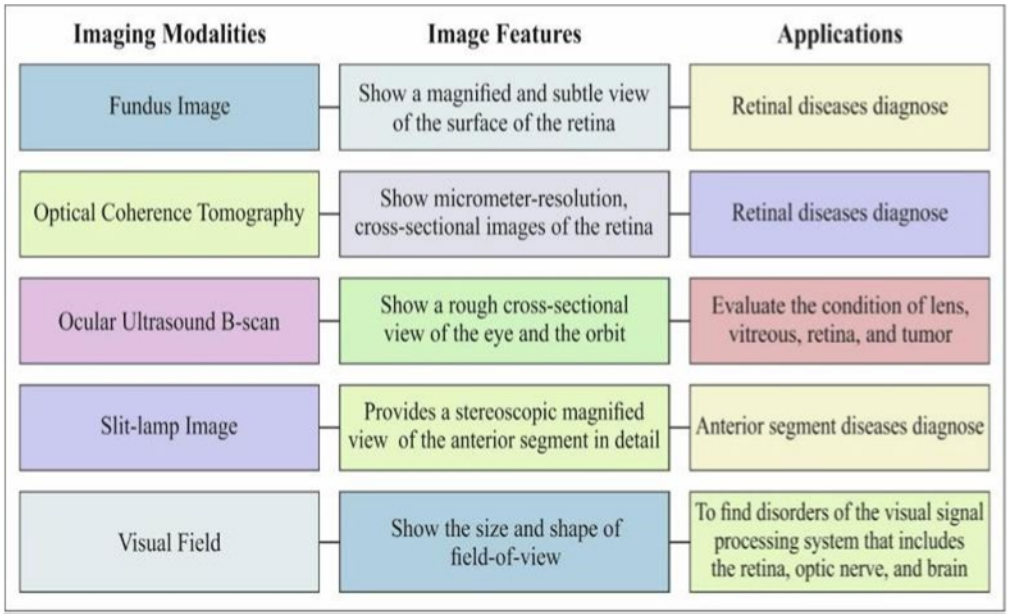

Figure: 42 Different retinal imaging techniques

FUNDUS PHOTOGRAPHY

The back of the eye has a layer of tissue called the retina that is light-sensitive. It is in charge of sending images to the brain and sensing light. The macula, which is situated in the middle of this nerve tissue, provides sharp, centered vision. Activities like reading, driving, and noticing little details need this vision. This vital tissue is affected by disorders of the retina. They may cause visual impairments, and in rare instances, they could be severe enough to cause blindness. The capacity to image the retina and the development of techniques for assessing the corresponding images are of great interest. A retinal camera designed especially for taking pictures of the vitreous, retina, choroid, and optic nerve regions of the eye is used during fundus photography. It is used to detect anomalies associated with eye diseases or to monitor the disease's course. For diseases including macular degeneration, retinal neoplasms, choroid abnormalities, and diabetic retinopathy, as well as for diagnosing glaucoma, multiple sclerosis, and other disorders affecting the central nervous system, it is deemed medically required.

Documentation of the retina, which is the neurosensory tissue in our eyes and is responsible for converting the optical pictures that we perceive into the electrical impulses that our brain can comprehend, is accomplished using fundus photography. Taking into account that the pupil acts as a portal for the light beams that illuminate and image that are produced by the

fundus camera, it is possible to take photographs of the retina directly. The patient is seated in front of the fundus camera by resting their chin on the chin rest and putting their forehead on the bar. Focusing and aligning the fundus camera is the responsibility of an ophthalmic photographer. Whenever the photographer hits the shutter release button, a flash is triggered, which results in the creation of a fundus a picture similar to the one seen in Figure (43, 44). These retinal pictures are used by ophthalmologists in order to monitor, diagnose, and treat vision-related conditions.

Figure: 43 Fundus photography ()

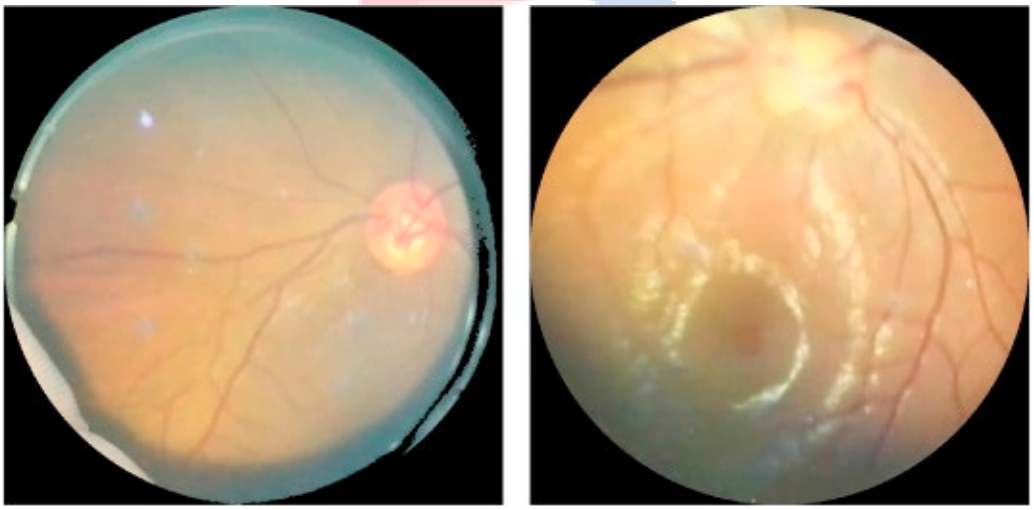

Figure: 44 Fundus image ()

In general, it is carried out with the purpose of evaluating anomalies in the fundus images, tracking the progression of a disease, planning the therapy for a condition, and determining the therapeutic efficacy of a recent surgical procedure. There are times when the photographs that are acquired are affected by a variety of issues, such as faulty placement, bad

lighting, out-of-focus, field mis-labeling, and so on. These problems lead to a deterioration in the quality of a fundus image, which complicates computer-aided diagnosis by making it harder to precisely segment the fundus and detect retinal diseases. This necessitates the collecting of photographs on several occasions, which significantly increases the workload for both patients and clinics. Consequently, it would be beneficial to have a system that automatically evaluates the quality of the photos captured throughout the process of image acquisition.

3D OPTICAL COHERENCE TOMOGRAPHY (OCT)

OCT model, which was developed by Drexler and Fujimoto (2015), is a well-known and efficient model that is widely used for non-invasive imaging modalities. Through the use of interferometry and confocal microscopy, it is possible to get three-dimensional cross-sectional maps of the retina via this technique. When it comes to 3D OCT pictures, the accuracy ranges from 10 to 15 μm. The resolution of the picture might be improved depending on the light source that was used there. On account of the fact that efficient scattering of light may be accomplished from the retinal cross-section, it is thus possible to use an illumination source with the greatest wavelength. A novel approach for predicting diabetic macular edema (DME) is thus suggested to be OCT. The use of OCT has become constantly advantageous for the production of angiograms for the purpose of measuring the vasculature of the retina.

OCULAR ULTRASOUND B-SCAN

The right (OD) and left (OS) eyes have been subjected to a B-scan ocular ultrasound scan, which was performed using a linear transducer operating at 12 MHz (SonoVet R3, Samsung Medison, South Korea). Figure (45) represents the image of ocular ultrasound B-scan. The trans palpebral technique was used in order to do the ultrasonographic examination. For the purpose of measuring the longitudinal globe length, a micro convex transducer was used. This was done since the linear transducer was unable to see the complete eye in a single picture. The animals were physically kept in stand posture with their heads held erect for the ultrasonography procedure, which took place in a partially darkened room. Neither anesthesia nor sedation were used during the examination.

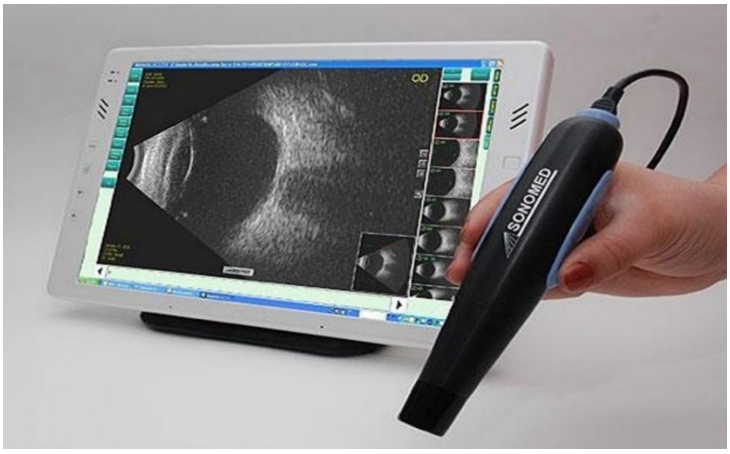

Figure: 45 Ocular ultrasound B-Scan

Immediately after the cutting of the eyelashes, above the closed upper eyelids was a sterile ultrasonic coupling gel. The gel was then gently rubbed in order to eliminate any air bubbles that had been caught between the eyelid and the transducer. After applying the least amount of pressure possible on the globe, The transducer was placed in a horizontal position., and the sweeping began in the dorsal direction before progressively moving in the ventral direction with increasing speed. Figure (46) displays the outcomes of the ocular ultrasound B-scan.

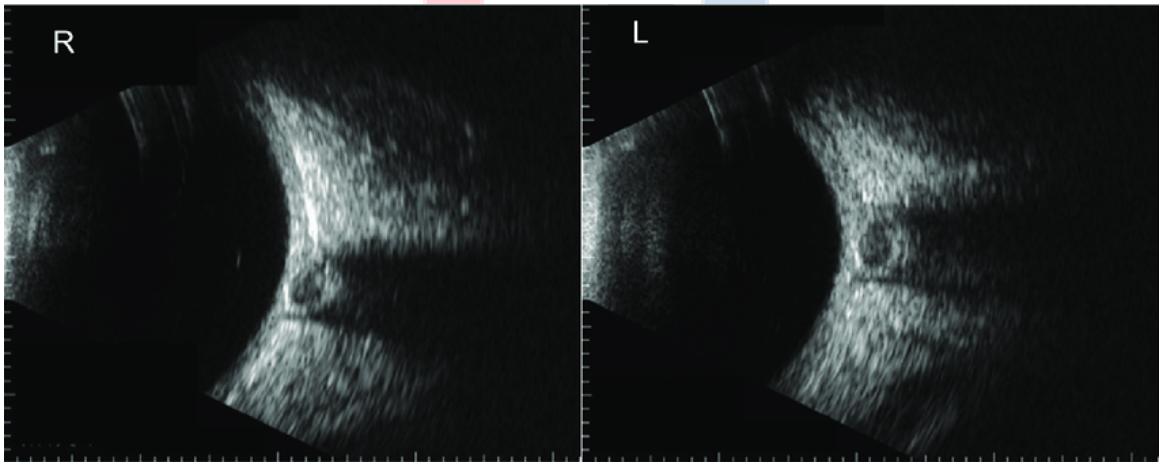

Figure: 46 Resultant image for B-scan

Next, the eye was inspected from the center of the canthus to the lateral canthus while the transducer remained erect. A horizontal scan was performed to complete each and every biometric measurement. When the posterior wall of the globe was clearly visible and the anterior and posterior lens capsules, the retina, and the cornea were all positioned

perpendicularly along the optical axis, the optimal alignment for biometric assessment was determined (50).

SLIT-LAMP PHOTOGRAPHY (SLP)

Imagery obtained using slit-lamp photography (SLP) is a technique that is readily accessible in all eye clinics and is quite inexpensive (figure(47)). The high resolution quality of SLP External views of the anterior eye components, including the cornea, is made possible via pictures. Use of various color-filtering illuminations in conjunction with topical staining of the eyes (e.g., Rose bengal, fluorescein, or lissamine green) might enhance the visibility of certain biomarkers, such as EDs. SLP isn't used with sufferers, although. Contrarily, Clinical professionals often manually insert their conclusions into electronic health records (EHRs) based on their subjective evaluations of biomarkers.

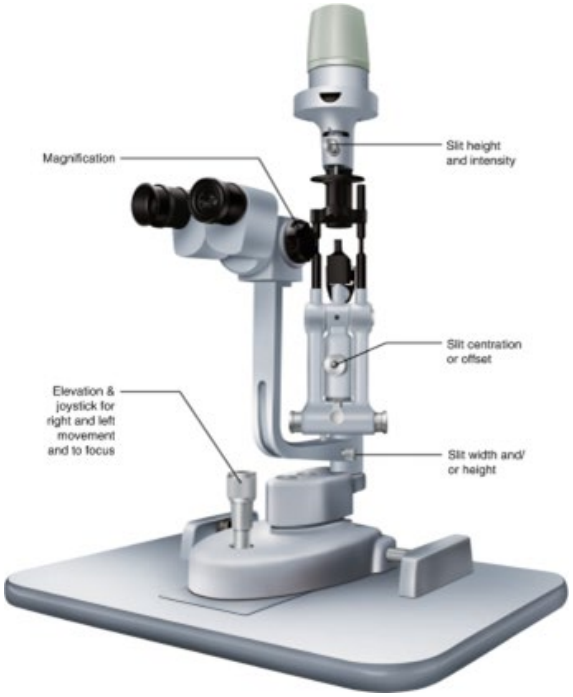

Figure: 47 Slit-Lamp Photography

The use of manual slit-lamp caliper measurements, drawings in the electronic health record, and free-text descriptions are all examples of subjective approaches. With regard to the quantification of certain MK biomarkers based on SLP pictures, there are no standardized and disseminated methodologies available (51).

HISTORY OF OPTICAL COHERENCE TOMOGRAPHY (OCT)

OCT is a nearly three-decade-old technology based on two widely used optical measurement techniques: "low-coherence interferometry "(LCI) and "white-light interferometry "(WLI). Interferometry is a commonly used technique that was first testified to by Sir Isaac Newton for estimating the quantity and echo time lag of backscattered light. LCI was first used to the detection of waveguides and optical fibre problems in communication networks. Fercher and colleagues reported the first biological use of LCI, whereby they used partly coherent light interferometry to quantify the axial length of the eye. A groundbreaking study that was published in Science in 1991 included lateral scanning to the interferometer's sample arm to illustrate a novel method. The technology was named OCT. With this OCT method, high-resolution cross-sectional imaging is made possible just by the spatial optical characteristics found within the tissue. Beam scanning may be done in two, three, or four dimensions (volume over time) by extending the scanning process to scan in either lateral or transverse directions. The degree of back-reflected display as an OCT picture, either in false color or in gray scale. Over the last three decades, OCT has advanced quickly in a variety of biological imaging applications. We present many variations of OCT, which we shall address in more detail later in this chapter. However, before moving on, let me draw your attention to a few other OCT-based biomedical imaging modalities. This is a brief summary and comparison of imaging depth and resolution (52).

OPTICAL COHERENCE TOMOGRAPHY

In the early 1990s, optical coherence tomography (OCT) was introduced. In dermatologic research as well as clinical dermatology, noninvasive imaging has become a useful technique. One such noninvasive imaging modality is OCT (53). Through the capacity to see the distinct layers of the posterior portion of the eye, images help doctors diagnose and track ocular disorders and abnormalities, as well as measure tissue integrity. While the majority of commercial OCT equipment provide automated layer analysis tools, commercial software may not be able to segment all the relevant layers or could need human processing or correction, especially when it comes to eyes with retinal diseases (54). OCT has been used more and more lately in a wide range of different disciplines, including dentistry, gastrointestinal, neurology, cardiology, and dermatology. Smaller, private ophthalmic clinics may be able to purchase more affordable, compact OCT equipment. A patient-operated, tiny device might enhance treatment monitoring and regular therapy (55).

The advantages of OCT are as follows:

- Easy (Short learning Curve)
- Rapid
- Non-Contact & Non Invasive
- Sensitive (7-10 micron resolution)
- Highly Reproducible

OCT imaging may be shown in a variety of colours that represent the various reflectivity levels, such as blue and black for less reflecting tissue, green for intermediate reflectivity, and red and yellow for highly reflective tissue. As an alternative, highly reflecting light—which is brighter than less conspicuous reflected light—can be shown on a grayscale display.

PRINCIPLE

Ocular tissue reflection of low-coherence light is intricately analysed as part of the Michelson interferometer, which is the basis for OCT imaging.

INTERFEROMETER (Michelson)

The light beam is divided into two by a semi-transparent mirror, which is then projected into mirrors spaced equally apart. The reflected light is then summed and detected by the detector (Figure (48)). The mirrors that are equally spaced reflect the light wave in the same phases. Nonetheless, the two mirrors reflecting the reflected light will have this disparity if one mirror is displaced by an amount less than the entering light's wavelength. This phase variation results in an interference pattern at the detector level.

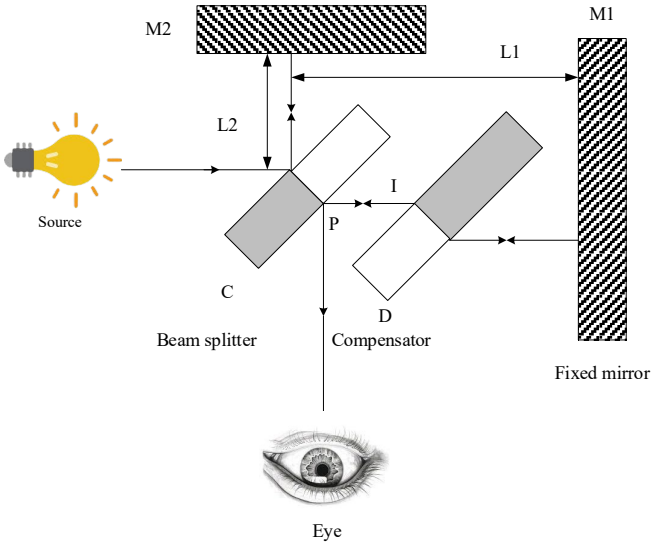

Figure: 48 Interferometer (Michelson)

In OCT instrumentation, there are two methods available: Time-Domain OCT (TD-OCT) and Fourier Domain-OCT (FD-OCT). (56)

BASIC OCT SYSTEM CONFIGURATION SETUP

No matter the particular type, An optical receiver with signal and image processing, a beam scanning device to control the sample's illumination, an interferometer with reference and sample pathways, and a light source are the fundamental parts of any OCT apparatus figure (49). In its most basic configuration, an OCT system sweeps the illuminating beam transversely over a sample while continuously measuring the sample's profile of reflectance parallel to the optical axis. Reflectance and ranging data are computed by signal processing, and the resulting cross-sectional or volumetric pictures are processed further. Ensuring that shot noise, the inevitable signal characteristic resulting from light's particle nature, will be the predominant noise term is a crucial design goal for all types of OCT devices. Achieving these criteria is essential since it will allow for the maximum speed, the deepest penetration of imaging, and the largest volume of imaging of samples. For every key OCT subsystem, there are broad considerations given in each of the sections below.

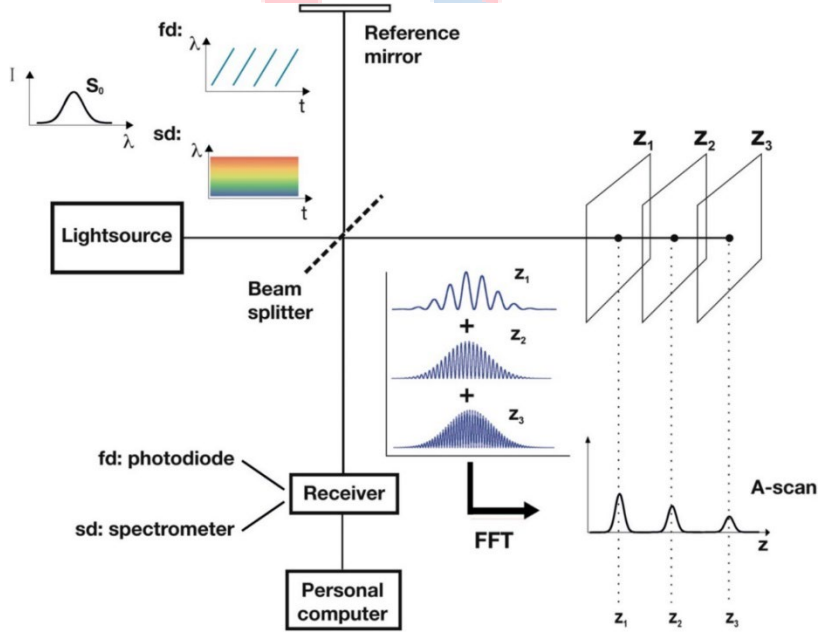

Figure: 49 Basic OCT system configuration

1. Light source: Although many various kinds of light sources have been employed for OCT, laser and superluminescent light sources are the most often used. The most significant general characteristics are wavelength, extension and spectral shape, spatial coherence and spatial coherence power, and noise. OCT light sources are often selected for a specific application

based on a wavelength that balances the effects of absorption and scattering on attenuation. Practical limitations have also had an impact, however, since it is impossible to achieve excellent performance in terms of other requirements at random wavelengths. Since the spectrum width of the source is correlated with the resolution along the optical axis within the sample, a significant amount of effort has gone into developing broadband light sources. The Fourier transform of the source's spectral distribution determines the axial point-spread-function of OCT; It is better to have a mostly Gaussian spectral distribution that behaves nicely. In addition to these temporal coherence characteristics, the light source must have a high spatial coherence to provide both outstanding signal-gathering compatibility and efficiency with realistic single-mode optical fiber. The light source must not only meet the criteria for temporal and spatial coherence, but also have low relative intensity noise and enough power—typically tens of milliwatts.

2. Interferometer: In OCT, the Mach-Zehnder and Michelson interferometer topologies are most often used. Crucially, the interferometer has to feature a reference arm with a consistent and tunable delay, low polarization mode dispersion, a dispersion which perfectly matches sample arm, and spectral bandwidth large enough to accommodate the whole spectrum of the light source. Nearly all Because optical fiber is inherently stable, OCT systems use interferometers built using beam splitters and single-mode optical fiber, circulators, polarization, and polarizer controllers. The telecommunications industry's need has led to the cheap cost and remarkable optical performance of these components.

3. Beam Scanning: Because optical fiber is inherently stable, almost all Interferometers for beam splitters, circulators, polarizers, single-mode optical fiber, and polarization controls are used in OCT systems. These components are inexpensive and have amazing optical performance because of the demand of the telecommunications sector. Despite the use of innovative techniques to regulate the distribution of light at the sample, each approach entails trade-offs between depth of field and transverse resolution, ultimately determining the size of the cross-sectional picture in optical coherence tomography. Typical systems employ Gaussian focal distributions, which induce quadratic variation in the depth of focus concerning the transverse resolution. This primer will go into depth in later parts about how various clinical imaging roles' patient interfaces and beam scanners are configured.

4. Optical receiver: The exact type of an OCT system determines how the receiver is designed, with spectral domain and frequency domain systems using radically different methodologies. A one-dimensional array of detector components and a spectrometer are

required for sd-OCT, but within fd-OCT, each polarization state's photo-diode is all that the receiver needs. To convert the optical interferometric signal into a low-noise, highly sensitive electronic signal, however, a few basic considerations must be made. Crucially, the application of interferometry essentially entails homodyning or heterodyning, where the optical interferometric signal into a low-noise, highly sensitive electronic signal. These results in a gain of order one million that is noise-free, which is proportional to the intensity of the reference electric field. Consequently, high strength preamplifiers—which are necessary for confocal or fluorescence imaging—are not needed for OCT receivers. OCT is essentially an interferometric method, therefore polarization fading—phenomena caused by a discrepancy between the polarization states returning based on the reference and sample routes —may affect receivers.

While it is possible to adjust the reference's polarization state should correspond with the typical condition of light returning from the sample, however, because many samples are birefringent and certain systems have sample paths where the polarization state varies rapidly over time, this is not always the case. A simple solution for polarization fading is to utilize polarization-diverse detection, where the receiver splits the reference arm's light is split into two orthogonal polarization eigenstates, which it measures. an example reflectance sample interferogram simultaneously in both states. The sum of squared amplitudes of these signals, which vary as cosine and sine functions independently, is then used to generate a polarization-independent signal.

5. Signal and image processing*:* The detected signal contains spatial range information in an interferogram, a feature shared by all OCT devices. Fourier transformation is one of the common signal processing procedures that may be easily used to decode the signal. Nevertheless, numerous systems do not consistently The interferogram is sampled at consistent wavenumber intervals, and the conjugate correlation between wavenumber and distance is investigated it is necessary for the Fourier connection supporting this signal processing. Therefore, an initial processing step into wavenumber space must be utilized to interpolate from the system's intrinsic sampling. To make up for any discrepancy in another common processing step is used, which is the dispersion of the reference and sample arms. This is usually achieved via a calibration that is carried out during system development and stays fixed, unless there are significant reconfigurations (57).

CATEGORIES OF OCT SYSTEMS

In two groups, the OCT systems can be narrowly distinguished as

1. Time-Domain OCT (TD-OCT)
2. Fourier Domain-OCT (FD-OCT)

The additional FD-OCT is classified into two subcategories as

a. Spectral-Domain OCT(SD-OCT)
b. Swept-Source OCT(SS-OCT)

TIME DOMAIN OCT (TD OCT)

The fundamental ideas of light interference and its function in OCT imaging are often shown using the Michelson setup with optical fibres, as seen in Figure 50. There are two different routes: the reference arm and the sampling arm the Michelson interferometer divides the light from the source into, and then merges the two sources of light at the interferometer's output. The two beams may satisfy any intermediate condition, cancel each other out, or enhance each other under certain circumstances (58).

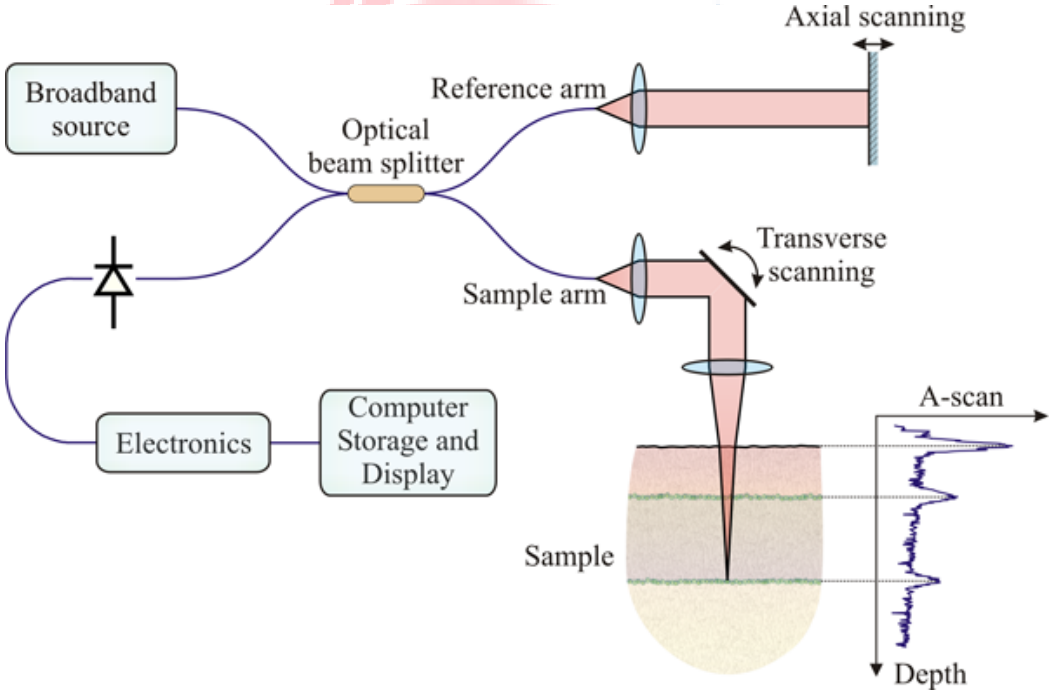

Figure: 50 Time Domain OCT system

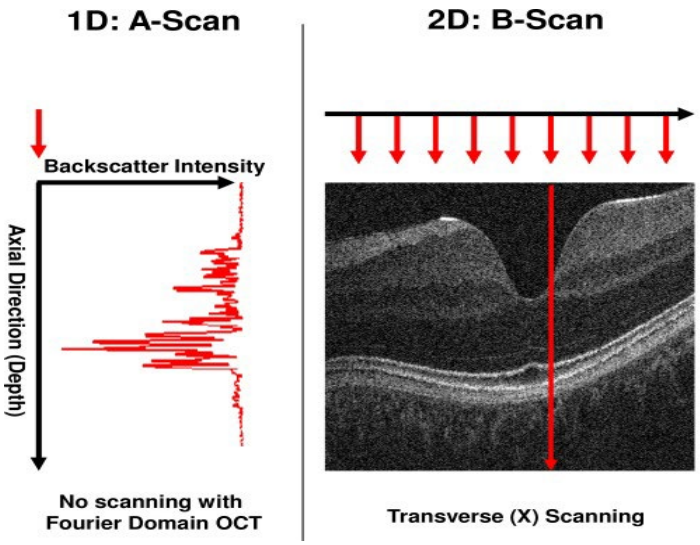

Figure: 51 OCT scanner coordinate system

Photo-detectors measure the associated interference. The mirror attached to the reference arm is scanned in a depth direction at each sample point, and the photodetector records the related light intensity. Consequently, a thorough depth profile of the sample reflectivity at the beam point, or A-scan, is generated. The sample beam is scanned laterally over the sample to create a B scan. Figure (51) displays the design of the OCT Scanning Coordinate System. An A-scan is obtained by scanning transversely (red arrows), and a B scan is created by combining several A-scans (15).

FOURIER DOMAIN OCT (FD-OCT)

The manual scan in the reference arms for the TD-OCT devices results in a low imaging speed. This is considered a drawback since it also leads to low signal sensitivity. Given that mechanical reference mirror scanning is not necessary to address this problem, FD-OCT is recommended. A beam splitter for an FD-OCT system is illuminated by a superluminescent diode (SLD), which has the benefit of a broad bandwidth range. This produces similar power splitting at the reference and sample arms. The spectrometer disperses the interference pattern produced by light returning from the sample at all depths and the corresponding reflections off the arm since the reference arm is adjusted to the length of the sample arm, capturing it on a charged coupled system (CCD).

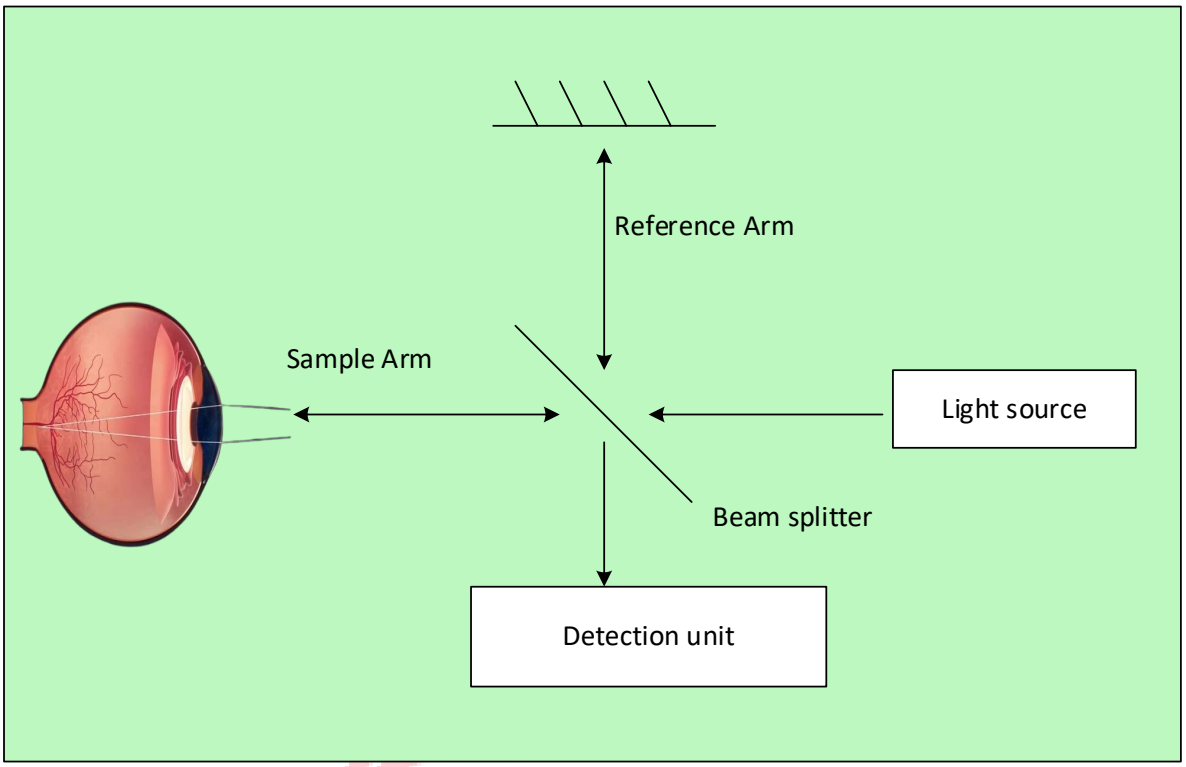

Figure: 52 Fourier Domain OCT system

A diagram illustrating the FD-OCT method is presented in Figure (52). By directing backscattered light to the CCD and measuring the spectrum of the processed interferogram, FD-OCT is capable of observing the inner layer profile at the focal point. By employing By using an inverse Fourier transform, more A-scan data may be acquired. Setting up the reference mirror, any sample motion is mitigated, thereby reducing OCT image distortion (59).

SPECTRAL DOMAIN OCT (SD OCT)

Spectral domain OCT was developed to overcome the limitations of TD OCT. Most of the components used in SD OCT and TD OCT are interchangeable. The two primary distinctions are: 1) SD OCT includes a spectrometer in the receiver; and 2) the length of the reference arm is fixed. Using the Fourier principle, this spectrometer evaluates the retina's reflected light spectrum and converts it into data on the depth of the structures. Figure (53) displays a schematic illustration of the SD OCT system. The interferometer output spectrum is converted into an optical reflectivity with depth map using the Fourier Transform. A fixed reference arm improves both the axial resolution and the speed at which A scans are recorded. One linear or circular sweep of the scanning beam over the sample yields a 2D slice, also

known as a B scan. It became possible to get many B scans for one analysis due to the rise in the pace of A scanning. As a consequence, depending on the quantity of A and B scans obtained, SD OCT enabled the imaging of structures in both 2D and 3D with varying resolution.

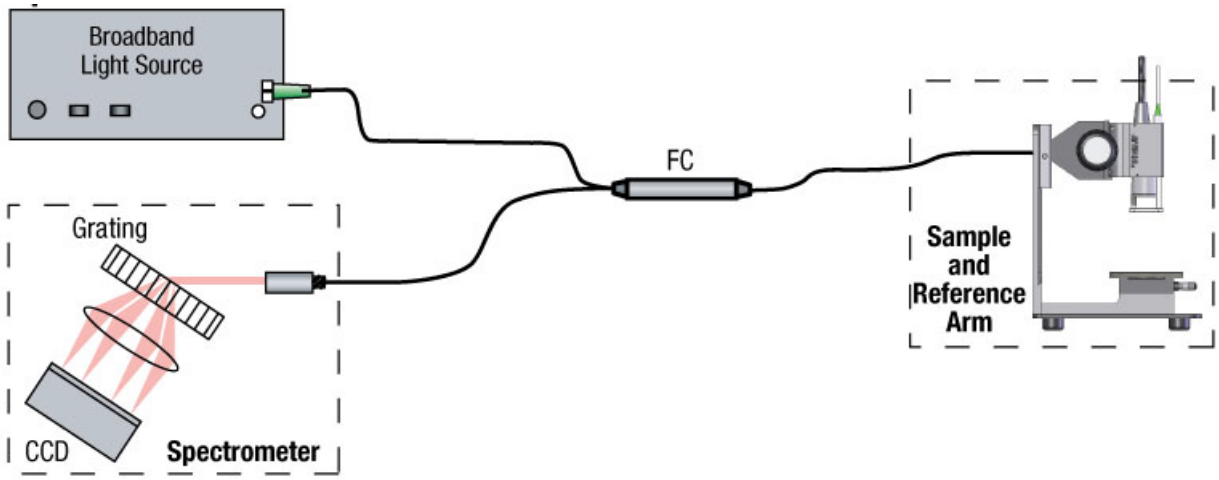

Figure: 53 Spectral Domain OCT system (60)

SWEPT SOURCE OCT (SS-OCT)

By employing a frequency-swept source, like a laser with easy customizable settings, it is possible to employ the frequency domain as a source for SS-OCT while relying solely on a single detector. SS-OCT, like FD-OCT, employs a stationary reference mirror to facilitate depth scanning while circumventing the need for mechanical scanning in the reference section.

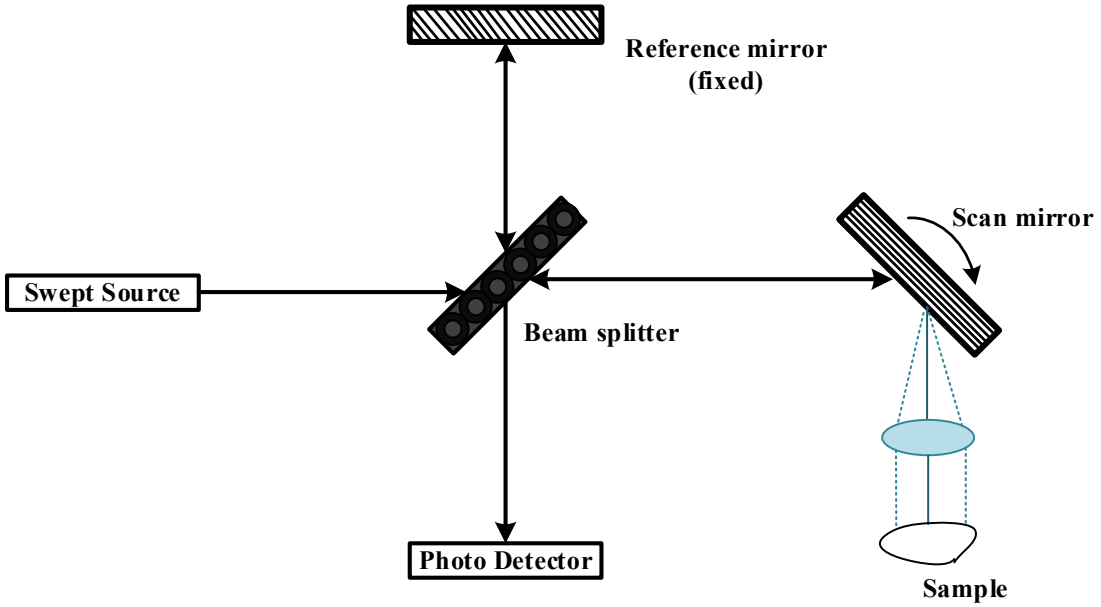

Figure: 54 Swept Source OCT system

Illustration (54) depicts a schematic of the SS-OCT method. Rather than conducting spectrum analysis over a finite wavelength, the sample is investigated with a source of narrow-band frequency variation. While SS-OCT's simplicity in detection via a single element photodetector improves its sensitivity to imaging depth, the restricted bandwidth of the tunable swept-source reduces its depth resolution. Additionally, the illumination source is costly (61).

THEORETICAL ASPECTS OF OCT SIGNAL EXTRACTION

By applying the wavelength-independent bifurcation ratio depicted in figure 1.7 to the beam splitter, the electric fields for a low coherent light source that is reflected into the sample and reference beams of the interferometer can be calculated as follows:

$$SB_E = RB_E = b(L)e^{-j(\omega t - ld)} \quad (1)$$

Here, SB_E - is sample beam for electric beam

RB_E - is reference beam for electric beam

L - Amplitude spectrum for electric field

D - Distance between the sample's several layers

Consequently, the attenuated electric field of the reference beam is as follows:

$$RB_E = r_B b(L) e^{-j(\omega t - 2ld_r)} \tag{2}$$

Where, r_B is the reference beam.

Light that strikes a particular specimen will be refracted through its multiple layers as a result of the specimen's refractive index variations and the presence of scattering particles. The expression for the back-reflected electrons that reoccur from the sample beam is:

$$SB_E = b(L) e^{-j(\omega t - 2ld_a)} \otimes r_a(D) \tag{3}$$

Where, r_a represents the amplitude reflectivity function of a specimen in a depth-dependent manner.

Subsequently, the beam splitter reintegrates the reference beam with the sample beams, producing the subsequent output:

$$E_{det} = \frac{1}{\sqrt{2}}(SB_E + RB_E) \tag{4}$$

Optical detectors, which function as square law intensity detection devices, provide the necessary assistance, incident light is transformed from an electric field to a photocurrent. The product of the average time of the incident electric field and the yields of its complex conjugate the following expression for the originated photocurrent:

$$I_{det}{}^{w_n}(D) = \frac{\zeta}{2}(SB_E + RB_E)(SB_E{}^* + RB_E{}^*) = \frac{\zeta}{2}(I_r + (SB_E{}^* SB_E{}^*) + 2Re\{(RB_E{}^* RB_E{}^*)\}) \tag{5}$$

The detector's response is denoted as ζ in amps per watt. DC components of current and interference generated within the provided specimen are represented on the component on the right-hand side of the initial two terms of the equation. In equation 5, the interference pattern generated between the reference and sample beams is represented by the final term. This pattern is subsequently employed in OCT to calculate structural information or the axial depth profile. Upon signal simplification, the expression for the AC component of photocurrent becomes as follows:

$$I_{ac}((W_n, \Delta D = \zeta B(W_n)\sqrt{r_B r_a}(\Delta D)\cos\,[2L\Delta D] \quad (6)$$

Utilizing a variety of OCT signal processing techniques, the depth-dependent reflectivity function $r_a(\Delta D)$ is recovered from any desirable specimen to obtain data regarding its axial structural profile. As shown in figure (54), light moves from the interferometer to a detector via propagation in a point-by-point scanning method. Following the resampling and DC background subtraction steps, the axial depth profile is produced by implementing the inverse Fourier transform on the structural information. A wide range of optical coherence tomography (OCT) techniques are applied to noninvasively analyze biological and industrial samples (62).

SYSTEM PARAMETERS OF OCT

A number of parameters, including axial and transverse resolution, phase stability, imaging speed and signal-to-noise ratio are metrics that assess the system's effectiveness. In this section, each parameter is examined individually.

1. Axial Resolution

OCT has an advantage over optical microscopy in both axial and transverse resolution.

The axial resolution is affected by the light source's coherence length, which has an inverse relationship with its bandwidth.

$$\triangle Y = \frac{2ln}{\pi}\frac{\delta^2}{\triangle\pi} \quad (7)$$

In the given context, δ signifies the central wavelength, while Y represents the bandwidth of the light source. An immediate deduction from equation 7 is that to attain a high axial resolution, a substantial source bandwidth is necessary. Furthermore, to attain a higher axial resolution, one must reduce the central wavelength. Conversely, the light with shorter wavelengths is considerably dispersed, which limits the depth of penetration for biological samples. The research community frequently employs 800 nm, 1060 nm, and 1300 nm wavelengths for OCT imaging to circumvent these formidable obstacles. This is because these wavelengths lie within the "optical window" in tissue, where light absorption is considerably less than scattering caused by light retardation.

2. Transverse Resolution

The focused pinpoint size is determined by the numerical aperture of the optical

focusing system, which is also accountable for the transverse resolution (λx). In mathematical notation, transverse resolution is expressed as:

$$(\lambda x) = \frac{4\delta}{\pi}.\frac{g}{D_i} \tag{8}$$

The variables D_i and g denote the focal length and diameter of the combined source beam and the focusing lens, respectively. The correlation between the size of the focused area and the depth of field was demonstrated for both high and low numerical apertures. To attain an excellent transverse resolution, an objective lens characterized by a large numerical aperture that concentrates the beam onto a minute area is necessary. However, depth of field is defined in relation to the confocal parameter $2zR$.

$$2zR = \frac{\pi\lambda x^2}{2\delta} \tag{9}$$

Depth of field and transverse resolution are inversely proportional; as one variable increases, the other decreases. Except for specific application domains, higher transverse resolution is typically favored over depth of field.

3. System Sensitivity

The sensitivity of the OCT system is determined by dividing the signal obtained from the ideal reflector by the system-introduced noise. The system sensitivity is also influenced by several parameters associated with optical power and A-scan rate. The mathematical definition of system sensitivity is as follows:

$$S_s = \frac{1}{4}.\frac{\varphi\delta}{ml}.\frac{O_s}{E_b} \tag{10}$$

The electronic detection bandwidth is denoted by E_b, the quantum efficiency of a detector is represented by φ, Planck's constant is denoted by m, and the speed of light is denoted by l. The relationship between the system sensitivity S_s and the optical power O_s incident on the sample surface is direct, while it is inversely proportional to the A-scan rate.

4. Phase Stability

Characterizing system performance requires phase stability, which turns into a crucial factor when discussing a variety of phase-sensitive processing techniques. The phase of dispersed light is highly responsive to optical frequency domain motions. Instability in the reference arm, electrical noise, a low SNR, axial or transverse perturbation, and other factors

may contribute to the motion.

The analysis of phase stability involves the computation of The phase disparity between consecutive A-scans at a particular position in depth λY, with the mirror positioned at the sample arm.

$$\triangle \varphi = 2n_s L_0 \, \lambda Y \tag{11}$$

In the given system, as denotes the index of refraction of the sample, ab represents the wavenumber in the air ($L_0 = 2\lambda/\pi_0$), and π_0 signifies the wavelength at the center of the source. Multiplication by two is performed in this case because the source beam has completed one round of travel.

5. Acquisition Rates

Speed of imaging is one of the parameters that raises concerns in relation to OCT. The initial TDOCT exhibited a scanning speed of 1 kHz, which subsequently became constrained by the reference mirror's speed. An additional advancement in the velocity of axial scanning empowers OCT to detect dynamic phenomena, including the cardiac activity of a tadpole. The development of FDOCT significantly enhanced both the pace of acquisition and the sensitivity of the system. The acquisition rate ceased to be reliant on the mechanical system and was instead managed by the discharge rate of the swept source beam or the CCD line scan camera. Under the present conditions, the axial scan rate was increased to 1-10 MHz and volumetric (4D) data was generated in real time (63).

IMAGE SEGMENTATION IN OCT:

Providing a quantitative tool to assist ophthalmologists in managing the great complexity of OCT data and developing a tool for better observation of distinct borders and individual layers is the driving force behind the clinical uses of OCT segmentation. This is the motivating point.

a. Global Segmentation: An AS-OCT picture includes the corneal edge and the area of the iris; however, some of the approaches that are now available only provide segmentation of a specific region, which is not the comprehensive segmentation that is required for ACA assessment.

b. Clinical Measurement: In the field of retinal image study, it has been discovered that

visual characteristics exhibited a satisfactory level of performance on glaucoma screening. On the other hand, medical characteristics that are specified by anatomic composition are far more important for the purpose of retinal evaluation and medical validation.

c. Multiple Modalities: The characteristics of the imaging, as well as the relative location and size of the iris and cornea, may vary from one AS-OCT modality to another. Several of the currently available methods are limited to a certain kind of AS-OCT picture, and thus are not capable of being directly adapted to other kinds of AS-OCT images (64).

SPECTRALIS OCT

Heidelberg Engineering launched the SPECTRALIS device (see in figure (55)) in 2006, which was based on the Heidelberg Retina Angiograph 2 (HRA2). It combines two complimentary methods of imaging: optical coherence tomography (OCT) and confocal scanning laser ophthalmoscopy (cSLO). It is a modular platform for ocular imaging that enables researchers and clinicians to customize their own devices by mixing and matching various imaging modalities. The device is sold as SPECTRALIS HRA, SPECTRALIS OCT, or SPECTRALIS HRA+OCT, depending on the combined modalities.

The SPECTRALIS device's cSLO section provides a range of laser sources with various illumination wavelengths and detecting techniques. These include green and blue wavelength range cSLO reflectance imaging, as well as fluorescence imaging modes for autofluorescence (blue and IR) and angiography (Fluorescein angiography FA, Indo-cyanin green angiography ICGA).

Two linear scanners that are powered simultaneously by the spectrometer's line scan camera read-out make up the OCT scanning unit. Therefore, the number of A-scans in a B-scan, or scan density, and the read-out time of the camera define the OCT frame rate. For the quickest scan pattern, the OCT2 module can handle a line rate of 85 kHz, which translates to a frame rate of around 110 Hz.

Software methods are needed to guarantee accurate and dependable placement of the OCT scan pattern because certain eye movements happens at frequencies that are faster than the OCT frame rate. Software-based motion compensation is necessary for a number of SPECTRALIS's most crucial software features, including image registration, auto-rescan capability, automated real-time (ART) noise reduction, and fovea-to-disc alignment.

Figure: 55 The SPECTRALIS HRA+OCT provides a wide range of imaging modalities, such as It integrating confocal (cSLO) imaging with OCT, and uses multicolor, fluorescein angiography, and OCTA.

Software methods are needed to guarantee accurate and dependable placement of the OCT scan pattern because certain eye movements happens at frequencies that are faster than the OCT frame rate. Software-based motion compensation is necessary for a number of SPECTRALIS's most crucial software features, including image registration, auto-rescan capability, automated real-time (ART) noise reduction, and fovea-to-disc alignment.

The SPECTRALIS enables Enhanced Depth Imaging (EDI) to improve visibility of the CSI and the choroidal vascular plexus by increasing sensitivity in depth. The environment is advantageous for lamina cribrosa imaging as well. The typical roll-off is depth-reversed for EDI. The sweet spot, or optimal imaging location, is shifted to the bottom portion of the exhibited OCT picture. In technical terms, the EDI mode is achieved by moving the reference mirror (65).

OPTICAL COHERENCE TOMOGRAPHY ANGIOGRAPHY (OCTA)

Expanding upon the foundational concepts of optical coherence tomography (OCT), optical coherence tomography angiography (OCTA) provides depth-resolved, non-invasive visualization of the chorioretinal microvasculature. Initial endeavors to achieve non-invasive visualization of the microvasculature employed a blend of optical coherence tomography (OCT) and the Doppler shift. While this approach proved effective in detecting flow within

larger vessels, its capabilities were constrained when it came to depicting smaller vessels and capillaries, particularly those oriented perpendicular to the detector. Motion artifacts were an additional drawback caused by the sluggish scanning velocities. With the significant advancement of OCT scanning rates, it became feasible to derive valuable insights from variations in signal phase and amplitude that occurred between consecutive scans. This notion served as the foundation for OCTA. The OCTA machine is figured below in figure (56) (65).

Without requiring the injection of a substance, OCTA technology can detect blood flow within the vessels of the area under investigation. The detection of differences between multiple OCT scans performed on the same area forms the foundation of OCTA technology. As the time intervals between image acquisitions are extremely brief, it is postulated that there are no structural modifications that take place. Therefore, any component of variation between consecutive measurements is classified as "motion" and encoded as blood flow by the OCTA device. OCTA is a highly suitable option for visualizing the choroidal vasculature, particularly in scenarios where serial imaging could be advantageous for disease management and follow-up. The provision of 3D data by OCTA enables the clinician to inspect the deep retinal vasculature more precisely and facilitates more precise localization of abnormal vessels (66).

Figure: 56 OCTA machine

Through the implementation of dense volume imaging, it becomes possible to obtain OCTA images that display resemblances to fluorescence angiography, the clinical gold standard. OCTA is a viable alternative to fluorescence angiography due to its elimination of the need for dye administration. Additionally, it is worth mentioning that fluorescence angiography produces only two-dimensional images of the fundus, whereas OCTA enables

the clear observation of blood circulation and anatomical features within the choroid, vitreous, and retina. By employing segmentation boundaries that have been adequately adjusted, one can also analyze the unique capillary networks of the retina, which consist of vessels with diameters of approximately 8 μm. Since the implementation of OCTA in clinical practice, the delineation of the separating boundaries has transformed (68).

Evolution of OCTA

They may be divided into three groups:

- OCTA based on phase signals
- OCTA based on intensity signals
- OCTA based on complex signals.

1. OCTA based on phase signals

In OCTA based phase signals there are 2 types which is listed below:

1. Doppler OCT
2. Phase-Variance OCT

1.1 Doppler OCT and the origins of OCTA

Doppler imaging is insufficient for the visualization of the retinal vasculature as blood flow in the face direction is predominantly perpendicular to the OCT beam. Blood velocity along the trajectory of the OCT beam can be quantitatively measured using classic Doppler OCT; however, blood flow measurements necessitate an comprehension of the Doppler angle, an acronym used to represent the angle created by the light beam and the blood vessel. Over time, It is possible to quantify the frequency shift of the interferometric fringe. The motion sensitivity is contingent upon the duration of sampling the Doppler signal at a specific location. Increased sampling durations result in enhanced sensitivity, However, this comes with diminished scanning velocity and spatial resolution.

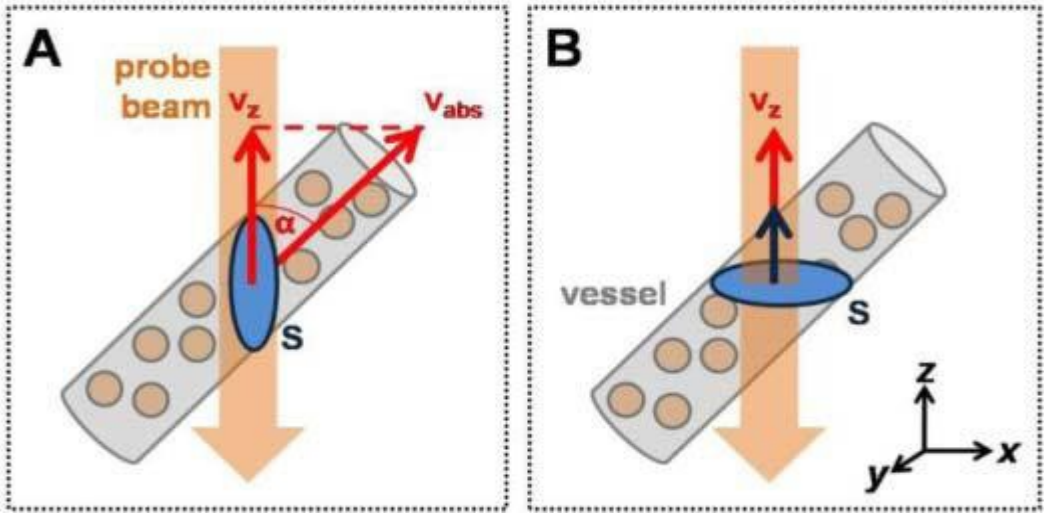

Figure: 57 Doppler OCT

Doppler frequency can be utilized to ascertain the velocity of an object due to its linear relationship with the relative motion of the reference and the sample. Laser Doppler velocimetry utilizes the principle of Doppler shift of light dispersed from moving particles to calculate flow velocities. By integrating these methodologies with OCT imaging, Doppler OCT (DOCT) is created, which provides access to velocity profiles and structural information of both flowing and scattering media. The Doppler OCT was illustrated in figure (57) Moreover; it is particularly significant for DOCT to detect flowing media that are embedded within scattering structures. In addition to tissue phantoms, small animal skin-flap models, and embryos, Doppler OCT imaging has been utilized to examine in vivo blood flow in the retina and skin. Nevertheless, the current capability of the over-the-counter system restricts imaging to blood vessels near the organ surfaces (69).

The utilization of optical Doppler tomography for the purpose of imaging blood vessels in the epidermis was illustrated. Doppler measurements with a high dynamic range were obtained utilizing time-domain OCT with an image scanning speed of 8000 A-scans per second. The advancement of spectral domain OCT (SD-OCT) facilitated direct access to the phase of A-scans and increased imaging rates. Blood flow visualization with swept source OCT (SS-OCT) was demonstrated by researchers through the quantification of Doppler signal variance and intensity variation in the absence of phase. in order to Observe blood flow through phantoms and the chorioallantoic membrane of a chick. Using SD-OCT, pulsatile blood flow in the retina was quantified (70).

1.2 Phase-Variance OCT

The phase variance optical coherence technique involves the acquisition of multiple B-scans at every location along the sluggish axis. When acquired at a single location, these time-separated repeat B-scans are denoted as BM scans or modulated B-scans. The fundamental tenet of this approach is that consecutive B-scans acquired at the identical location fail to identify any phase transition in areas characterized by either stationary or minimally moving objects. In contrast, adjacent B-scans undergo a phase transition in areas where scatterers are in motion. The phase of the backscattering light undergoes temporal variation in successive B-scans due to the motion of the scatterer. For motion detection, the phase difference calculated between consecutive B-scans within a BM-scan is crucial. The equation for the phase change component is as follows: Δ_τ represents the phase change, j designate the j^{th} frame of the B-scan in a BM scan Y signifies the depth position, t_p signifies the time point, and φ signifies the time interval between consecutive B-scans.

$$\Delta_\tau(Y, t_p) = \tau_{j+1}(Y, t_p + \varphi) - \tau_j(Y, t_p) \tag{12}$$

The computed total phase change encompasses various components, including phase noise resulting from sample bulk motion, SNR-based phase change, and contributions from moving scatterers that result in phase errors. The term "phase change term"$\Delta_\tau(Y, t_p)$ refers to the phase change induced by moving scatterers. This particular term functions as the primary data source for motion contrast. By conducting iterative B-scans at every slow-axis position, contrast is produced for motion-affected regions across the entire volume. It is possible to compute the phase variance between consecutive frames, as illustrated in the subsequent equation.

$$PV_{OCA} = \frac{1}{m-1}\sum_{j=1}^{m-1}\left\{\left(\tau_M^{j+1} - \tau_M^{j} - \tau_M^{Bulk\ Motion}\right) - \frac{1}{m-1}\sum_{j=1}^{m-1}\left\{\left(\tau_M^{j+1} - \tau_M^{j} - \tau_M^{Bulk\ Motion}\right)\right\}\right\}^2 \tag{13}$$

The quantity of frames contained within each BM scan is represented as 'm' in the equation above, while 'M' represents the total number of BM scans. The notation τ_M^j denotes the j^{th} frame of the nth BM scan, while the notation τ_M^{j+1} signifies the $j+1$st frame of the nth BM scan (71).

2. OCTA based on intensity signals

Intensity signal based OCTA is broadly divided in 2 categories namely,

1. Speckle-Variance OCT
2. Correlation-Mapping OCT
3. Split-Spectrum Amplitude-Decorrelation Angiography (SSADA) Algorithm

2.1 Speckle-Variance OCT

Doppler OCT was the initial implementation of an OCT method functional expansion. Nevertheless, the blood flow measurement was angularly dependent, and blood flow that ran perpendicular to the scanning beam rendered the method insensitive. To mitigate this apprehension, Barton and Stromski developed an alternative flow extraction methodology. The researchers implemented a TD-OCT system that was outfitted with Doppler capability in order to measure the speckle change in the OCT signal. It has been shown that speckles in OCT signals function as both a noise source and a carrier of information concerning the microstructure and flow of tissues.

Barton and Stromski formulated the hypothesis that the flow measurement methodologies originally developed for laser speckle could be adapted to incorporate flow assessments into (OCT). Barton and Stromski formulated the hypothesis that the flow measurement methodologies originally developed for laser speckle could be adapted to incorporate flow assessments into OCT. By utilizing only, the amplitude information from the OCT signal, the authors successfully produced a flow image of hamster skin and an in vitro tube phantom by quantifying the speckle variance in the adjacent 4-pixel region. The initial application of speckle analysis to OCT images was to determine depth-resolved flow. The inter-frame speckle variance signal can be acquired through the execution of numerous imaging passes at a single transverse location, as described in the following equation:

$$FLOW_{SV}(a,b) = \frac{1}{K}\sum_{j=1}^{K}(J_i(a,b) - K_{mean})^2 \quad (14)$$

In the given context, N denotes the number of B-scans that are repeated at a specific location, $J_i(a,b)$ signifies the intensity value in the j^{th} B-scan at depth position a and lateral

location b. Additionally, $K_{mean} = \frac{1}{K}\sum_{j=1}^{K} J_i(a,b)$ In order to improve the contrast of the image and the signal-to-noise ratio when observing microcirculation in tissues undergoing high and low bulk motion, the separation interval of the suggested technique was adjusted (either through adjustments to the number of repetitions or the field of view). By virtue of its hardware-accelerated speckle variance OCT and 100 kHz A-line rate, it was possible to visualize blood flow in the human retina using a custom-designed SS-OCT system.

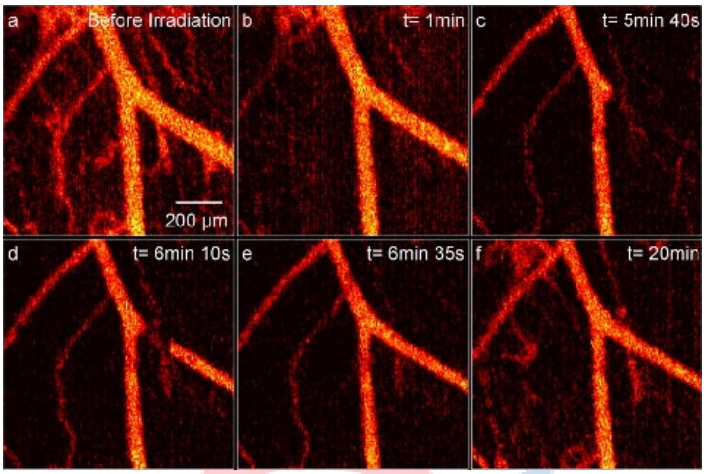

Figure: 58 Speckle-Variance OCT image

The system outlined in the report implemented graphics processing units to facilitate the visualization of blood flow within the human retinal capillary network in real time. As opposed to fluorescein angiography (FA), The speckle variance OCT method exhibited what appeared to be an increased capillary density. In addition, speckle variance OCT identified the terminal capillaries that encircle the foveal avascular zone (FAZ) with greater accuracy. Varying speckles OCT was subsequently evaluated by comparing the retinal capillary network encircling the FAZ using confocal scanning laser microscopy and fluoroscopic analysis in healthy human eyes and donor eyes. In the periphery, radial peripapillary capillaries encircle the disc. The results demonstrated that speckle variance OCT could reliably and reproducibly measure and evaluate the morphometric dimensions of the human foveal zone, in addition to stratifying the foveal circulation into inner and deep capillary plexuses. These results provided additional evidence that speckle variance OCT can be utilized to image the human retina. The figure (58) represents the Speckle-Variance OCT output image (72).

2.2 Correlation-Mapping OCT

An additional OCTA method utilizing intensity signals was unveiled by Jonathan and

Enfield in 2011. Utilizing the time-varying speckle effect and subsequent observation of the phenomenon in which vascular regions and their immediate surroundings display more pronounced speckle signals than non-flow regions (also known as static tissue), Jonathan proposed a more direct method for flow signal detection. As a result of determining the correlation between adjacent scans' OCT signals, they dubbed their technique correlation mapping. By applying a predetermined threshold to the correlation coefficient values of static tissues and flow regions, it becomes feasible to differentiate micro-vasculatures from the latter. This is because flow regions exhibited lower correlation magnitudes than static tissues. A pair of B-scans was obtained at an identical transverse position. A flow signal was further acquired by cross-correlating a grid from frame C(I_C) with the corresponding grid from frame D (I_D).using the subsequent equation.

$$CM_{OCTA}(a,b) = \sum_{s=0}^{N}\sum_{r=0}^{M} \frac{[I_C(a+s,b+r)-\overline{I_C(a,b)}][I_D(a+s,b+r)-\overline{I_D(a,b)}]}{\sqrt{[I_C(a+s,b+r)-\overline{I_C(a,b)}]^2+[I_D(a+s,b+r)-\overline{I_D(a,b)}]^2}} \quad (15)$$

Where $\bar{I}$ represents the mean intensity value within the grid and M and N denote the grid size. $I_j\{a,b\}$, which is the same notation as previously demonstrated, denotes the intensity value in the j^{th} B-scans at the depth position z and the lateral location x. As a result of the grid displacement across the complete B-scan, a two-dimensional (2D) map is generated. The correlation values were recorded within the range of -1 to 1. A value of 0 indicated weak correlation, while values of -1 and 1 represented strong inverse correlation and strong correlation, respectively. The grid size utilized in the research was selected arbitrarily to achieve the highest possible image quality. Increased grid sizes yield superior signal-to-noise ratios; nevertheless, they may introduce additional processing time, distorting characteristics, and the disappearance of tiny vessels. Correlation mapping successfully demonstrated the capillary pattern in a prototype of a multi-layered capillary tube and the capillary network of volar forearms from rodents and humans during their inaugural exhibition. The figure (59) represents the Correlation-Mapping OCT process.

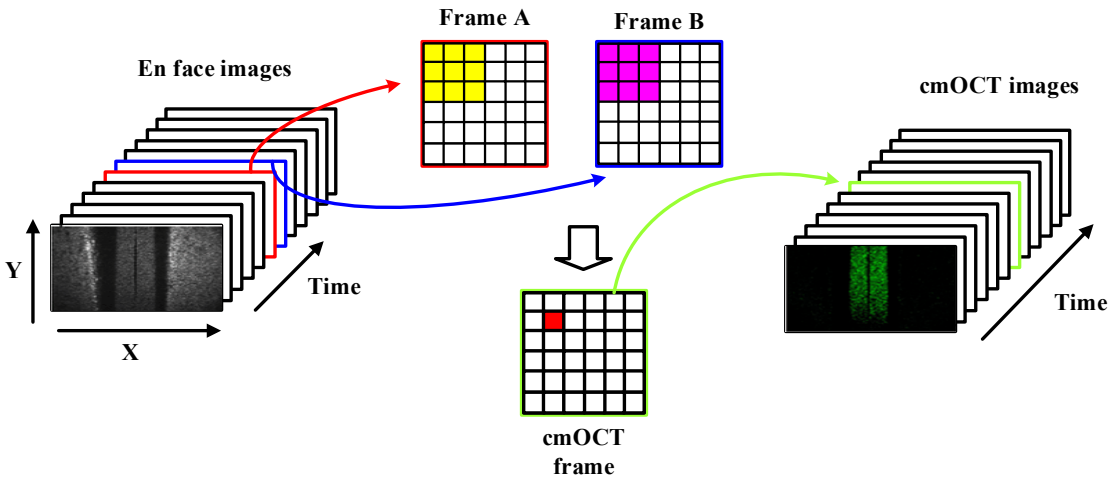

Figure: 59 Correlation-Mapping OCT

By applying a correlation mapping technique to pairings of en-face images, full-field OCT can be used to generate En-face non-scanning flow imaging. Full-field OCT relies on megapixel cameras to acquire en-face images of 2D, as opposed to the majority of OCT approaches. OCT with a full field of view is able to generate 2D or 3D images with a resolution of 1µm. which is equivalent to or greater than the cellular resolution observed in epidermis tissue, due to the exclusion of significant depth-of-field information. To enable in vivo functional imaging of blood vessels, the study introduced full-field OCT correlation mapping as its initial application (73).

2.3 Split-Spectrum Amplitude-Decorrelation Angiography (SSADA) Algorithm

Utilizing the same time-varying speckle effect concept, a split-spectrum amplitude-decorrelation angiography (SSADA) algorithm was introduced in 2012 to improve the correlation mapping method. This algorithm aimed to extract the flow signal and differentiate between inert tissues and vessels. The amplitude decorrelation algorithm, as opposed to correlation mapping, produces the flow signal through the computation of Decorrelation between two B-scans that occur consecutively. To address the interference caused by aggregate motion of tissues, an additional technique was implemented: By utilizing a split-spectrum technique, the degree of sensitivity to axial pulsatile bulk motion was reduced. To further enhance the signal-to-noise ratio, split-spectrum and amplitude decorrelation were combined. Using SSADA, the entire OCT spectrum was partitioned into several narrower bands, and the inter-B-scan decorrelation was computed for each subband.

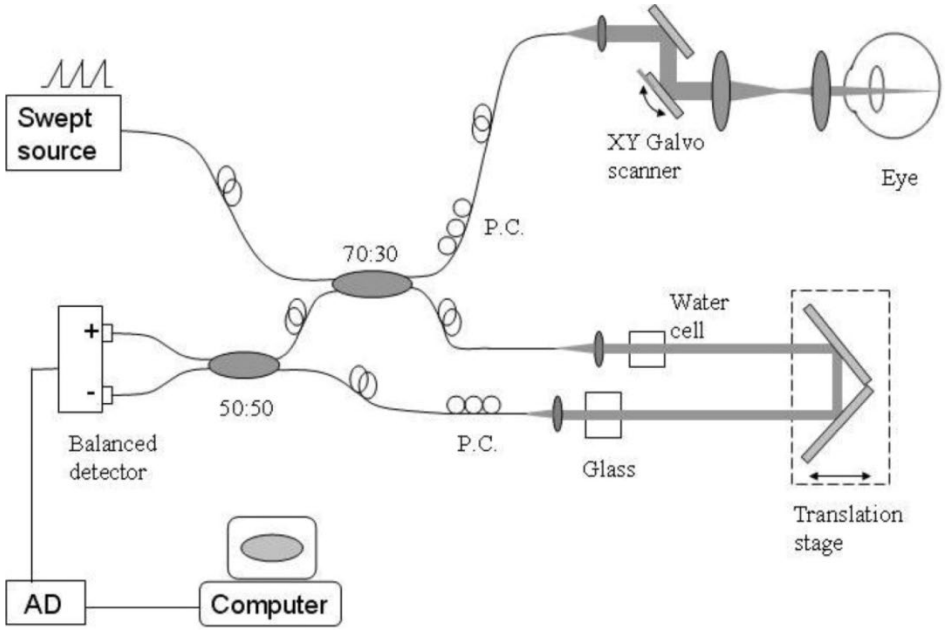

Figure: 60 SSADA Algorithm

One potential approach to improving the ratio of decorrelation signals to noise while minimizing the time required for scan acquisition is to increase the number of divided spectrums. The optimal split-spectrum number was subsequently determined to be nine. Spectrum splitting is employed to differentiate blood flow the SSADA method generally yields axial resolutions that are three times less precise than those of conventional OCT images. The figure (60) is illustrated for the Split-Spectrum Amplitude-Decorrelation Angiography (SSADA) Algorithm. To provide an example, consider an OCT system utilized for angiographic imaging with an axial spatial resolution of 5µm microns. In this case, the SSADA algorithm yields an axial resolution of approximately 15µm for flow imaging. SSADA has been shown to distinguish diseased eyes from healthy controls in the detection of retinal diseases such as AMD and glaucoma by identifying capillary networks and The macular and optic disc regions of the human retina contain blood vessels (74).

3. OCTA BASED ON COMPLEX SIGNALS

In general, complex signals -based OCTA can be divided into two groups:

1. Optical Microangiography (OMAG)
2. Multiple Signal Classification OMAG
3. Imaginary Part-based Correlation Mapping OCT

3.1 Optical Microangiography (OMAG)

The third classification determines the flow signal by using the OCT intensity information, and the signal's phase or coherence information. Optical microangiography

figure (61) is a representation of the complex-signal-based OCTA technology. Despite the fact that calculating the flow signal utilizing phase change induced by particulate motion is susceptible to bulk motion and the Doppler angle, relying solely on intensity information to measure the flow signal may reduce the flow detection sensitivity if the induced change occurs exclusively in phase signal. To enhance its sensitivity, The intensity and phase components of the OCT signal were integrated into the calculation of the flow signal. Phase variation induced by pulsatile bulk motion may be mitigated through the application of phase compensation techniques. Subtracting consecutive complex signals yields the flow indication ascertained by the OMAG algorithm subsequent to phase compensation, as illustrated in the subsequent equation:

$$OMAG_{OCTA}(a,b) = \frac{1}{M-1}\sum_{j=0}^{M-1} |D_{j+1}(a,b) - D_j(a,b)| \qquad (16)$$

In the given context, M denotes the number of B-scans that are repeated at a specific location, while $D_j(a,b)$ represents the complex signal, which consists of phase and intensity values, in the j^{th}B-scan at depth position a and lateral location$b$. The final flow intensity is determined through coherent averaging, which involves by averaging the differences in the absolute values of complex signals between each pair of B-scans, as specified in the equation.

By employing the Hilbert transformation, OMAG can discern the orientations of the mobile blood cells in relation to the direction of the incident OCT beam. Consequently, OMAG is capable of generating flow images with or without directional information. By taking into account the compromise between B-scan repetition count and the scanning duration (with more repetitions resulting in a greater ratio of signal to noise), they successfully generated a high-quality flow image using four repetition of the B-scan at the identical location during the initial demonstration. Subsequently, the capillary network was also discernible with adequate image quality in two B-scans conducted at identical location, it was disclosed.

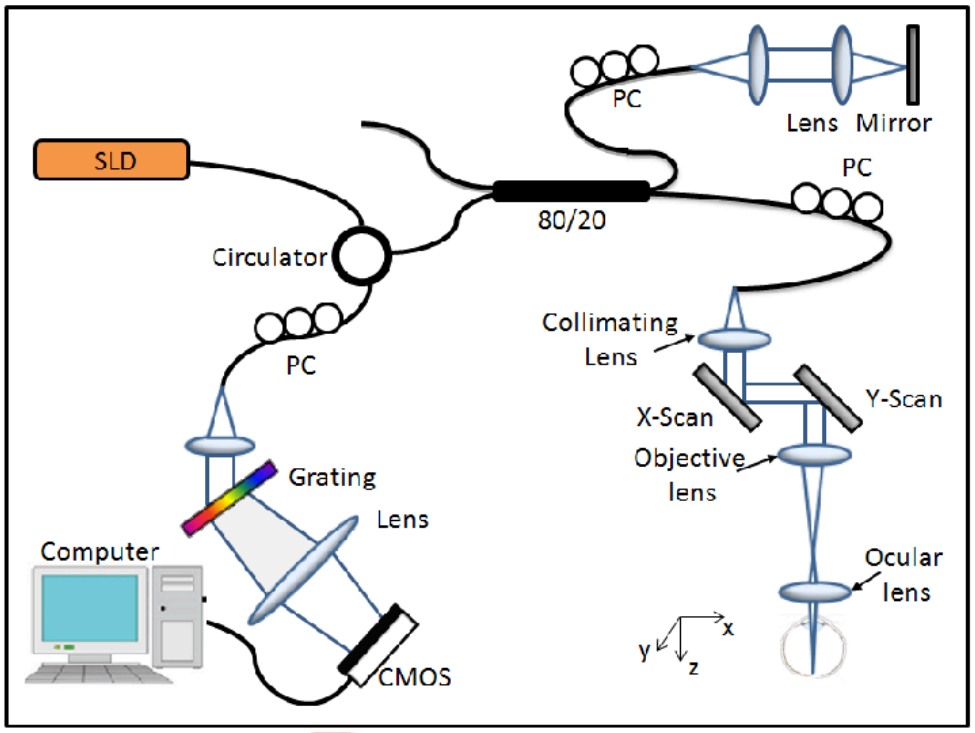

Figure :61 Optical Microangiography

Optical microangiography is being utilized to visualize the patterns of microcirculation. within the retina, cutaneous tissue beds, and rodents. Subsequent research demonstrated that the instrument's exceptional sensitivity in detecting retinal capillaries, choriocapillaris, and radial retinal capillaries enabled it to distinguish between healthy and pathological eyes. Thus, it may contribute valuable information to the progression of the disease (75).

3.2 Multiple Signal Classification OMAG

Detecting the flow signal requires an additional classification signals using the OMAG method, which is an approach to super-resolution spectral estimation based on the orthogonality principle. The OCT signal at each voxel was represented by the proposed method in the form of a superposition of three separate components: Hemordynamic signal (primarily originating from moving red blood cells), tissue signal (comprising stationary and slowly moving tissue structures), and noise (comprising system noise and discharge noise).

Eigen decomposition permits the OMAG method for classifying multiple signals to differentiate flow of signal induced by Red blood cells (RBCs) are separated from noise and inactive tissue through the decomposition of the backscattered OCT signal into orthogonal basis functions. By establishing a correlation between the product of blood concentration and flow velocity, the flow signal obtained using this technique enabled the Functional

microvascular network visualization in cutaneous tissue in vivo.

Adaptive nature of this technique is its defining characteristic: in opposition to arterial flow signal with the inert tissue signal, it denies the latter. This is accomplished by suppressing the static tissue signal under the ensemble signal composition's Eigen components. In contrast to The typical OMAG, which classifies multiple signals The OMAG method produces OCT angiograms of the volume of scanned tissue without the need for phase adjustments due to bulk tissue movement. It was demonstrated that the flow signal acquired via this methodology facilitated the observation of operational microvascular networks within living epidermis tissue. Furthermore, A correlation was observed between this signal and the product of flow velocity and blood concentration. The adaptive nature of this technique is its defining characteristic: in opposition to the blood flow signal with the inert tissue signal, it denies the latter. This is accomplished by suppressing the static tissue signal per the ensemble signal composition's Eigen components. Hence, in contrast to traditional OMAG, the multiple signal categorization OMAG approach generates OCT angiograms of imaged tissue volume without the need for phase compensation caused by bulk tissue motion.

It was demonstrated that the flow signal acquired via this methodology facilitated the observation of operational microvascular networks within living epidermis tissue. Furthermore, this signal exhibited a correlation with the product of blood concentration and flow velocity. The adaptive nature of this technique is its defining characteristic: to contrast the blood flow signal with the inert tissue signal, it denies the latter. This is accomplished by suppressing the static tissue signal per the ensemble signal composition's Eigen components. Hence, in contrast to traditional OMAG, the multiple signal categorization OMAG approach generates OCT angiograms of imaged tissue volume without the need for phase compensation caused by bulk tissue motion.

3.3 Imaginary Part-based Correlation Mapping OCT

As a remedy for the indistinct an adverse consequence arises as the dimension of the correlation window is augmented. in order to attain a higher signal-to-noise ratio in OCT image correlation mapping, OCT imaging of imaginary part-based correlation was proposed. By employing this methodology, it becomes possible to generate microcirculation maps that exhibit enhanced quality in terms of flow images while simultaneously reducing the sensitivity of vessel detection.

The researchers achieved a sophisticated scientific symbol in the spatial domain by

implementing a Fourier transform in the domain of wavenumbers. The extracted imaginary portion of an OCT signal, which corresponds to the complex OCT signal between consecutive B-scans was subsequently correlated to acquire flow information to attenuate the inaccurate flow signal caused by tissue motion, a sub-pixel cross-correlation registration based on the intensity of the OCT signal was implemented and Before calculating the correlation, Kasai estimator was utilized to register the difference between two B-scans, similar to how phase correction of bulk tissue motion is performed.

To generate a two-dimensional correlation map, The complete picture had The grid shifted, mimicking the methodology used in all of the intensity-based correlation mapping for OCT. The correlation values are quantified on a scale of -1 to 1. A 0 value denotes a poor correlation, in contrast, a strong inverse correlation is represented by a value of -1 and a strong correlation by a value of 1. Similar to OMAG, complex signals provide phase and intensity features that allow phase shifts caused by red blood cell (RBC) curve alterations to be detected, without affecting their intensity.

Consequently, OCT-based correlation mapping based on imaginary parts exhibits enhanced sensitivity towards motion, thereby potentially facilitating the extraction of blood flow data from tiny vessels with greater sensitivity. The technique was assessed on an in vivo mouse ear as well as an in vitro phantom. In contrast to the conventional correlation mapping OCT technique, their findings revealed minute blood vessels, which the intensity-based correlation mapping OCT approach did not include. This work is the first attempt to apply phase information to conventional intensity-based correlations mapping in order to improve the signal-to-noise ratio and sensitivity to small vessels without increasing the size of the grid (76).

Imaging Artifacts in OCTA

On the other hand, much as with any other imaging technique, OCTA may potentially have artifacts. Erroneous diagnoses and needless treatments are also possible outcomes of artifacts. Among the many types of artifacts, there are three primary categories:

1. OCTA technology artifacts regardless of device type
2. Artifacts caused by data collecting and image processing methods
3. Motion based Artifacts (77)

- OCTA technology artifacts regardless of device type

There are 3 types of artifacts in the device type independent they are listed

below;

1. projection artifacts
2. shadowing artifacts
3. window artifacts

1. Projection artifacts

OCT-A compares subsequent OCT B scans that were taken at precisely the same cross-section in order to identify contrast that is caused by blood that is continuously flowing. The existence of shadowgraphic flow projection artifacts, on the other hand, makes it difficult to analyze vascular networks at deeper levels.

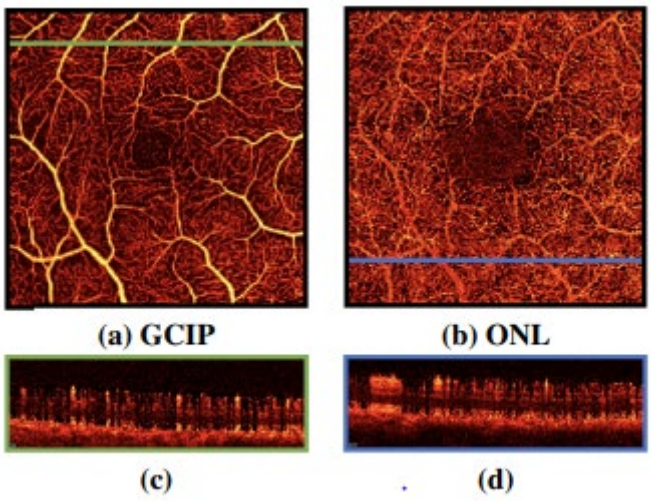

Figure: 62 The en face angiograms that were obtained by maximum projection for the (a) GCIP (GCL and IPL) and the (b) ONL are shown below. The cross-sectional angiograms that are shown in (c) and (d) are in accordance with the green line in (a) and the blue line in (b), respectively.

A fake blood flow that should be avascular is what the projection artifact gives the impression of being. By observing two characteristics, we are able to visually detect the projection artifact that is caused by large vessels in OCT-A: in en-face angiograms, the arteries from the superficial retina duplicate the vascular pattern found in the deep retinal layers. (see figure 62(a) and (b)); in cross-sectional angiograms, it appears as elongated flow signals just beneath (a) GCIP (b) ONL (c) (d) The first figure. The en-face angiograms that were obtained by maximum projection for the (a) GCIP (GCL and IPL) and the (b) ONL are shown below. The cross-sectional angiograms that are shown in (c) and (d) are under the green line in (a) and the blue line in (b), respectively (78).

2. Shadowing artifacts

In contrast to the false flow signal introduced by projection artifacts, the true flow signal is eliminated by shadow artifacts figure (63). Caused by OCT signal attenuation are shadowing artifacts. Retinal pathology, such as retinal detachments, hyperreflective foci, or drusen, may be the cause of this signal attenuation. Shadowing is possible under massive vessels., however, even in healthy eyes. External characteristics, such as vitreous floaters, cataracts, or hemorrhage, may also contribute to shadowing. Vignetting, which may result from misalignment of the OCTA apparatus or imaging in nearby areas susceptible to pupil aperture correction, constitutes an additional significant cause of shadowing.

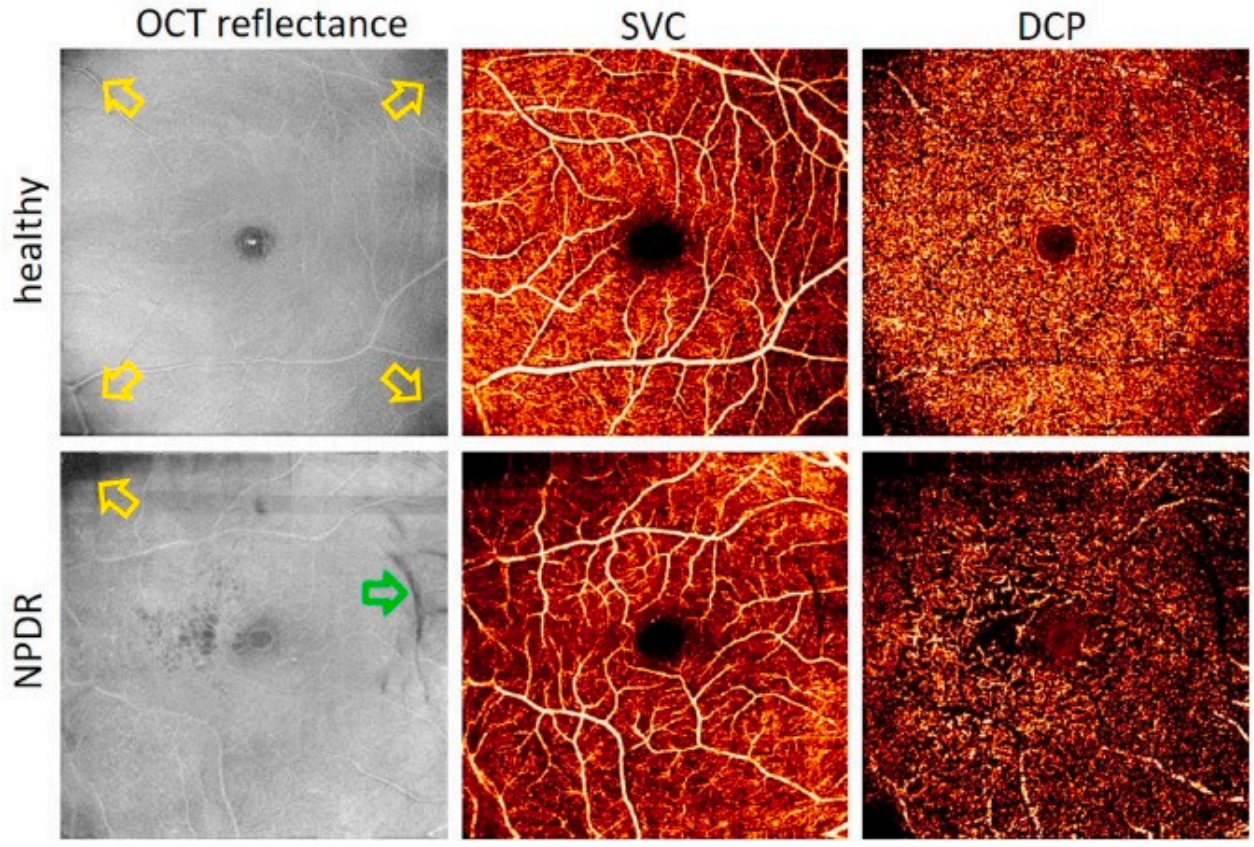

Figure: 63 Shadowing artifacts. Vignetting (yellow arrows) in the deep capillary plexus (DCP), superficial vascular complex (SVC), and OCT reflectance channel (left column) causes shadows in the en- face image of a healthy volunteer (top row). Shadowing artifacts are more visible in deeper levels. Vignetting and a vitreous floater shadow (green arrow) are seen in eyes with non-proliferative diabetic retinopathy (NPDR; bottom row).

In addition to mimicking the appearance of real pathology, like capillary dropout,

shadowing artefacts can also resemble apparent neovascularization brought on by projection artefacts. Therefore, any data associated with ischemia, such as nonperfusion area and vascular density, may be substantially affected by shadowing artifacts. Other pathological developments can also be concealed using shadowing artifacts; for instance, a region undergoing neovascularization can be obscured.

It is possible for shadowing anomalies to be sufficiently powerful to obstruct the OCTA flow signal's recovery. In contrast to numerous OCTA anomalies, this signifies that intense shadows cannot invariably be mitigated or offset. Conversely, regions that are significantly impacted by shadowing artifacts ought to be identified and excluded from quantitative analysis. Due to the intricate interplay among the diverse features capable of discerning shadowing artifacts, algorithms designed to detect such artifacts have traditionally depended on machine learning techniques (79).

3. Window artifacts

The window artifact occurs when the imaging depth range that the operator chooses does not cover the complete thickness of the tissue that is of interest to the operator. In the event that the imaging depth is set too shallow, for instance, it may ignore deeper arteries or structures, which results in an inadequate image of the vasculature. On the other hand, if the imaging depth is set too deep, it may contain signals from layers that are close to it, which may lead to overlap and confusion in the interpretation of blood flow patterns. The figure (64) describes the visualization to choroid through retinal pigment epithelium loss

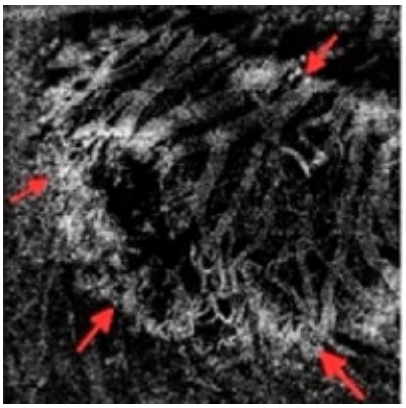

Figure: 64 Window artifact

The appearance of window artifacts in OCTA may be attributed to a number of different causal causes. When analyzing blood flow, one of the most important factors to consider is the selection of segmentation borders, which define the layers that are being

examined. In the event that these limits are not established correctly, it may lead to the inclusion of vascular structures that are either insufficient or excessive. Furthermore, the refractive index of various tissue layers might have an impact on the accuracy of depth segmentation, which subsequently contributes to the appearance of window artifacts (80).

- Artifacts caused by data collecting and image processing methods

There are 2 types of artifacts based on the image processing and data collection

1. segmentation artifacts
2. duplication of vessels artifacts

1. Segmentation artifacts:

The automated segmentation algorithm erroneously identified the boundaries of the superficial vascular layer, leading to a deviation of over 50% in the diameter of the total thickness in a B-scan. Severity was attributed to this artifact if it was detected in excess of 10% of the total B-scans that comprised the en face angiogram figure (65) and (66).

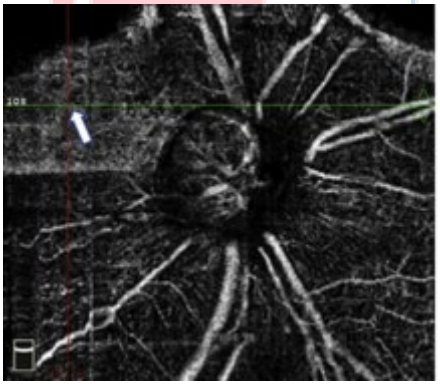

Figure: 65 Error in segmenting a en-face image

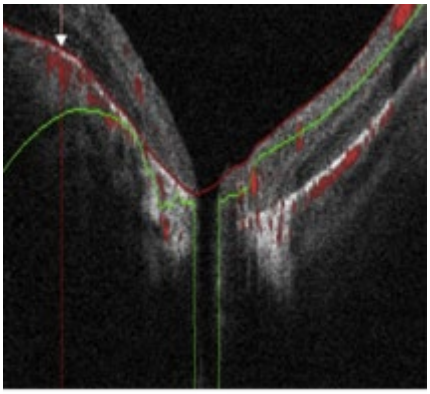

Figure: 66 B-scan segmentation error (81)

Different slabs' microvascular networks are seen in OCTA en-face pictures. Slabs are

tissue layers that are divided into the choriocapillaris, outer avascular retina, deep plexus, and superficial plexus. These layers are bounded by two limits of the retinal layer. Segmentation artifacts are caused by any mistake in determining the precise location of the retinal borders. Segmentation mistakes are more common in eyes with retinal diseases and pictures of poor quality.

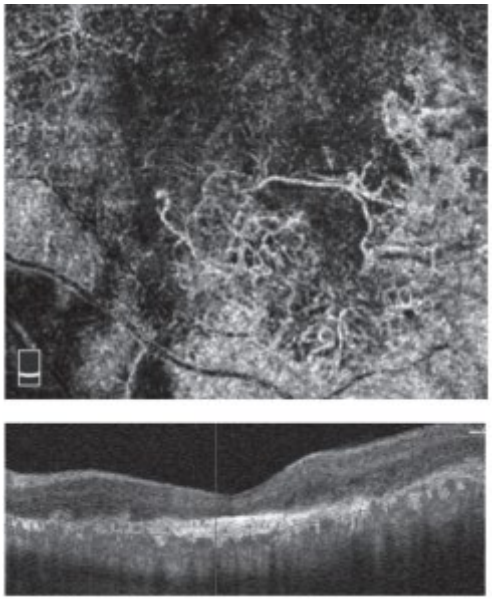

Segmentation artifact. (**Figure:** 67) En face segmented outer retinal slab (OCTA) demonstrating massive choroidal veins disguising themselves as neovascularization due to segmentation mistake in the retinal pigment epithelium.

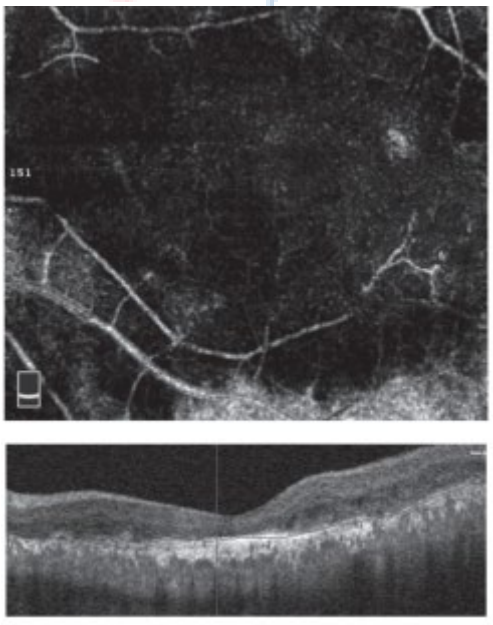

Figure: 68 en face OCTA at the outer retinal slab after segmentation correction. Note the

removal of large choroidal veins (82).

2. Vessel duplication artifacts

When referring to OCTA, the term "vessel duplication artifacts" refers to the appearance of blood vessels that are replicated or mirrored in the subsequent imaging findings. Artifacts like this might be caused by a number of different sources. For instance, an OCTA picture of the retina that a blood that is flowing in a horizontal direction. It is possible for the software to incorrectly perceive the same vessel as two independent vessels, resulting in a duplicated appearance. This incorrect interpretation might be caused by a tiny movement that occurs during the imaging process or by faults in the segmentation algorithm. The picture may give the impression that there are two vessels that are parallel to one another rather than just one (83).

- Motion based Artifacts

There are 3 categories based on the motion related artifacts,

1. Motion artifact
2. Blink artifact
3. Banding artifact

1. Motion artifact

One of the most important components of OCTA collection is making sure that eye motion is given the appropriate amount of compensation. To identify temporal shifts in the optical coherence tomography (OCT) signal that are associated with blood flow in capillaries, it is necessary to detect and adjust for eye movements with a high degree of precision. Sampling strategies and different eye-tracking implementations, thus, are important factors in evaluating a device's overall performance. when it comes to the observation of blood circulation at the capillary level.

Here, two distinct ways that eye movements affect the collection of OCTA results are discussed. First, there must be a spatial overlap between these B-scans in order to detect changes in the OCT signal that correspond to blood flow. As a result, the scans must overlap within the lateral breadth of the probing beam, which is normally on the order of 15 micrometers. In the second place, wider eye movements have the potential to result in geometrical distortion or the absence of data from the volume scans of OCTA. Volume scans

are often obtained in a matter of seconds or sometimes even minutes. On this time scale, saccades, changes in fixation, or changes in head posture are likely to be the causes of significant eye movements.

Image registration of the subsequent B-Scans might be used to compensate for slow eye wanders inside the B-Scan plane, It successfully eliminates the temporal signal shift in regions with stagnant tissue (see to figure (69) for further information). OCTA signal may be severely degraded when there is inadequate spatial overlap between the B-Scan samples. This can occur when there is eye movement that is perpendicular to the B-Scan plane or when there are bigger eye movements (also known as "saccades"). In the event that no countermeasures are adopted, this will result in the OCTA volume scans to have missing data as well as geometrical aberrations. The goal of motion artefact adjustment is to ensure that the OCTA data collected from one visit to the next is free of errors that could potentially affect the precision of quantitative change assessments.

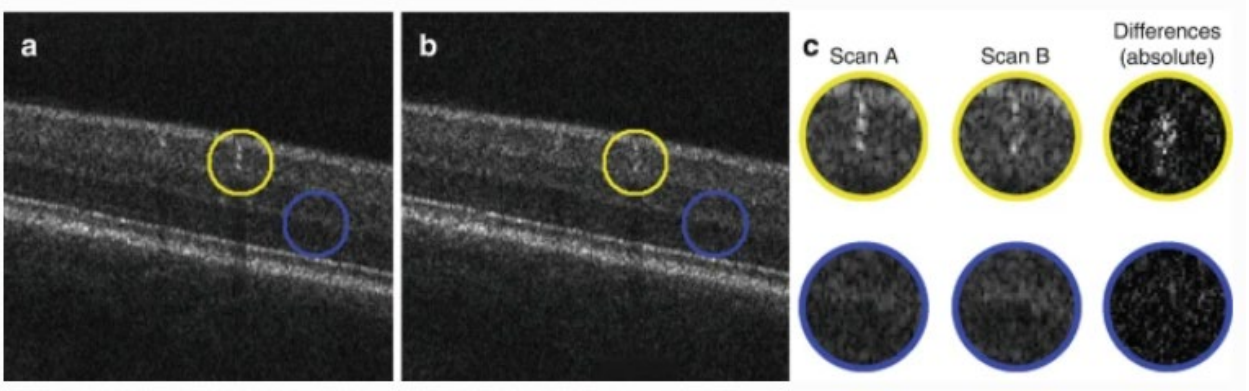

Figure: 69 An example of the OCT signal intensity's temporal progression following bulk motion correction. (a, b) OCT images of structures were obtained. Both images depict inert tissue (blue circle) and a larger blood vessel (yellow circle) with their respective locations indicated. (c) When these regions are magnified and the absolute differences are computed, it is possible to observe more pronounced signal fluctuations in the blood vessel in comparison to the inert tissue.

Two primary strategies exist for reducing the impact of motion artifacts in OCTA. One method is to get several independent measurements of the OCTA volume and then combine the information during post-processing. In contrast, the second method involves real-time monitoring. One benefit of employing the post-processing approach is the reduction in acquisition times. Practically speaking, the quick scanning axis is usually oriented perpendicularly, and just two volume scans are used. The final volume is achieved through

the process of interpolating and averaging the various input volumes. While it is common practice to supplement larger data voids from one volume with information from the other volume, achieving results free from distortion is not always guaranteed.

The real-time monitoring methodology utilizes precise eye motion measurements that occur in real-time. B-scans that are compromised by excessive motion are re-obtained. When eye motion is slow, real-time observations can also be used to actively manage the OCT scanners so that the beam stays on the nominal scanning path (eye deviations). Acquiring data using the real-time monitoring method can be occasionally sluggish due to data filtration triggered by vigorous eye movement. On the contrary, the volumes acquired through real-time monitoring exhibit geometric accuracy and are sampled uniformly, devoid of any voids caused by absent data (84).

2. Blink artifact

One of the most prevalent types of motion abnormalities in OCTA is known as blink artifacts. These artifacts are brought about by the fast movement of the eyelids that occurs throughout the imaging process. The blinking of a patient causes a quick shift in reflectance patterns, which the optical coherence tomography (OCTA) interprets as blood flow. This causes false positive signals to be produced in the pictures that are obtained. It may be difficult to adequately evaluate the vasculature of the retina when there are blink artifacts present since they can severely decrease the quality of OCTA pictures. Blink artifact is defined by the presence of horizontal black band indicating missing scans. Figure (70) indicates the blink artifacts in OCTA systems.

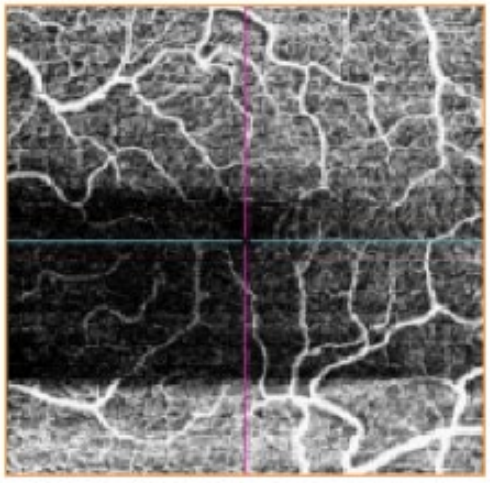

Figure: 70 blink artifacts

Artifacts caused by blinking often appear in the OCTA pictures as streaks that are either bright or dark. It is possible for these streaks to mask the real vascular architecture since they are often perpendicular to the direction in which the blood vessels are flowing. There is a possibility that quantitative measurements and analyses of the retinal vasculature might be inaccurate due to the presence of blink artifacts. This is of utmost importance in research or clinical settings, where accurate measurement of blood flow is essential for the identification and surveillance of numerous ocular diseases (85).

3. Banding artifact

Banding defect is sometimes referred to as Quilting defect, which is described as a pattern of artifacts that lies in a rectilinear orientation (figure (71)). Motion correction software does not perform an appropriate correction of multiple saccades in both the horizontal and vertical directions, which results in a rectilinear pattern that is accompanied by distortion. There was a distinction made between the quilting process, which included none, minimal, moderate, and substantial stages.

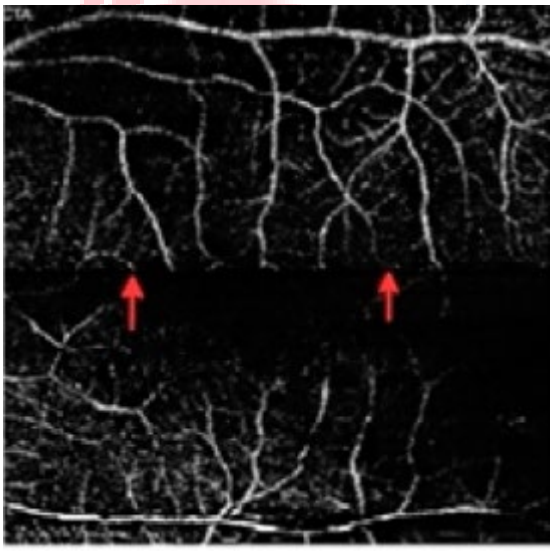

Figure: 71 Banding artifact

Due to the fact that OCTA is reliant on light sources, artifacts are extremely prevalent and can result in inaccurate interpretations of OCTA images. These may result from eye movements, intrinsic eye characteristics OCTA image processing, presentation, or capture techniques. One notable classification of artifacts consists of shadow artifacts, which manifest as an attenuated signal concealed by an obstruction or absorbing or scattering surface. Reduced OCTA signals from the retinal vasculature as a consequence of drusen, subretinal haemorrhage, retinal haemorrhage, or media opacity which leads to a decreased OCTA signal from the choroidal cell membrane (CC), are instances of shadow-causing artifacts.

A further possible source of artifacts is subretinal fluid (SRF), which is a characteristic feature of numerous chorioretinal diseases. Neovascular eye disease, including RPE atrophy, age-related or myopic macular degeneration, like geographic atrophy when it comes to AMD, or exudative CC disease, including patchychoroidal disease or choroidal tumor, or CSC, can all manifest as SRF (86).

WORKING FUNCTION OF OCTA

Multiple B-scans (cross-sectional scans) of the identical region are gathered by OCTA in order to identify variations in motion contrast, amplitude, intensity, or phase. The techniques used vary depending on the device. Since that the choroid and retina are fixed tissues and immobile things do not alter their signals in contrast to moving objects, it is thought that the solitary moving particle inside them—blood—is the source of the changes in values. Because of their biconcave shape, erythrocytes reflect light. After that, several axes of scanning are carried out to provide a 3D picture (87).

Functional of OCTA extension of structural OCT that detects motion contrast in the vasculature by doing multiple B-scans. Moving things will cause more of a shift in appearance from one photograph to the next than stationary ones. It is possible to produce a picture that emphasizes movement by searching for changes over time. The net intended consequence is to see blood flow, as the only motion that is predicted in the retina is the flow of blood via capillaries. Choices about implementation must be taken, and these choices may result in variations in function and performance, similar to any oversimplification of practical application. These implementation considerations include bulk eye movements not due to blood flow management, how findings are shown, how flow is recognized, and what distinguishes a difference between B-scans.

Thus, a variety of hardware and software options are generated, each involving a trade-off in terms of cost, possible issues, or performance. A simplified schematic of the operation of OCTA in comparison to structural OCT imaging is shown in figure (72). In traditional structural OCT imaging, a series of B-scans at various retinal regions are conducted in a "raster" scan pattern to provide a 3D volume or picture cube. A high density of A-scans is covered by the raster scan in a portion of the fundus. However, numerous images of the same retinal region are required in order to produce vascular contrast and detect motion.

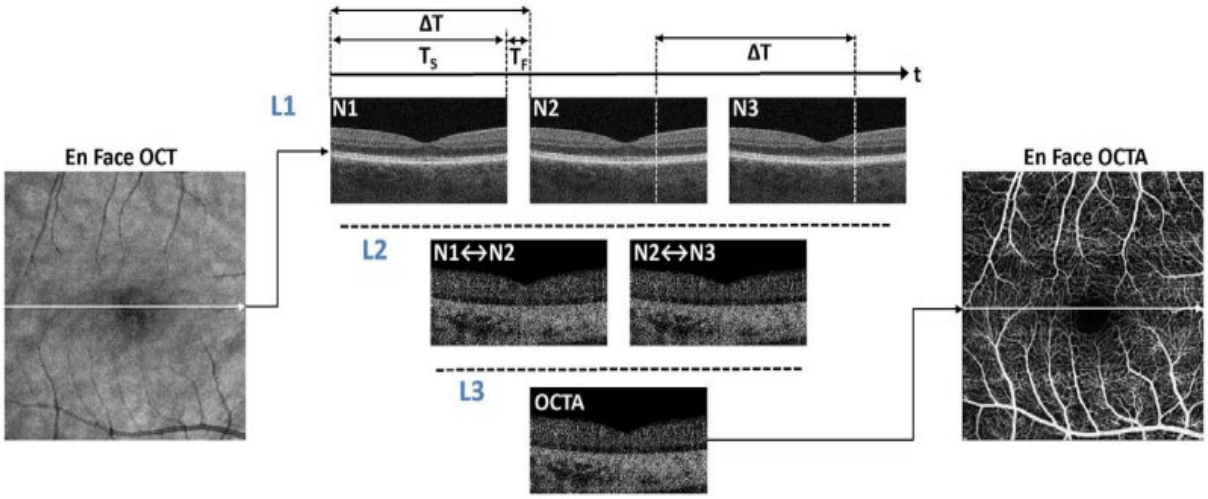

Figure: 72 OCTA (optical coherence tomography angiography) simplified schematic diagram.

To identify signal changes brought on by flowing erythrocytes, In the same area (row L1, N1 to N3), many B-scans are performed, and the structural images are compared pixel by pixel. A motion contrast picture is subsequently shown, showing the variations between the repeated B-scans (rows L2 and L3). To create a motion contrast picture (row L3), Repeated B-scan comparisons can be done pair-wise or in various combinations with various techniques. To generate volumetric OCTA data throughout a section of the retina, repeated B-scans are performed using a raster scan pattern at progressively displaced locations in the retina. Similar to fluorescein or "indocyanine green angiography" (ICGA), The OCTA volume, which is typically displayed by segmenting the different retinal layers and projecting an en-face image, enables the 3D imaging of the microvasculature.

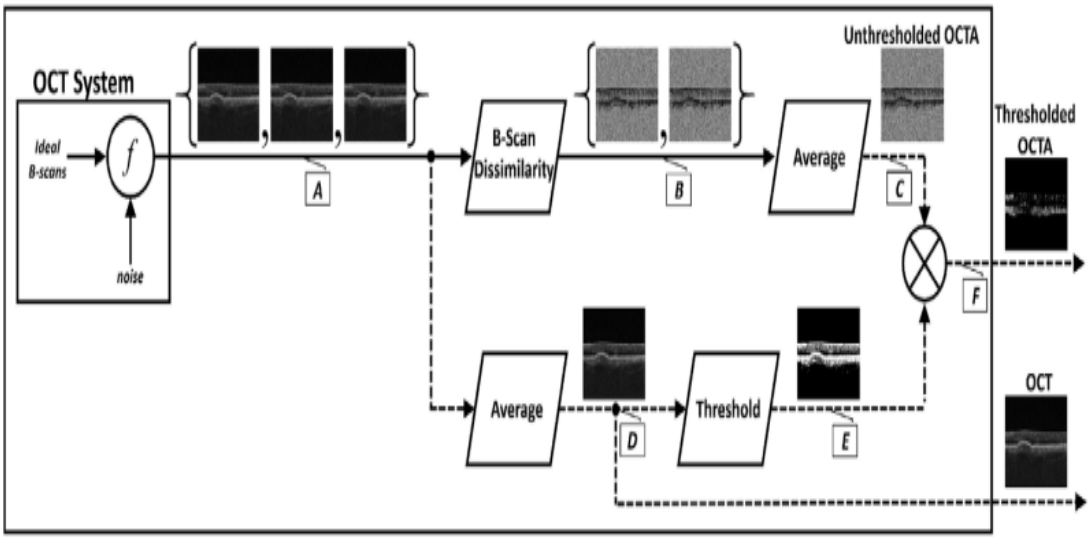

Figure: 73 OCTA processing flowchart in detail.

According to the figure (73) the same site is used to capture several Bscans (block A). The picture (represented by f) is blended with the noise contained in the B scans. To boost the signal to noise ratio, Compute the decorrelation between pairs of B-scans (block B) to create motion contrast. Block C then generates an average. It is also averaged for repeated B-scans (block A) to produce an OCT picture with a higher signal to noise ratio (block D). Block D measures the OCT image signal pixel by pixel as well. If the signal is below a threshold, block E generates a mask. This threshold mask is then used to remove the wrong pixels from the OCTA image (block F) that are associated with low or noisy OCT pixels. Next, the masked OCTA picture is shown. The processing settings and features that greatly influence OCTA pictures are exclusive to commercial equipment (88).

RETINAL BASED DISORDERS

Over the last several years, OCTA has been utilized in numerous studies to identify different retinal conditions. The information on the present research on a few of the retinal illnesses is going to be covered in the following parts.

After DR, it is the second most common retinal vascular disease, and it often results in considerable vision impairment, particularly in people who are middle-aged or older. Hypertension, smoking, diabetes, and open-angle glaucoma are all variables that might increase the likelihood of developing RVO. Ischemia of the macular region, often known as ME, is the most common cause of central vision loss. Some of the neovascular problems that may lead to vision loss include vitreous hemorrhage and neovascular glaucoma. These complications are a substantial cause of vision loss. An illustration of the superficial retinal plexus's anatomy can be seen in figure (74) to illustrate an example of RVO.

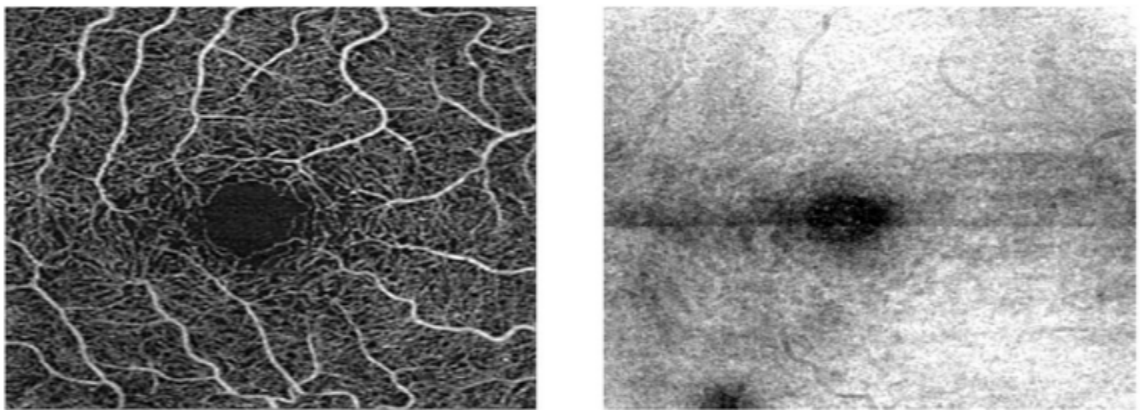

Retinal superficial plexus structure image

Figure: 74 A picture of the retinal superficial plexus's structure in an RVO case. (89, 6)

RVO has been associated with systemic conditions, hypertension, hyperlipidemia, and diabetes mellitus in particular. Depending on which veins are impacted, retinal vein occlusions may be classified 2 types namely;

1. Central retinal vein occlusion (CRVO).
2. Branch Retinal Vein Occlusion (BRVO) (91).

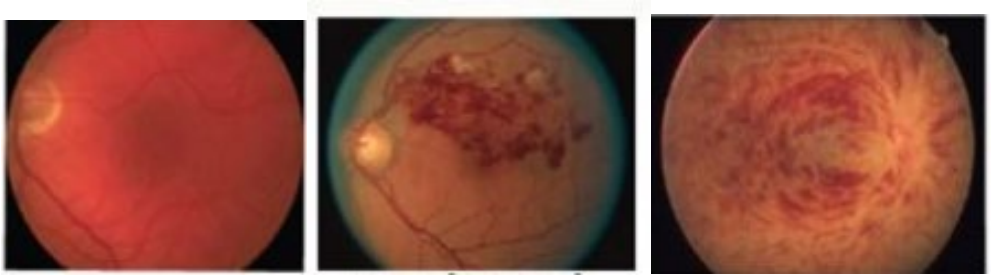

Normal Retina BRVO CRVO

Figure: 75 Normal retinal vs. BRVO vs. CRVO

1. Central retinal vein occlusion (CRVO)

Retinal apoplexy was the term Liebreich used to characterize the clinical manifestation of retinal vein blockage in 1855. In 1878, Michel recognized as a medical entity brought on by thrombosis.When Duke-Elder and Dobree said in 1967 that "since that time (von Michel's) the condition has been the subject of almost continuous research but even today, many points both in the etiology and in the intimate mechanism of the obstruction are still unelucidated," they summed up the state of research on retinal vein occlusion with accuracy.

There is a blockage in the region of circulation that is responsible for draining blood from the retina. In most cases, it takes place at the point where an artery and a vein intersect. Occlusion may be caused by a number of reasons, including but not limited to hypertension, glaucoma, hyperviscosity syndromes, diabetes mellitus, cardiovascular disease, anemia, vasculitis, and other similar conditions.

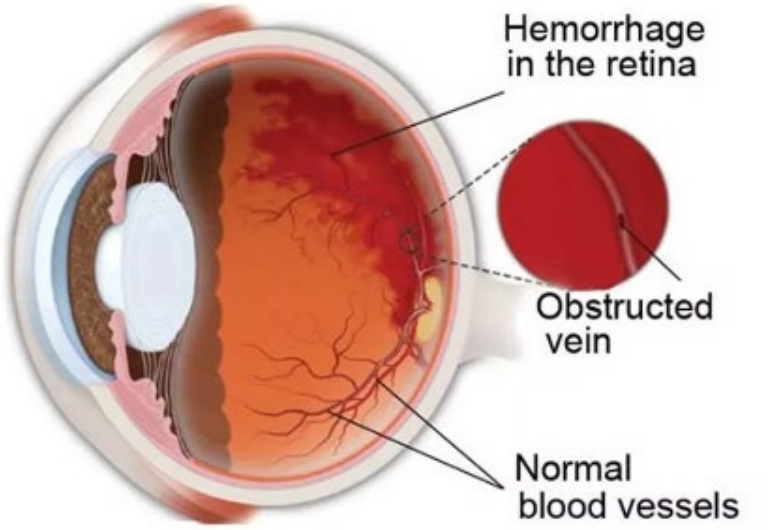

Branch retinal vein occlusion (BRVO), causing bleeding in parts of the retina.

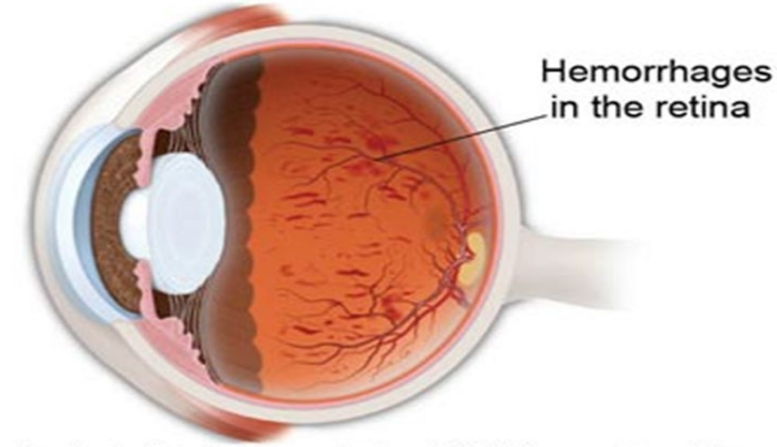

Central retinal vein occlusion(CRVO). The main vein of the eye is blocked, causing hemorrhages(bleeding) in the retina

Figure: 76 Physical differences between BRVO and CRVO

These three primary consequences of occlusion pose a danger to vision: macular edema, macular ischemia, and neovascularization. All three of these problems are associated with occlusion. Each of these two forms of RVO is characterized by a unique combination of anatomical and clinical characteristics. A visual representation of the physical distinction between the CRVO and the BRVO seen in Figure (76) (3).

Retinal vascular disorders such as CRVO may result in serious ocular morbidity. It usually affects both men and women equally and is more frequent in those over 65. There

may be comorbid systemic vascular disease, such as diabetes and hypertension, in this group. When younger people exhibit the clinical signs and symptoms of CRVO, there may be an underlying inflammatory or hypercoagulable etiology. The prevalence of CRVO is reported to be between <0.1 and 0.4% in population-based research.

Although CRVO is often a unilateral condition, there is a 1% yearly chance of getting any form of blockage of the retinal arteries of the adjacent eye, and up to 7% of people with CRVO may acquire within five years in the fellow eye. of the first eye's commencement. Comparing individuals with CRVO to a reference group without ocular illness, the former show a substantial decline in vision-related quality of life along with higher healthcare expenses and resource use. The ability to carry out everyday tasks may be impacted by CRVO, particularly in situations with bilateral CRVO or when coexisting ocular illness impairs vision in one eye. CRVO has two forms: ischemic and non-ischemic its discussed below (93, 94).

1.1 Ischemic CRVO and Non-Ischemic CRVO

The more severe type of CRVO is known as ischemic CRVO, or iCRVO for short." low VA (≤ 0.1)", Cotton-wool patches, and relative afferent pupil defect are the most obvious signs of retinovascular outflow obstruction (RVO). iCRVO has the potential to result in neovascularization and potentially loss of vision. Early vision and visual fields are quite important in the process of differentiating CRVO patient. Among patients with iCRVO, the initial VA is 20/200 or worse in 99% of cases, in contrast, 22% of individuals with non-ischemic CRVO had the same outcome.

Additionally, it was demonstrated that patients with ischemia CRVO had a far more severe visual field deficit than those without ischemia CRVO. particularly in cases with central scotoma. The peripheral inferior nasal visual field deficiency was the problem that occurred the most often. In the meanwhile, central scotoma and peripheral vision abnormalities are more severe in patients with ischemia congenital retinal vascular occlusion (iCRVO) than they are in patients with non-ischemic congenital retinal occlusion (CRVO). FA was the method that ophthalmologists used to diagnose iCRVO in the past. At this time, however, functional tests such as electroretinogram, visual field, afferent pupil deficiency, and vision reveal that the individual is superior.

In order to verify iCRVO, ultra-wide area fluorescein angiography, also known as (UWFA), has become more popular. Thomas's study employed UWFA to calculate the baseline ischemia index (ISI), which was then utilized to calculate the CRVO grade.

According to FA, The ratio of the non-perfused retina to the entire visible retina is known as the ischemia index. This ratio is determined according to FA. As a result of an ISI that is more than 35%, the categorization of CRVO as ischemia is both sensitive and specific. In light of this, UWFA is more helpful in the prognosis. According to the findings of a recent research, there is a favorable correlation between the disc regions and the occurrence of neovascularization. There is a twenty percent increase in the likelihood of neovascularization in eyes that have more than thirty degrees of non-perfusion of the retina. iCRVO may be diagnosed using a non-invasive method called retinal oxygen saturation assay. The idea behind it is that the color of blood is determined by the oxygen saturation of the hemoglobin, and that the ischemic retina is able to extract more oxygen than the healthy retina.

It has been shown that between 10 and 33 percent of original non-ischemic cases undergo the shift from non-ischemic to ischemic CRVO. The likelihood that non-ischemic CRVO will become ischemic CRVO within the first month depends on the initial state of blood flow and eyesight. The risk is greatest during the first month. There is a strong correlation between ischemic conversion and retinal hemorrhage, and the degree of ischemia is utilized to differentiate between ischemic CRVO and non-ischemic central retinal vein occlusion. Color Doppler Imaging (CDI) is a technique that measures the minimum central retinal venous velocity in order to differentiate between ischemia and non-ischemic retinal vein occlusion (RVO). There is a continuum from non-ischemic CRVO to ischemic CRVO that includes damage to the macular, retinociliary, and visual systems. This development is not completely understood.

There is a correlation between risk variables and the switch from non-ischemic to ischemic coronary artery disease (Figure (77)). There is a correlation between a greater incidence of iCRVO and factors such as advanced age, women who are above the age of 65, hypertension, stroke, and obesity. The adipocytosis, which controls diabetes and obesity, is secreted by lipocytes. Not only does adipo play a significant part in RVO and neovascularization, but it also has the potential to become a novel therapy target. In addition to contributing to the circulation of aqueous humor, ciliary vessels are responsible for perfusing the macular area and the head of the optic nerve. Occlusion of the ciliary vessels is another potential complication of non-ischemic CRVO, which may also cause abnormalities in the central or peripheral vision fields. Macular retinal ganglion cells, which are associated with the prognosis of ischemic CRVO, are damaged when ciliary arteries do not get enough blood flow across the retina. Glaucoma is induced when ciliary arteries are blocked, which

leads to the accumulation of aqueous humor and a rise in intraocular tension. Glaucoma may eventually lead to the development of non-vascular glaucoma (NVG). In addition to this, VEGF (Vascular endothelial growth factor) is an indication that may be used to measure the degree of iCRVO. Both ischemia and non-ischemic CRVO may cause macular edema, however ischemic CRVO is the only condition that can cause ischemic harm to the retinal cells of the macular region. When macular edema progresses into macular hemorrhage, the microstructure of the eye becomes more severe. As a result of the process, VEGF is increased, which in turn activates NF-κB and inflammatory factors ("IL-8 and TNF-α"), resulting in the development of iCRVO and NVG.

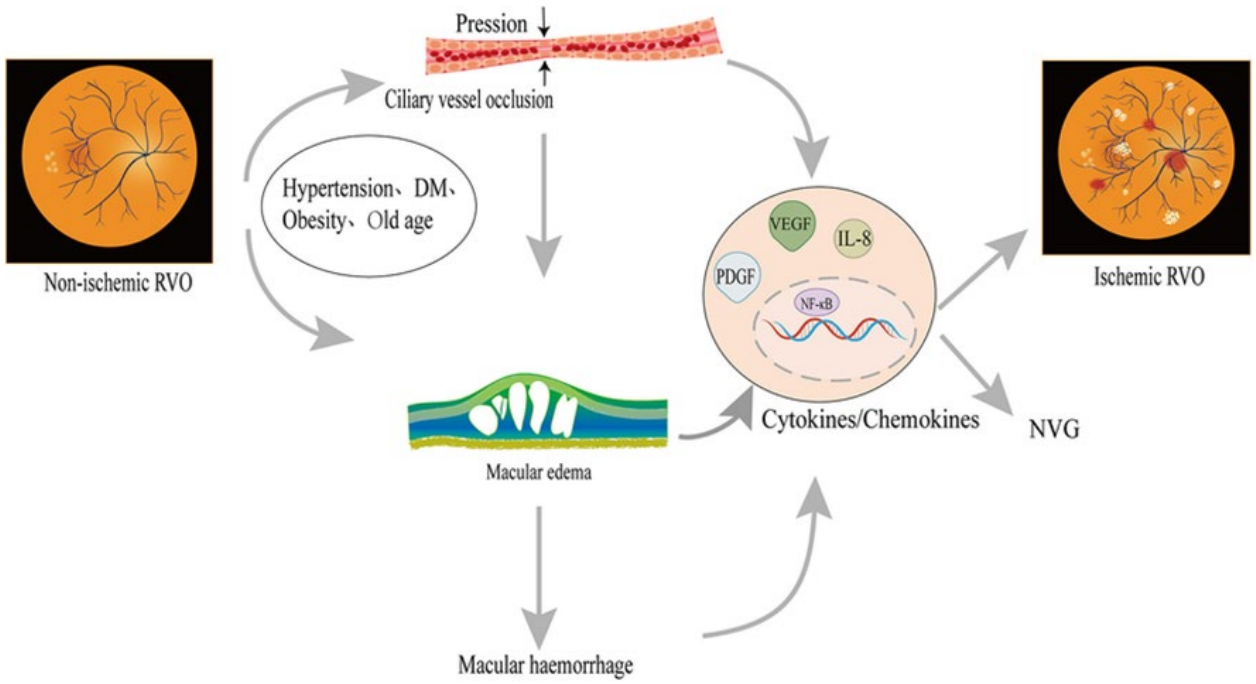

Figure: 77 Potential process by which iCRVO develops from non-ischemic CRVO

It is believed that thrombotic variables and arterial hypertension are the main risk factors for iCRVO. even if the exact pathophysiology is yet unknown. Increased hydrostatic resistance from central venous blockage causes blood flow stagnation, retinal ischemic damage, and increased retinal non-perfusion (RNP). RNP and VEGF have a positive feedback loop. While greater VEGF worsens retinal ischemia and hence increases RNP, it also plays a significant role in the illness. RNP enhances VEGF and vein occlusion. In the meanwhile, VA imperfection is more severe in iCRVO because retinal ganglion cells were permanently damaged by retinal ischemia and RNP. A permanent loss of central vision results from the loss of photoreceptors in the macular, which also causes the production of inflammatory

chemicals including VEGF, placenta growth factor, and interleukin 6 and 8. In the anterior and/or posterior segments, VEGF stimulates the creation of new blood vessels. This leads to vascular ingrowth into the vitreous cavity, which in turn causes macular edema, subsequent vitreous hemorrhage, and even NVG (Neovascular glaucoma) (95).

1.1 Natural History of central retinal vein occlusion

The acute phase of CRVO is characterized by macular hypoxia, intraretinal hemorrhage, and central macular edema. Visual impairment is one of these symptoms. There is a varying degree of long-term vision impairment in the majority of cases, despite the fact that in certain instances, Normalization of the retinal venous circulation may take place with little impact on vision. CME that is chronic may lead to the dispersion and clumping of retinal pigment epithelium cells below the fovea, which can also result in the loss of photoreceptors. Ischemia of the macular tissue and the creation of epiretinal membranes are two other long-term causes of decreased macular vision. However, depending on the severity of retinal ischemia, there is also the possibility of anterior segment neovascularization, which may lead to the development of neovascular glaucoma. An increased risk of anterior segment neovascularization and, less frequently, posterior segment neovascularization for the patient is linked to increasing severity of retinal ischemia.

During the CVOS investigation, 34 percent of eyes that were originally non-ischemic evolved into the ischemic group by the time the three-year study came to a close. During the first four months of the trial, the progression of ischemia was the fastest, and it continued to proceed constantly throughout the full course of the study, which lasted for three years. One-sixth of the patients who participated in the CVOS trial acquired anterior segment neovascularization, and ten percent of the patients who were previously categorized as non-ischemic also exhibited this phenomenon. During the 18-month follow-up in the central venous bypass experiment (CVBS), “20.8%” of the control group's initially non-ischemic eyes were converted to the ischemic category. Ten the rates of ischemic conversion have been observed to be somewhat greater by other writers. Glacet-Bernard found that after one year, 54 percent of eyes that had originally shown as non-ischemic had transitioned into the ischemic group. Additionally, 12 percent of eyes had iris neovascularization, and 9 percent developed neovascular glaucoma. In the CVOS trial, there was a 35% probability of developing anterior region neovascularization in eyes that were originally categorized as having an ischemic condition (96).

1.2 Pathogenesis

Uncertainty and debate continue to surround the pathophysiology of chronic recurrent pulmonary oedema (CRVO). It is thought that the lamina cribrosa structure located directly behind and in the area of where the blood flow from the central retinal veins is restricted. There is a possibility that a number of variables, such as local anatomical vulnerability, changes in vascular wall, hemorrheologic inclinations, and thrombotic tendencies, all are contributing factors. The theory that a thrombus located in the (CRV), close to the lamina cribrosa, is what causes a CRVO is founded on the anatomical characteristics of the lamina cribrosa. Additionally, the hypothesis is supported by an autopsy study of eyes that sustained CRVO for an extended period of time, wherein the lamina cribrosa was shown to have thrombosis-related findings.

It is possible that the CRV in the area of the lamina cribrosa is susceptible to blockage due to the different anatomical configurations around it. Because the adventitial sheath of the central retinal artery and the adventitial sheath of the CRV are identical, it is possible for the vein to be compressed by the arterial wall, which is stiffer. This is more likely to occur in individuals who have arteriosclerotic vascular disease. It has been proven via post-mortem examinations that healthy eyes possess a CRVO natural constriction at this point. Furthermore, it has been seen that the alterations become more prominent with advancing age. At this particular location, it has been established that the CRV has high blood velocities, which also suggests the existence of a constriction is there. These alterations might then result in increased shear pressures, which would cause damage to the endothelial cells. This damage, in turn, could result in the proliferation of endothelial cells and perhaps the development of thrombus. The morphology of retinal venous endothelial cells is generally homogeneous and different from that of artery cells. Nevertheless, the venous endothelial cells in the posterior lamina cribrosa area exhibit features that are similar to those of arterial cells, which lends credence to the notion that this is an area of haemodynamic stress.

The theory that was presented previously assumes that the degree of blockage to venous outflow in the area of the lamina cribrosa is varied and that the variance in the clinical presentation is caused by either a total or partial occlusion of the CRV. According to the findings of other researchers, the variance in the clinical picture may be attributed to the geographic location of the obstruction in the CRV. They postulate that a more severe or ischemic-type clinical presentation will arise from an occlusion of the CRVO in the lamina

cribrosa region, which will lead to a more complete restriction to CRV outflow. A blockage located farther posterior to the lamina cribrosa, on the other hand, will cause a less severe or non-ischaemic clinical state. This is because some venous outflow via venous tributaries situated in the retro cribrosal region of the CRV will be allowed by an obstruction posterior to the lamina cribrosa. These tributaries have the potential to develop anastomoses with the veins that are located in the surrounding area.

The macula of the retina gives humans the ability to see in great detail. The fovea, which is a little pit in the center of the eye, is exclusively made up of cones, and it is responsible for the highest level of visual acuity one may experience. According to one theory, the breakdown of the blood–retinal barrier (BRB) is the root cause of macular edema that is associated with CRVO. Macula edema is caused by a number of other factors, including hydrostatic and osmotic pressure, all of which contribute to the buildup of fluid and the swelling of tissue over time. Damage to the tight junctions that connect capillary endothelial cells, in conjunction with vitreomacular traction and adhesion, is the root cause of this condition. Vasopermeability factors, including as VEGF, are able to seep into the vitreous fluid as a consequence of the breakdown of the BRB (97).

1.3 Risk factors

Arteriosclerotic vascular risk factors, diabetes, ageing, hypertension, and glaucoma are the primary risk factors for chronic recurrent obstructive vascular occlusion (CRVO). There is a correlation between higher levels of physical activity, increased alcohol intake, and the use of estrogens in postmenopausal women, which results in a reduction in the risk of CRVO.

The use of antithrombotic medications is a regular practice among patients who are of an older age. There was a higher incidence of coronary revascular occlusion (CRVO) among individuals who were taking aspirin and warfarin, according to the research, even after correcting for other risk factors. There is a lack of clarity on whether this is a result of the increased cardiovascular risk profile of patients who are taking these drugs or if it is related to other variables. However, It appears that there is no discernible protective benefit to using anticoagulants in people who are at risk of developing CRVO. This is due to the fact that additional research has revealed that patients who had previously taken warfarin also acquired CRVOs.

Hemorrhageologic changes in blood constituents might potentially contribute to RVO. Due to its distinct anatomical features, the lamina cribrosa may exhibit a greater degree of the high flow resistance of the retinal venous circulation. This resistance restricts the retina's

capacity to adjust to changes in blood viscosity and keeps it from contracting in response to increased intraocular pressure. Blood viscosity has been brought up as a potential factor in RVO for more than 30 years. Erythrocyte aggregability, erythrocyte deformability, plasma viscosity, and haematocrit level are the four parameters that affect blood viscosity. Numerous investigations have looked at the significance of changed blood haemorrheologic features in RVO, with sometimes contradictory findings. The differences in techniques of evaluating the rheologic parameters, small numbers in several of the research, and different patient groups might all be contributing causes to the differing results. The erythrocyte deformability index with RVO and whole blood viscosity have been observed to significantly correlate in a more recent case-controller, suggesting that hemorrheologic variables may have some function in the etiology (98).

2. Branch retinal vein occlusion

The most frequent retinal vascular cause of vision loss is (BRVO), which occurs three times more often than CRVO and is second only to diabetic retinopathy. There is little question that local anatomical variables like arteriovenous crossings as well as systemic ones like hypertension contribute to the development of branch retinal vein blockage. Vision loss due to branch retinal vein blockage is painless and manifests as hazy or distorted vision. The most prevalent retinal disorders seen in clinical practice is BRVO. In a large series, 90% of the patients were over 50 years old, indicating that it is often a condition mostly affecting the elderly. Since the disease's consequences contribute significantly to visual disability, early diagnosis and treatment are crucial.

Leber first described BRVO in 1877. One of the major vein's branches is obstructed in BRVO. It is described as a segmental intraretinal hemorrhage brought on by a blockage in the vein that drains the corresponding retinal region, with a size not surpassing the midline. In just 9% of cases does it occur bilaterally; it is often unilateral. Clinically, those with BRVO may not exhibit any symptoms at all or may complain of reduced vision. The degree of macular damage resulting from intraretinal edema, hemorrhage, or capillary non-perfusion is correlated with loss of vision at diagnosis. Macular edema, capillary non-perfusion, delayed venous filling in the region of occlusion, and microvascular anomalies in the latter stages are among the distinctive fluorescein angiographic findings in BRVO. More recently, optical coherence tomography has been used to show subretinal hemorrhage and serous macular detachment.

2.1 Risk factors

Arteriovenous crossings and other local anatomical variables, as well as systemic ones like hypertension, are unquestionably the source of BRVO. Two systemic risk factors for BRVOs are cardiovascular disease and high blood pressure. Among the risk factors for the eyes are hyperopia and glaucoma. Many individuals may not be aware that high blood pressure may impair vision by causing damage to the veins in the eye, even though most people are aware that high blood pressure and other vascular illnesses offer concerns to general health.

The most prevalent ailment connected to BRVO is high blood pressure. Thrombogenic factors include hyperviscosity syndrome, diabetes mellitus, and arterial hypertension. It is believed that the focused narrowing of the vein at the site of obstruction is the triggering mechanism in BRVO because of the significant correlation with systemic atherosclerosis and the observation that blockage often occurs at the location of an arteriovenous crossing.The primary cause of BRVO is thought to be arterial compression of the vein. A turbulent vein's flow may result from compression of the vein. A local environment that is conducive to the production of intravascular thrombus is produced by the turbulent flow combined with pre-existing endothelial vascular injury from various causes (99).

HISTOLOGY

Understanding the layers of the eye from a histological perspective is crucial for understanding the pathophysiology of various diseases as well as for understanding certain treatment modalities. Anatomically speaking, the eye may be broadly understood as a collection of overlapping tissue layers. The profile of a tiny, nonperfused arteriole nearest to the fovea provided no endothelial cells within it at all, according to histology using antibodies against (red, identifying lower level membrane) and endoglin (green, labelling endothelial cells). A little distance upstream in the partly perfused segment of the vessel, there was also no endoglin staining. Nevertheless, robust endothelium staining higher upstream in the artery's well-perfused sections provided the presence of a whole vasculature. The outer layers of eye are muscles, conjunctiva, auxiliary glands, lids, and eyelashes. Three concentrically stacked tissue layers make up the interior anatomy of the eye: The outer layers consist of the cornea and sclera. The intermediate vascular layer, known as the uvea, is further separated into the ciliary body, choroid, and iris. Nervous tissue makes up the retina, which is the deepest layer (92, 101, 100).

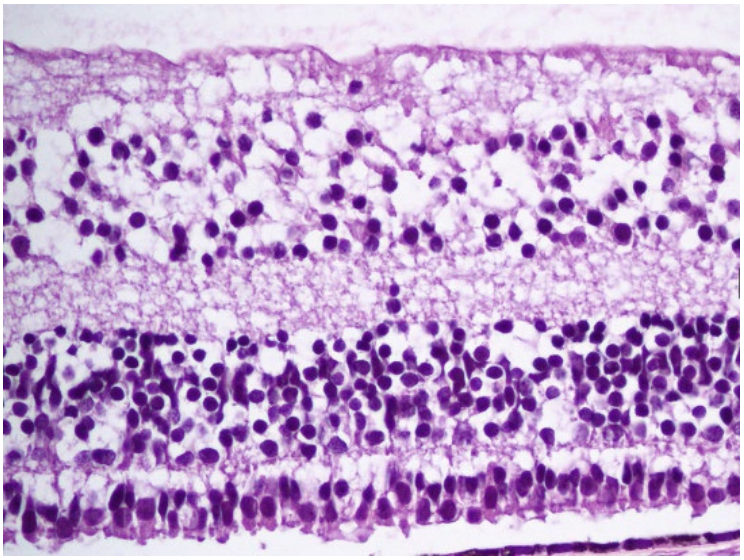

Figure: 78 Retina-very high

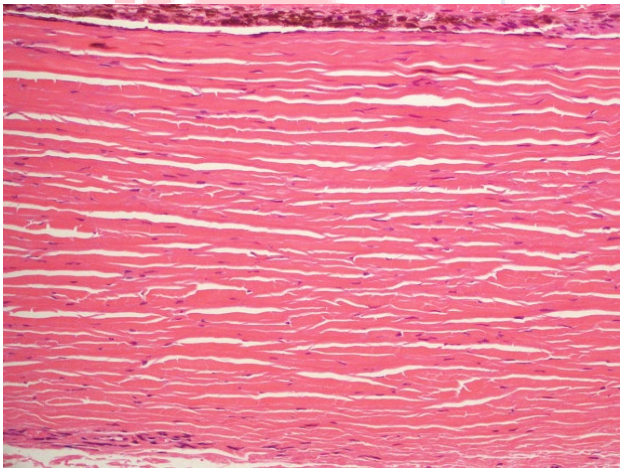

Figure: 79 Striated muscle tissue

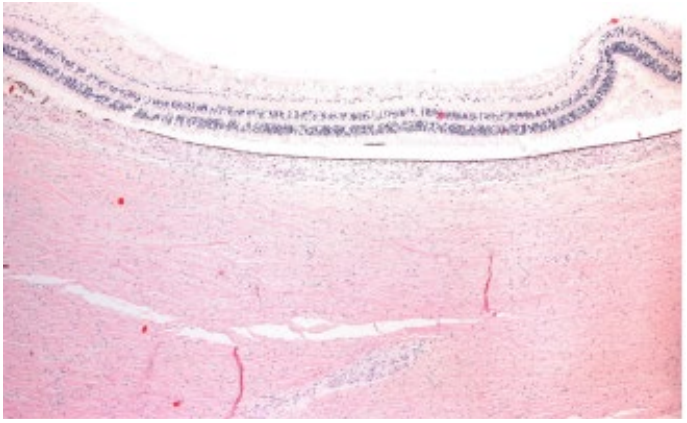

Figure: 80 Formation of Morgagnian globules

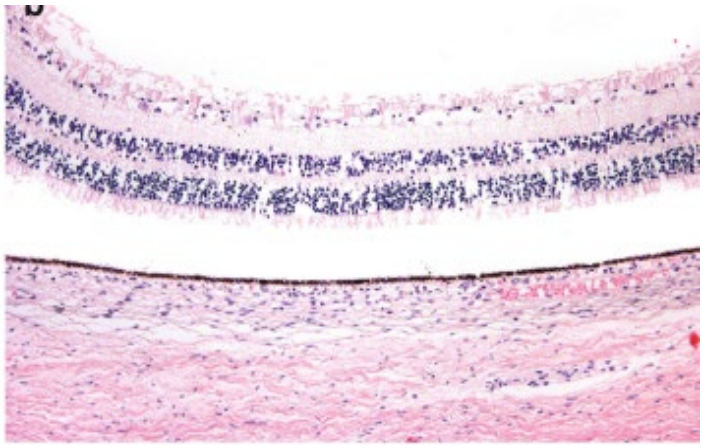

Figure: 80 Formation of Morgagnian globules

BURDEN OF CENTRAL RETINAL VEIN OCCLUSION DISEASES IN INDIA

A vascular condition of the eyes known as CRVO is known to produce severe visual morbidity, including abrupt blindness. An estimated 2.5 million individuals worldwide suffer with CRVO. From 40 years of age to 65 years of age and beyond, the incidence of CRVO rises by a factor of more than ten. In 2006, the projected yearly direct cost for the management of CRVO among Medicare beneficiaries was almost $1.3 billion. Furthermore, CRVO has a much greater financial cost than glaucoma. Compared to glaucoma, the one- and three-year per-patient direct medical expenses linked to CRVO are, respectively, 24% and 15% greater [6], even though glaucoma is 24 times more common than CRV. The various off-label therapies for iCRVO aim to reduce or postpone the development of CRVO-related problems, including neovascularization (NV) and macular edema (ME). Neovascular glaucoma (NVG) and vitreous hemorrhage (VH), which may result in blindness and severe visual morbidity, are two of the complications associated with NV. There are two types of CRVO: non-ischemic and ischemic.

The milder kind of CRVO, known as nonischemic CRVO, may go away on its own or develop into the ischemic variant. More severe ischemic CRVO (iCRVO) may cause VH or NVG. FA, OCT, and funduscopy may all be used to diagnose and characterize the severity of CRVO. A variety of criteria are used to identify ischemia in CRVO depending on the results of these tests or exams [10]. Although the precise epidemiology of iCRVO is still unclear, one research indicates that iCRVO accounts for around one-fifth of all occurrences of CRVO. According to a different research, 34% of individuals with non-ischemic CRVO advance within

three years, while 15% of patients progress to iCRVO within four months. Untreated problems resulting from iris NV or NVG cause partial or total vision loss in over 90% of individuals.

Intravitreal anti-vascular endothelial growth factors (anti-VEGFs), intravitreal steroid depots, laser therapies, and several surgical procedures are now used to control the consequences of CRVO. It is uncertain how often these off-label medicines cause difficulties for iCRVO patients; these rates have not been thoroughly examined A thorough systematic study recording data on the whole spectrum of iCRVO therapies is also required. The expenses linked with various therapies, as well as the corresponding rates of complications. Documenting the clinical results, rates of posttreatment problems linked to interventions, and financial results of therapies used to address iCRVO issues is the aim of this comprehensive literature review (102).

METHODS OF DISSECTIONS OF HUMAN EYE

The anterior chamber, vitreous, and retina are removed during dissection, and the eyecup is kept as a hemisphere for enzymatic digestion (see to Fig. 2). By keeping the eyecup in place throughout the surgery, you may prevent choroidal cell contamination of the RPE and retain an intact Bruch's membrane. In order to stop pigmented mesenchymal cells from seeping into the inner side of the Bruch's membrane, we take great care to avoid scraping the RPE/choroid membrane. If present as a contaminant, these pigmented mesenchymal cells will proliferate more quickly and contribute to the culture, even if they resemble RPE in appearance but are smaller in size. These pigmented cells' non-epithelial morphology may be a factor in the various morphologies that other researchers have found in RPE cultures. When deciding the tool to utilize to scrape the RPE from the Bruch's membrane, we have taken extra care.

We require a rounded tool to avoid puncturing the Bruch's membrane since we are extracting the RPE cells while they are still within the eyecup. The angled and double-bevelled spoon blade makes it simple to remove RPE sheets without jeopardizing the Bruch's membrane. Furthermore, dispase is the best enzyme digestion we have investigated since it maintains cell-cell connections while disrupting the RPE cell-basement membrane interactions. One of the main worries while extracting RPE is that if the cell body experiences enough shear stress, it may start secreting extracellular matrix (ECM). Because of this, we carried out a number of experiments with different temperature, dispase exposure times, and agitation levels throughout the enzyme digestion process. As a result, we were able to determine the best course of action

for simple RPE removal. In order to improve our control over the space between sheet fragments during plating, we finally attempt to collect RPE sheet pieces that are comparable in size and form. After a month in culture, if everything is done properly, the wells will develop into an epithelial monolayer (see Figure (82)). Protocols for RPE cell extraction, culture, and functional verification of the resultant RPE epithelial monolayers are included (101, 102).

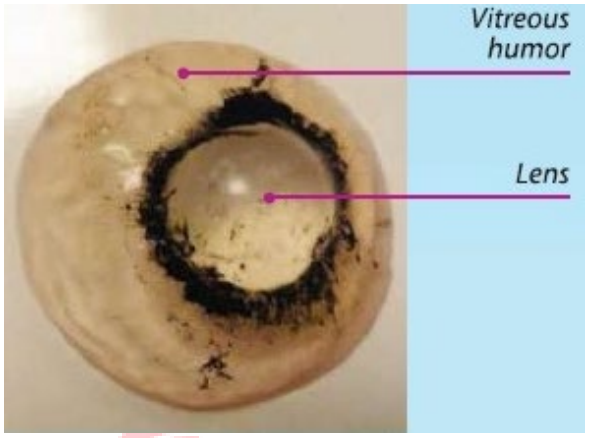

Figure: 82 Vitreous humor and lens

The vitreous humor, a transparent fluid that fills the back of the eye, aids in keeping the eyeball shaped. The lens is harder jelly lump which is easily separated from the vitreous humor.

Figure: 83 The retina

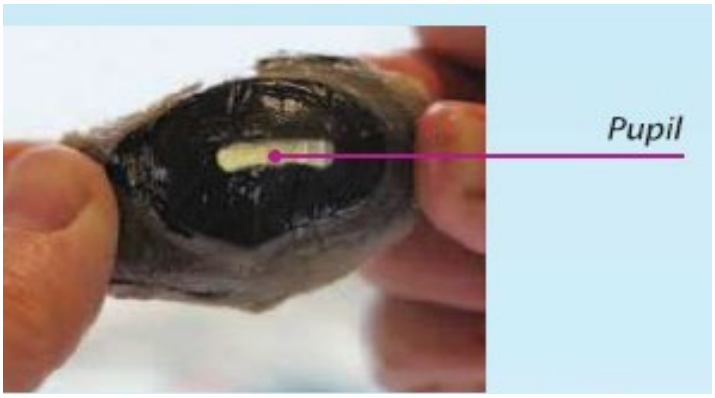

Figure: 84 The pupil is a hole in the iris and is protected by the cornea

Figure: 85 The iris separated from the cornea

FACTORS FOR DIAGNOSING IN CRVO

1. RAPD

A relative afferent pupillary defect (RAPD) represents the left–right asymmetric impairment of the anterior visual input pathway from the retina to the lateral geniculate nucleus. RAPD is an important ophthalmologic biomarker because of its objectiveness, unlike subjective functional tests such as the visual acuity and visual field, which are dependent on the patient response. inically, RAPD is assessed using neutral density filters in the swinging flashlight test (SFLT), and it is observed to correlate with alterations in retinal structure and asymmetrical vision field loss. For more accurate pupillary response recording, electronic pupillometry with infrared monitoring is used in the interim. The application of recent advancements in OCT angiography (OCTA) to the study of the link between glaucomatous optic neuropathy (GON) and peripapillary and macular vascular alterations (capillary density

and peripapillary choroidal capillary structure) has drawn interest (106). A combination of parameters was used to identify ischemic CRVO, and it was discovered that RAPD, together with electroretinogram, perimetry, and visual acuity (VA), was the most accurate indicator to distinguish between ischemic CRVO in the acute phase (103).

2. Disc edema

Swelling of the optic nerve's intraocular part is known as optic disc edema. The occipital cortex receives the visual information from the retinal ganglion cell's axons, which leave the eye via the scleral lamina cribrosa. Tissue edema is caused by the compression of the fibers in the lamina cribrosa, which also raises intercellular matrix pressure. Peripapillary hemorrhages, hyperemia, loss of optic disc borders, optic nerve head bulging, and vascular congestion are some of the symptoms of optic disc edema. The obstruction of both retrograde and orthograde axoplasmic transport in the optic nerve results in optic disc edema.

Symptoms:

- Visual loss
- Vomiting
- Ocular motility pain
- diminished ability to see color
- Diplopia
- Nausea

3. Development of collateral vessels:

As a result of the hemodynamic overload and hydrostatic changes brought on by RVO, collateral vessels progressively form within the optic disc or in the retina to promote blood outflow within the first six months, collateral vessels are evident under a microscope, and they fully mature in the next 24 months. The link between collateral vascular growth and structural and functional results in RVO eyes is generally poorly understood. Retino-choroidal shunt vessels were found to be thick, looping collateral vessels in CRVO that were situated within or near the optic disc (104).

The collateral veins on the optic nerve that link the choroidal and retinal circulations are called optociliary shunt vessels (osv), sometimes referred to as retinochoroidal shunt vessels of the optic disc or retinochoroidal venous collaterals. They are a nonspecific indicator of chronic retinal venous congestion and are linked to many diseases, such as central retinal vein blockage, optic nerve sheath meningioma, chronic glaucoma, and chronic papilledema. The central retinal vein, which travels through the optic nerve's middle and

empties into the superior ophthalmic vein, is where retinal blood exits the eye in healthy individuals. In the pre-laminar area of the optic nerve, optociliary shunt vessels are collateral venous routes that carry blood from the retinal venous circulation to the peripapillary choroidal veins. They are caused by the progressive expansion and dilatation of pre-existing anastomotic capillary channels, which happen under various situations as a compensatory reaction to the high pressure of the central retinal venous circulation.

There are two types of optociliary shunt vessels: acquired and congenital. Rare are the congenital instances. They show the connection between the choroidal venous and retinal venous circulations, a vascular abnormality. The majority of the time, acquired optociliary shunt vessels are linked to eye disorders that result in reduced retinal venous outflow (109). The degree of retinal ischemia may be related to the quantity of collaterals. The most frequent reason for their appearance is central retinal vein occlusions (CRVO) figure (86).

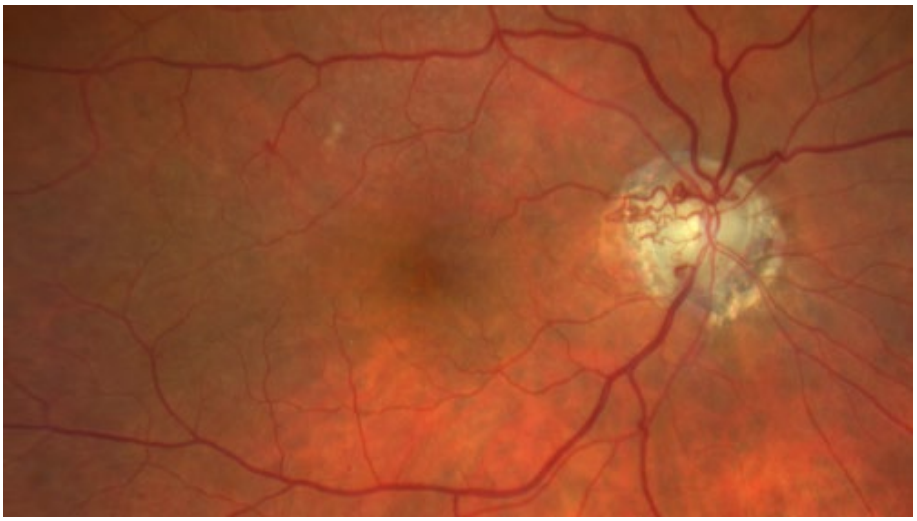

Figure: 86 Optociliary shunt vessels in an individual with blockage of the central retinal vein

It has been suggested that the pressure difference between an obstructed artery and a nearby unblocked vessel might induce blood to flow via collateral channels in retinal vein occlusion, despite the fact that nothing is known about the physiological importance of OSVs in CRVO. Furthermore, blood flow was drained via retinal veins into vortex veins and choroidal circulation through OSVs, according to an indocyanine green angiography investigation. When paired with B scan, OCTA technology enables segmented assessment of retinal capillary networks. Due to these benefits, OCTA may be a better method of identifying OSVs than color fundus photography, indocyanine green angiography, or fluorescein angiography; In addition to providing a dye-leakage-free imaging of the microvasculature, OCTA also gives three-dimensional data on the OSVs located in the optic disc.

OSVs are identified using OCTA photos, which include en face images of the neural retina, the neural retina and choroid, B scan images with flow overlay, and complementary color fundus shots. In order to establish if we had found a suspected OSV, we first examined the neuronal retinal slab. Neural retinal clab analysis is performed to validate the identified putative OSV. Next, utilizing the choroidal slabs looked for the link between the OSV and the choroidal veins. If there were discrepancies between the two graders, the misunderstanding was cleared up by C.H., another retina expert. The diameter on the thickest portion of the greatest OSV was used to determine the diameter of the OSVs. The closest vessels that were split off from the central retinal vessel were identified as the central venous initial branches (105).


RELEVANCE

RELEVANCE

The primary retinal vein, which is situated posterior to the lamina cribrosa of the optic nerve system, becomes obstructed due to thrombosis, which is the most frequent cause of central retinal vein constriction. Central retinal vein blockage comes in two flavors: ischemic (nonperfused) and non-ischemic (perfused). Approximately 70% of cases with CRVO are not ischemic. Patients with CRVO often report that their vision in one eye becomes distorted or hazy very rapidly. It won't be painful to lose your sight. Neurological signs such diminished movements of the extraocular muscles, paresthesias, speech impediments, weakened muscles, increased deep tendon responses and ptosis, suggest a diagnosis other than CRVO. The patient may report nonspecific symptoms of visual disturbance or noticeably diminished vision, depending on the kind of CRVO. In a similar vein, they could have a generally normal exam or show indications of color vision loss, reduced visual acuity, or an afflicted eye with an afferent pupillary deficiency. The large number of hemorrhages seen across the retina give central retinal vein occlusions on ocular fundus examination an image of "blood and thunder." Cotton wool patches, injury in retinal nerve fiber layer and optic disc are the expansion of additional fundus finding process. In situations with non-ischemic CRVO, an ophthalmoscopy test often shows tortuosity and mild enlargement of the retinal veins along with hemorrhages in all quadrants. Symptoms of ischemic central retinal vein blockage usually include widespread 4-quadrant bleeding, venous expansion, and substantial retinal edema (106).

We conducted a search of PubMed and Google Scholar beginning with its commencement and extending until June 2021. Ten studies out of the first fifty five offered detailed information on COVID-19 patients that had CRVO. Studies show that 60% of patients were male and that their average age was "39.3 ± 11.6 years." The most prevalent presenting complaints were blurred vision (“40 %”) and reduced vision (“50 %”) respectively. From five days to six weeks after the first complaint of fever, symptoms began to appear. After diabetic retinopathy, the second most common kind of retinal vascular disease is RVO. CRVO is one of its varieties. In the industrialized world, the incidence of CRVO is 0.8 per 1000, while the average number of retinal vein occlusions is 5.20 per 1000. The two subtypes of CRVO are ischemic (non-perfused) and non-ischemic (perfused). Although ischemia CRVO has a less favorable outcome, non-ischemic CRVO is linked to

small visual abnormalities and high visual activity. Ninety percent of patients over 50 had CRVO. Other traditional risk factors include age, diabetes mellitus, glaucoma, hypertension, and hyperlipidemia. As a result, CRVO is often associated with age-related illnesses (107).


METHODOLOGY

1. METHODOLOGY

RESEARCH QUESTION

When individuals over 50 have Central Retinal Vein Occlusion (CRVO), how do the collaterals alter over time?

AIMS AND OBJECTIVES

1. To investigate the progression of collateral vessels following Central Retinal Vein Occlusion in patients aged 50 and older using OCT angiography.
2. To evaluate and measure changes in retinal blood flow parameters in patients with central retinal vein blockage that's 50 years of age or older using OCT angiography.

In order to examine the subsequent parameters in patients diagnosed with Central Retinal Vein Occlusion during four periodic visits on the 1^{st}, 3^{rd} ,6^{th} and 9^{th}months:

1. Vessel density in superficial capillary plexus
2. Vessel density in deep capillary plexus
3. Longest foveal avascular zone on superficial capillary plexus
4. Mean foveal avascularzone on deep capillary plexus
5. Longest foveal avascular zone on deep capillary plexus
6. Mean foveal avascularzone on deep capillary plexus
7. Choriocapillaris vascular density

STUDY DESIGN

A prospective observational study will be implemented at a solitary center for the duration of one year.

STUDY SETTING

The study has been conducted at the Army Hospital Research and Referral Centre, Advanced Centre of Ophthalmological and Visual Sciences, New Delhi-110010.

STUDY PERIOD:

The research will be conducted for duration of one year. From November 1, 2022 to December 31, 2023

SAMPLE SIZE: 26

The formula for calculating sample size is given below

$$n = \frac{t^2 \times (1-P)}{m^2} \quad (17)$$

n= required sample size

t= confidence level at 95% (standard value of 1.96)

p= estimated prevalence

m= margin of error at 5%

INCLUSION CRITERIA:

A patient in the age range of 50 to 70 years old who has a clear media occlusion of the central retinal vein that permits the acquisition of an OCT Angiography scan of all four quadrants of the central 3 x 3 mm^2 area.

EXCLUSION CRITERIA:

1. Co-existing Central retinal Vein Occlusion
2. History of previous Branched retinal vein occlusion/ Central retinal vein occlusion
3. Pre-existing diabetic retinopathy
4. Pre-existing age related macular degeneration
5. Patient unwilling for follow up for 09 months

STUFY TOOLS:

1. A structured proforma for gathering fundamental information (age, gender, date of examination) and collateral vessel findings in CRVO.
2. OCTA device
3. ImageJ with Java 8 (version ij154)
4. Operating system: windows 10

CLASSIFICATION OF COLLATERAL VESSELS, IMAGE ANALYSIS, AND OCT ANGIOGRAPHIC ASSESSMENT OF PARAFOVEAL VESSEL DENSITY

For analysis, the OCTA scan with the greatest picture quality was selected. Using the AngioVue Analytics software (version2017.1.0.151) of the OCTA device, the parafoveal vascular density (VD) of the SCP and DCP was measured in the 3 X 3 mm2 OCTA picture. Within a ring-shaped region of interest that is centered on the fovea and has inner and outer ring diameters of 1 mm and 3 mm, respectively, the program determines the area occupied by blood vesicles. Automatic reporting of the parafoveal VD as a proportion of the entire region is provided. The segmentation boundaries that are utilized to display SCP, DCP, and the

entire retinal thickness are automatically defined by the OCTA device's built-in software. From the internal limiting membrane (ILM) to 9 µm above the inner plexiform layer (IPL), the SCP slab was divided. The DCP slab was divided into segments starting 9 µm above the outer plexiform layer (OPL) and ending 9 µm below the IPL. The internal border of the whole retinal slab is determined by the built-in software at the ILM, while the external boundary is set at 9 µm below the OPL. Manual correction of the segmentation boundaries was carried out in situations of automated software segmentation mistake caused by macular edema or macular thinning. If an eye's central macular thickness (CMT) was 300 µm or more, it was considered to have macular edema related to RVO. Additionally, CMT was recorded using the same integrated program.

In the 3 X 3 mm2 en face angiograms of each eye, every collateral vessel was found. Using corresponding cross-sectional scans with angiographic flow overlay and 3D projection artifact removal (PAR) technology to remove projection artifact, the images were further examined to determine the location of each collateral vessel. Collateral vessels that were seen on en face OCT but did not have a matching flow identified on OCTA were eliminated. Based on whether the collaterals were coursed via the SCP or DCP and the position of parent vessels related to the collateral itself, the collaterals that were chosen for study were categorized into one of four types: true superficial, true deep, superficial diving, and foveal collateral. True superficial collaterals and true deep collaterals, respectively, are the collaterals that join parent blood vessels in the SCP and the DCP, respectively.

Superficial diving collaterals are those that link two superficial vessels together via the DCP. Collaterals that join two superficial blood arteries by spanning the horizontal raphe over the fovea are known as foveal collaterals. Folveal collaterals may be distinguished from superficial diving collaterals because the SCP's segmentation ends closer to the fovea. Using color fundus photos and FA pictures, the collaterals were further divided into veno-venular (V-V) and arterio-venous (A-V) categories (109).

DATA MANAGEMENT AND STATISTICAL ANALYSIS

Depending on the type of result, several statistical techniques are used in the data analysis. The researchers may want to determine if there is a statistically significant difference in the mean values between the two groups if the outcome data are continuous

variables. The paired t-test (for matched samples) is perhaps the most used statistical technique for comparing the differences between two samples if the data is normally distributed (110).

The relationships between the various parameters were found using the Pearson correlation coefficient (111). The Statistical Analysis System ("v.9.1, SAS Inc., Cary, NC") was used to conduct the analyses. The proportions were compared using chi-square tests, and the mean values of the chosen variables were compared between subgroups using t-tests (112). A significant level will be fixed at a p value less than 0.05 .

There are four periodic visits of $1^{st}, 3^{rd}, 6^{th}$ and 9^{th} month.There is no major difference between the $1^{st}, 3^{rd}, 6^{th}$ month in BCVA so we can consider as a single group (first group) and second group would be 9^{th} month. To calculate the p-value for a two-sample t-test comparing the BCVA values between the $1^{st}, 3^{rd}$,6^{th} month and 9^{th} month we utilize the students t-test formula eq (18).

$$t = \frac{\overline{X_1} - \overline{X_2}}{\sqrt{\frac{s_1^2}{n_1} + \frac{s_2^2}{n_2}}} \tag{18}$$

Here, first group in BCVA: $\overline{X_1}$ denotes the mean, s_1 represents the standard deviation and n_1 is the sample size. Similarly, the second group in BCVA: $\overline{X_2}$ is the mean and s_2 denote the standard deviation for the sample size n_2.

The greatest number of logically independent values that may fluctuate in a data sample is referred to as degrees of freedom df. To compute degrees of freedom, take the number of elements in the data sample and remove one.

$$df = n_1 + n_2 - 2 \tag{19}$$

Ophthalmologic examination comprised fluorescein angiography (FA), Goldmann applanation tonometry, OCT, OCTA, slit-lamp biomicroscopy of anterior and posterior segments, and best corrected visual acuity (BCVA) evaluation using standard Early Treatment Diabetic Retinopathy Study (ETDRS) charts. Spectral-domain optical coherence tomography (Spectralis HRA+OCT) was used to get structural OCT images. The

methodology for acquiring structural OCT images included improved depth imaging (EDI) and dense scans , raster and radical with a high number of frames (ART > 25) as well as improved depth imaging (EDI). For the study, only high-quality photos (Topcon's quality index > 80) were taken into account. From 3 x 3mm^2OCTA acquisitions, automatic segmentation into superficial capillary plexa (SCP), deep capillary plexa (DCP), and choriocapillaris (CC) was achieved (113).

Patient's result image is initially loaded into the ImageJ software. Following this, the Image Type is modified to 8-bit image. Following this, the threshold value is modified to accommodate vessel analysis and reduce noice. Then we start analyzing. Vessel Density in Superficial Capillary Plexus: We use OCTA to capture images of the superficial capillary plexus. Define the region of interest (ROI) for vessel density measurement. Calculate vessel density as the percentage of the area occupied by vessels in the defined ROI. Vessel Density in Deep Capillary Plexus: We capture OCTA images specifically focused on the deep capillary plexus. Ensure consistency in imaging parameters across visits. Quantify vessel density as a percentage of the total area in the ROI.

Longest Foveal Avascular Zone on Superficial Capillary Plexus. We identify the foveal avascular zone on OCTA images of the superficial capillary plexus. Measure the longest linear distance across the avascular zone. Mean Foveal Avascular Zone on Superficial Capillary Plexus. We focus on OCTA images of the deep capillary plexus to locate the foveal avascular zone. Capture images consistently across visits. Longest Foveal Avascular Zone on Deep Capillary Plexus. We identify the foveal avascular zone on OCTA images of the deep capillary plexus. Measure the longest linear distance across the avascular zone. Mean Foveal Avascular Zone on Deep Capillary Plexus. We focus on OCTA images of the deep capillary plexus to locate the foveal avascular zone. Ensure consistency in image quality and positioning. Choriocapillaris Vascular Density. We acquire OCTA images specifically targeting the choriocapillaris. Follow a standardized imaging protocol for capturing choriocapillaris vascular patterns. Finally, we plot the result as a correlation matrix that displays correlation coefficients between each pair of parameters. Highlight significant correlations and also Provide as result excel sheet.


RESULTS

RESULTS

A collaterals after occurrence of CRVO using OCTA for 26 patients results received at the Advanced Centre of Ophthalmologic and Visual Sciences, ARMY Hospital.

1. Sex Distribution of cases in study

Out of the 26 cases 20 were (77 %) males & 6 (23 %) were females with male to female ratio 3.33:1. There was remarkable male dominance.

Gender	Number of Cases	Percentage
Female	6	23 %
Male	20	77%
Total	**26**	**100%**

Table: 7 Sex Distribution of cases in study (n =26)

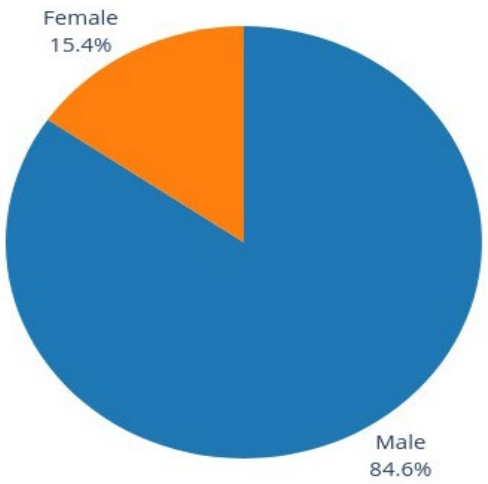

Figure: 87 Pie chart of sex distribution

2. Age distribution of study population in different genders of study population

`The subjects' ages varied over fifty years. With a mean age of 53.4 (standard

deviation of 8.76), the age group 61–70 years accounted for the greatest number of cases (46.1%), next to 51–60 years (42.3%).

Age Group	Number of Cases		Total (Percentage%)
	Females	Males	
51-60	1	10	11(42.3%)
61-70	4	8	12(46.1%)
71-80	1	2	3(11.5%)
Total	**6**	**20**	**26(100%)**

Table: 8 Age distribution of study population (n=26)

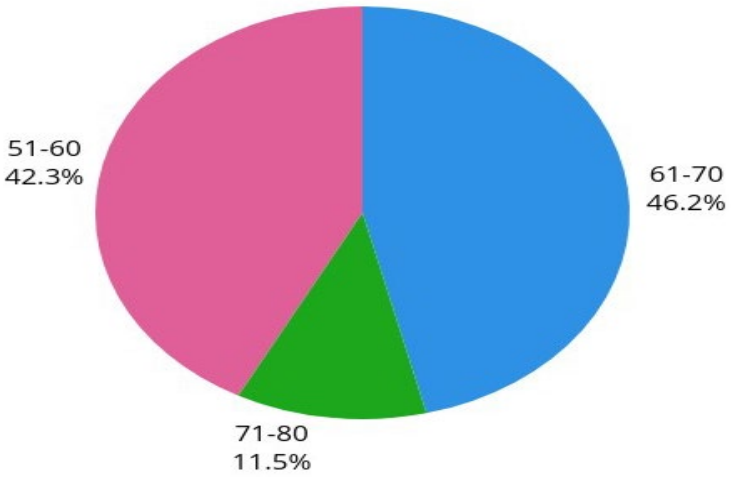

Figure: 88 Pie chart of age distribution in study population

3 . Disc edema

Among the 26 patients, 13 patients (50%) have swelling of the nerve fiber layer at the optic nerve head. Out of the 13 patients 4 were (66.6%) females and 9 (45%) were males with male to female ratio 2.25:1. The domination of male was remarkable.

Patient group	Total patients	Patients with swelling	Percentage of female patients	Percentage of male patients
Female	6	4	66.6%	-
Male	20	9	-	43.4%
Total	**26**	**13**	**-**	**-**

Table: 9 Patient demography and characteristics

Maximum number of patients belonged to age group 51-60 years (46.1%) followed by 61-70 years (46.2%) with a mean age of 60.3.

Age group	Number of cases		Total (%)
	Female	Male	
51-60	1	5	46.1%
61-70	3	3	46.1%
71-80	-	1	7.6%
Total	**4**	**9**	**100%**

Table: 10 Traits specify to age

4. Hemorrhages at macula

Hemorrhages at the macula causes deterioration of visual acuity within seconds or minutes. A frequent effect of extreme myopia that, if left untreated, can lead to poor vision is myopic macular neovascularization (m-MNV), which often displays as a macular hemorrhage. In the study there is a meal hemorrhages at macula with 20 cases (76.92%) compared to females with 6 cases (23.07%). Hemorrhages at macula is higher in age group within 50 to 60 years with 11 cases (42.30%) of which males are more frequently involved than female with 10 (38.46%) cases and 1 (3.84%) case respectively.

Patient group	Number of cases		Total (%)
	Female	Male	
51-60	1	10	42.3%

61-70	4	8	46.1%
71-80	1	2	11.5%
Total	**76.93%**	**23.07%**	**100%**

Table: 11 Age and gender distribution of Hemorrhages at macula

5. SCP vessel density in 1^{st} visit

Vessel density of the SCP was found using OCTA imaging method. Out of the 26 patients 13 (50%) cases between the range of 21 to 30 and 8 (30.76%) between the 30 to 40 range.

Range of VD	SCP Vessel density in 1^{st} visit		Total (%)
	Female (%)	Male (%)	
1-10	1 (16.6%)	2 (10%)	3(11.5%)
11-20	-	2(10%)	2(7.7%)
21-30	1(16.6%)	12 (60%)	13(50%)
31-40	4(66.6%)	4 (20%)	8(30.7%)
Total	**6(100%)**	**20(100%)**	**26(100%)**

Table: 12 Range of SCP Vessel Density and Gender Distribution in First Visit

6. DCP vessel density in 1^{st} visit

An investigation of the DCP (Deep Capillary Plexus) vascular density in the 26 patients included in the research indicated that 18 patients reported ranges between 81 to 90. None of the patients, remarkably, were in the 70–80 range. This distribution highlights the group's variation in DCP vessel density, with a noteworthy lack of values falling within the defined range of 70–80.

Range of VD	DCP Vessel density in 1^{st} visit		Total (%)
	Female (%)	Male (%)	
51-60	1(16.6%)	4 (20%)	5 (19.23%)
61-70	-	3 (15%)	3
71-80	-	-	-
81-90	5(83.3%)	13 (65%)	18 (69.23%)
Total	**6**	**20**	**26 (100%)**

Table: 13 Range of DCP Vessel Density and Gender Distribution in First Visit

7. Measurement of FAZ

In contrast to traditional photography, the digital format of the images allows us to work with them. The higher FAZ seen in the unadjusted picture is most likely the result of the contrast's loss of detail. Since the picture's size remains unchanged after the modifications, it seems improbable that this area reduction is an artifact. OCTA can poroduce quantitative parameters, including the area of the FAZ of the SCP. The mean FAZ area was significantly larger at superficial retinal layer compares to DCP. At baseline, the CRT was correlated with the DCP, and at month 6 the macular vascular density in the SCP had considerably dropped. There was a significant rise in the FAZ and FAZ perimeter at months 6 and 12. At month 12, there was a negative correlation between the changes in BCVA and the macular vascular density in SCP.

FAZ MEAN : SCP

Range of VD	FAZ MEAN : SCP		Total (%)
	Female (%)	Male (%)	
41-50	2 (33.3%)	1 (5%)	3 (11.5%)
51-60	1 (16.6%)	4 (20%)	5 (19.23%)
61-70	-	5 (25%)	5 (19.23%)

71-80	1 (16.6%)	5 (25%)	6 (23.07%)
81-90	1 (16.6%)	3 (15%)	4 (15.3%)
91-100	-	-	-
101-110	1 (16.6%)	2 (10%)	3 (11.5%)
Total	**6 (100%)**	**20 (100%)**	**26 (100%)**

Table:14 Gender-wise distribution of mean FAZ in SCP

FAZ LONGEST: SCP

Range of VD	FAZ LONGEST: SCP		Total (%)
	Female (%)	Male (%)	
51-60	2(33.3%)	1 (5%)	3 (11.5%)
61-70	-	2 (10%)	2 (7.69%)
71-80	2 (33.3%)	9 (45%)	11 (42.3%)
81-90	-	3 (15%)	3 (11.53%)
91-100	-	2 (10%)	2 (7.69%)
101-110	1 (16.6%)	1 (5%)	2 (7.69%)
111-120	-	-	-
121-130	1 (16.6%)	2 (10%)	3 (11.53%)
Total	**6 (100%)**	**20 (100%)**	**26 (100%)**

Table:15 Range and gender-wise distribution of longest FAZ in SCP

FAZ LONGEST: DCP

Range of VD	FAZ LONGEST: DCP		Total (%)
	Female (%)	Male (%)	
71-80	1 (16.6%)	2 (10%)	3 (11.53%)

81-90	-	5 (25%)	5 (19.23%)
91-100	3 (50%)	6(30%)	9 (34.61%)
101-110	-	2 (10%)	2 (7.69%)
111-120	-	-	-
121-130	2 (33.3%)	3 (15%)	5 (19.23%)
131-140		2 (10%)	2 (7.69%)
Total	**6 (100%)**	**20 (100%)**	**26 (100%)**

Table: 16 Gender-wise distribution of longest FAZ in DCP

FAZ MEAN: DCP

Range of VD	FAZ MEAN: DCP		Total (%)
	Female (%)	Male (%)	
61-70	1 (16.6%)	2 (10%)	3 (7.69%)
71-80	-	5 (20%)	-
81-90	3 (50%)	6 (30%)	9 (34.61%)
91-100	-	2 (10%)	2 (7.69%)
101-110	-	-	-
111-120	2 (50%)	3 (25%)	5 (30.76%)
121-130	-	2 (10%)	2 (7.69%)
Total	**6 (100%)**	**20 (100%)**	**26 (100%)**

Table: 17 Gender-wise distribution of mean FAZ in DCP

11. CHORIOCAPILLARIS VD

In clinical practice the analysis of the choriocapillaris vessel density is used to identify the choriocapillaris changes in early phases.

Range of VD	CHORIOCAPILLARIS VD		Total (%)
	Female (%)	Male (%)	
30-40	2 (50%)	4 (20%)	6 (23%)
41-50		2 (10%)	2 (7.69%)
51-60	3 (50%)	8 (40%)	11 (42.3%)
61-70		2 (10%)	2 (7.69%)
71-80	1 (16.6%)	4 (20%)	5 (19.23%)
Total	**6 (100%)**	**20 (100%)**	**26 (100%)**

Table: 18 Choriocapillaris vessel density

P-VALUE

A p-value of < 0.05 will be considered statistically significant. The p-value for our study is lower than 0.05 for only 4 of the 26, members to were studied. This indicates that there is a statistically significant connection or difference in the data being studied for these 4 members.

Table: 19 Comparison of BCVA between two groups with t-test results

S.No	BCVA		P-VALUE (Paired t-test)
	First group	Second group	
1	0.42 ± 0.36	0.46 ± 0.53	< 0.015
2	0.37 ± 0.28	0.46 ± 0.53	0.76
3	0.46 ± 0.29	0.33 ± 0.33	0.69
4	0.46 ± 0.56	0.21 ± 0.25	< 0.01
5	0.42 ± 0.36	0.44 ± 0.42	0.92

6	0.46 ± 0.29	0.33 ± 0.33	0.06
7	0.38 ± 0.28	0.21 ± 0.25	< 0.025
8	0.38 ± 0.33	0.44 ± 0.42	0.61
9	0.38 ± 0.33	0.37 ± 0.28	0.92
10	0.42 ± 0.35	0.46 ± 0.53	0.92
11	0.46 ± 0.29	0.33 ± 0.33	0.13
12	0.37 ± 0.28	0.21 ± 0.25	< 0.03
13	0.37 ± 0.28	0.44 ± 0.42	0.24
14	0.42 ± 0.35	0.37 ± 0.28	0.6
15	0.42 ± 0.31	0.42 ± 0.35	0.8
16	0.35 ± 0.28	0.46 ± 0.53	0.3
17	0.36 ± 0.28	0.46 ± 0.53	0.42
18	0.36 ± 0.33	0.33 ± 0.33	0.53

PHOTOGRAPHS

PHOTOGRAPHS

Let's talk about a few of the 26 patient samples as an example. In the case 1figure (89-94) demonstrates a male patient with OS and OD who was evaluated over the course of four visits at the 1^{st}, 3^{rd},6^{th} and 9^{th}months, Each phase's ART and HR show a discernible difference. OS was affected by the CRVO.

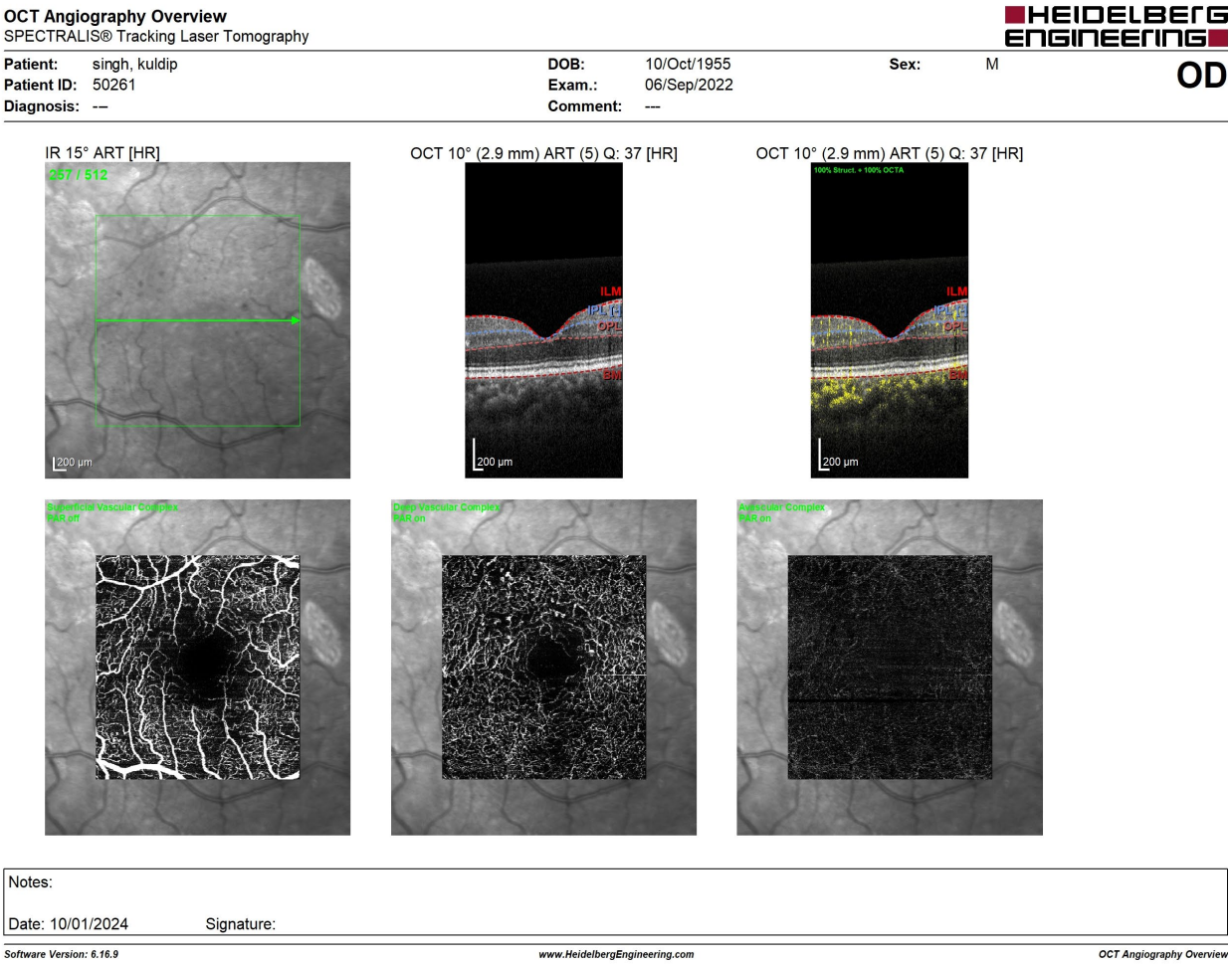

Figure: 89 This image was taken on September 6, 2022, during the first visit for OD.

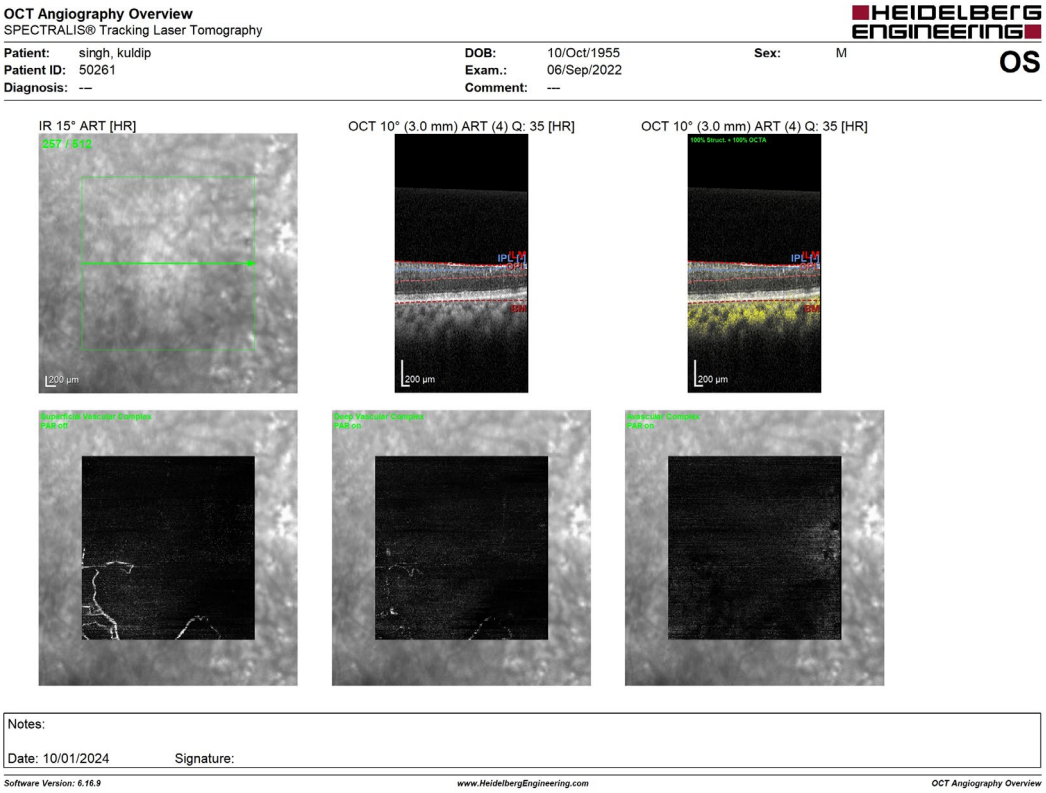

Figure: 92This image was taken on September 6, 2022, during the first visit for OS.

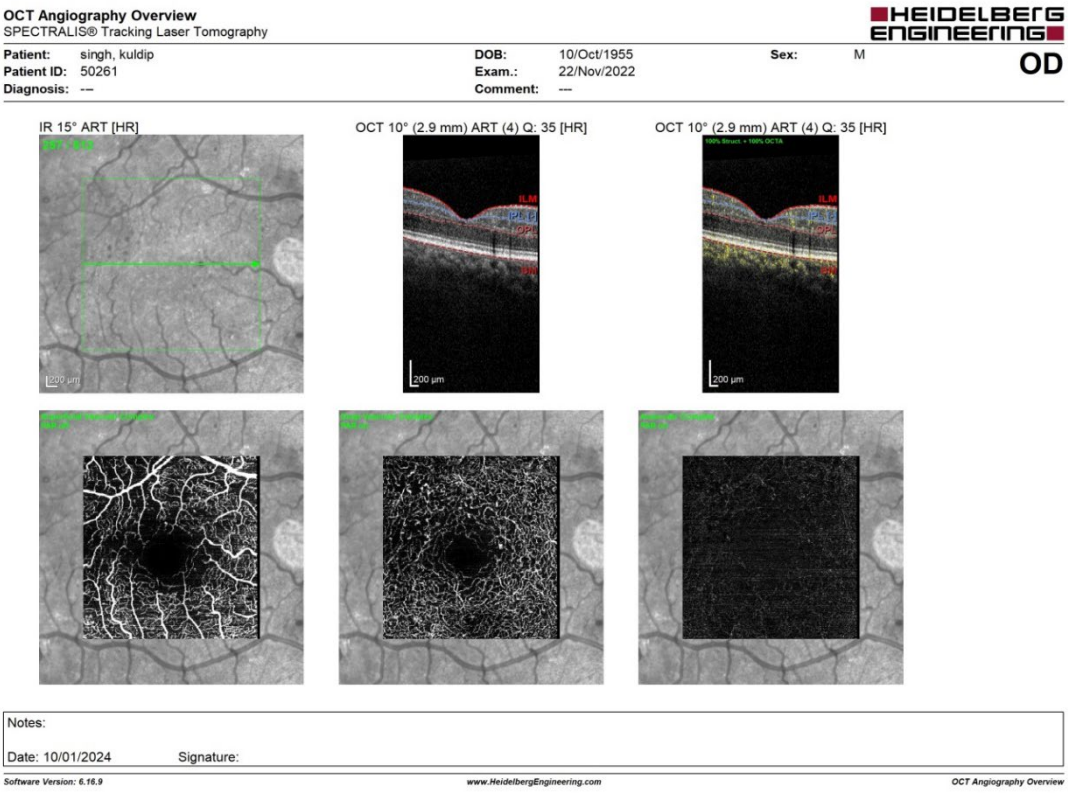

Figure: 93 This image was taken on November 22, 2022, during the second visit for

OD.

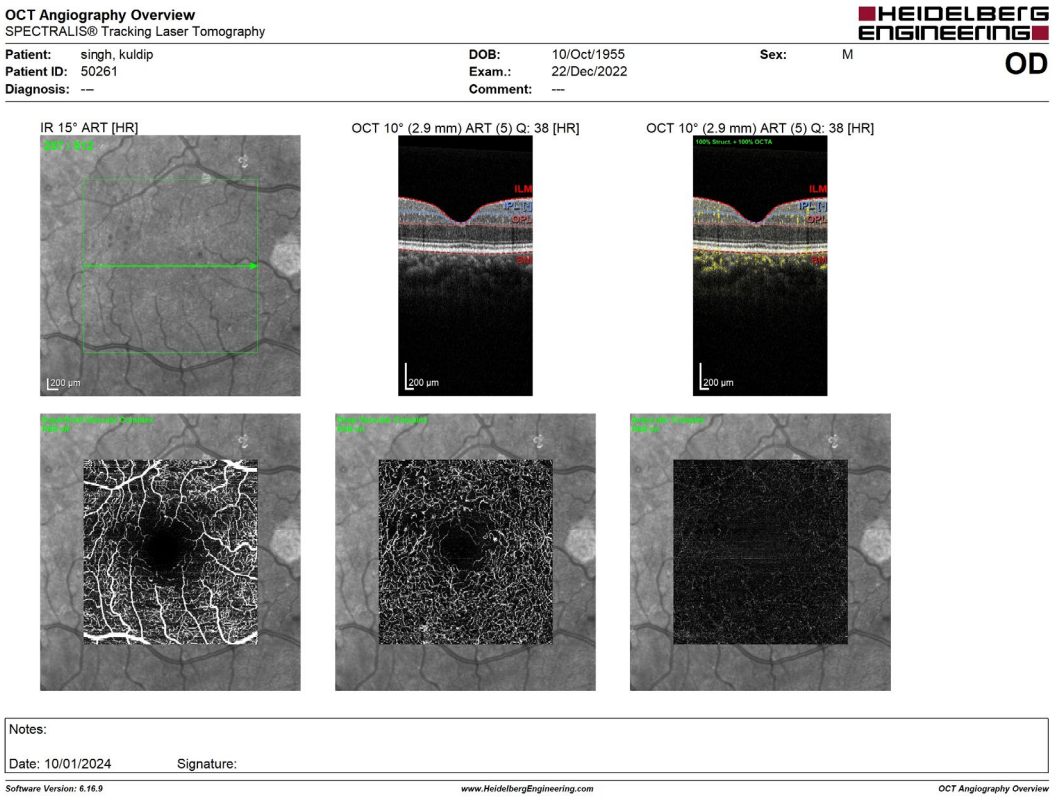

Figure: 94 This image was taken on December 22, 2022, during the third visit for OD.

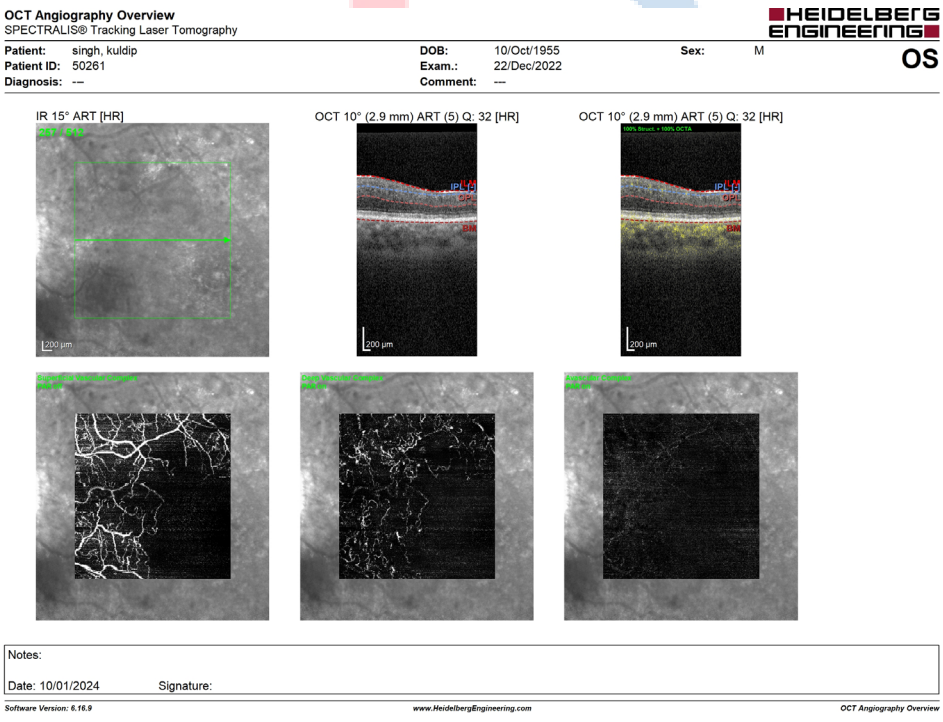

Figure: 93 This image was taken on December 22, 2022, during the third visit for OS.

The blink artifact, which results from the patient's eyelid moving quickly, is one of the most common kinds of artifacts. Which are the source of the interference in the OCTA (Fig 94)

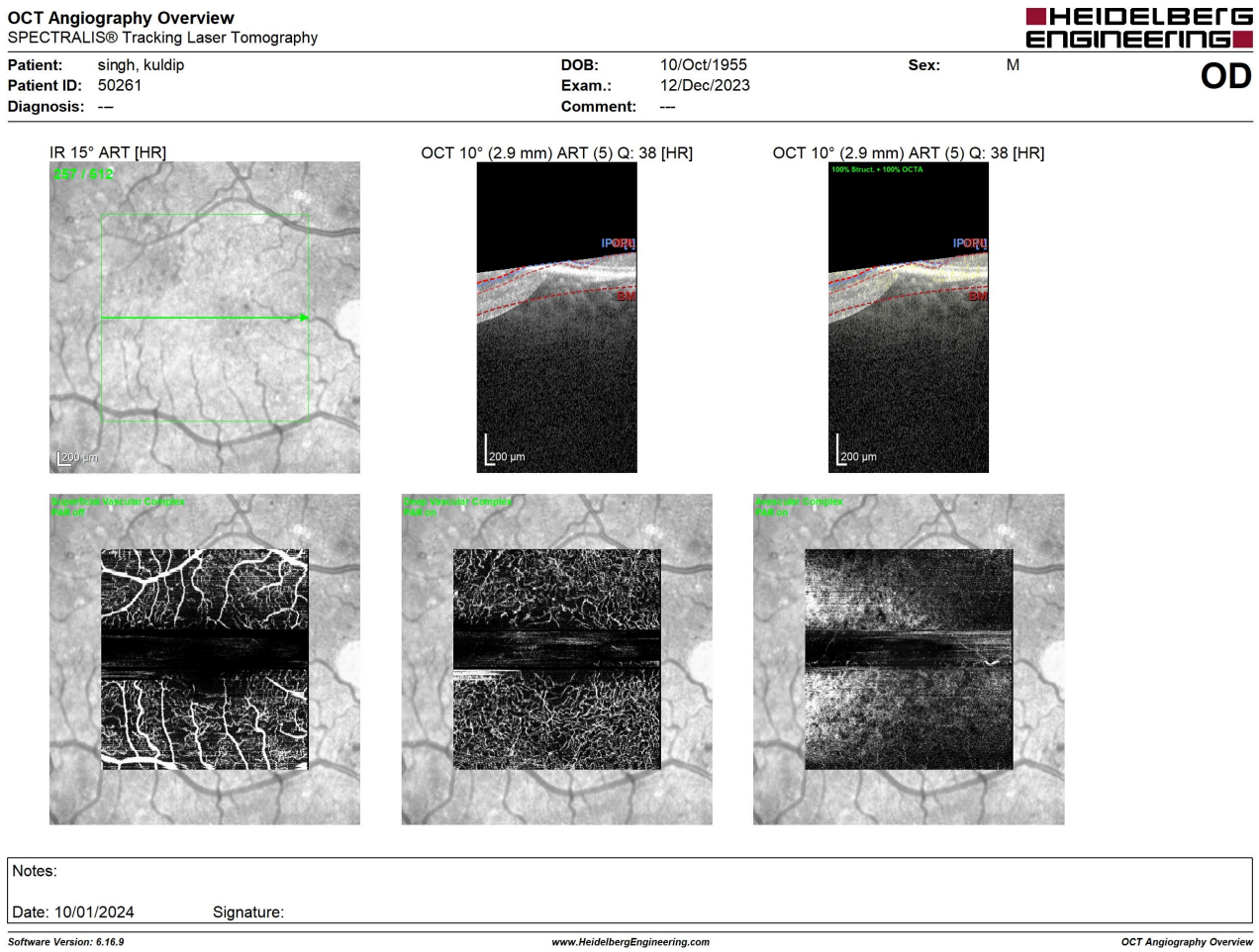

Figure: 94 Cause of blink artifact during December 22, 2022, third visit for OD.

This patient was diagnoised and presence of CRVO is resulted in the OD. Case 2 outcome is shown in figure 95-100.

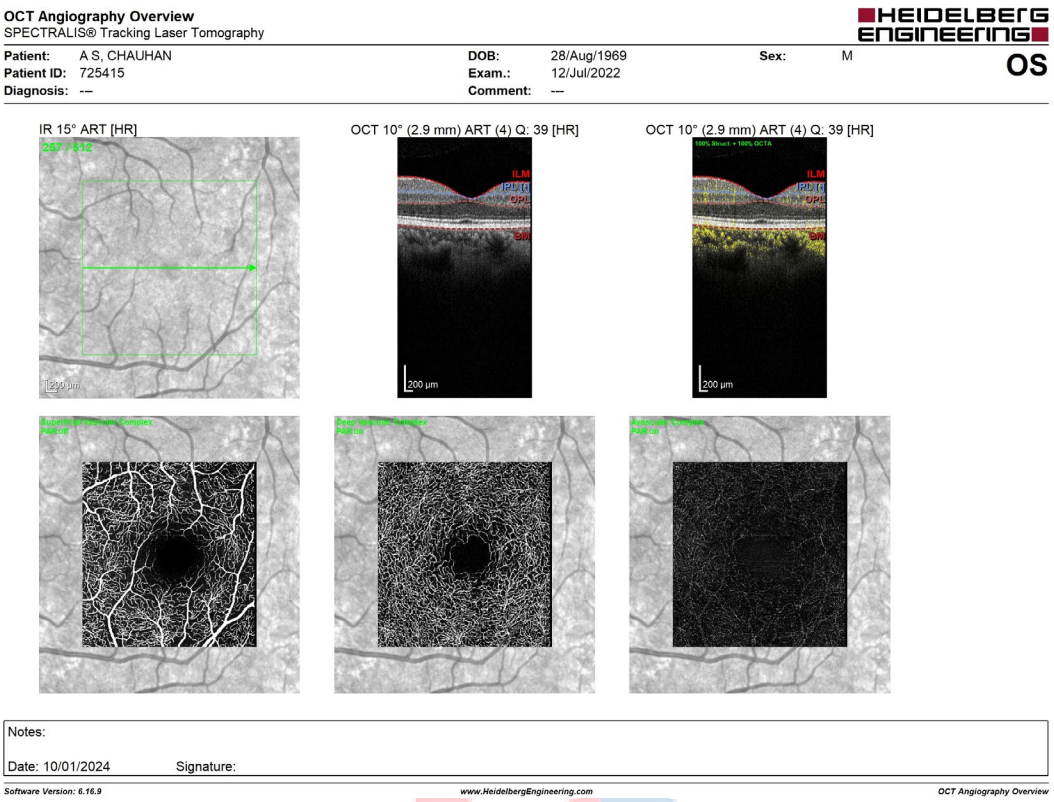

Figure: 95 This image was taken on July 12, 2022, during the first visit for OS.

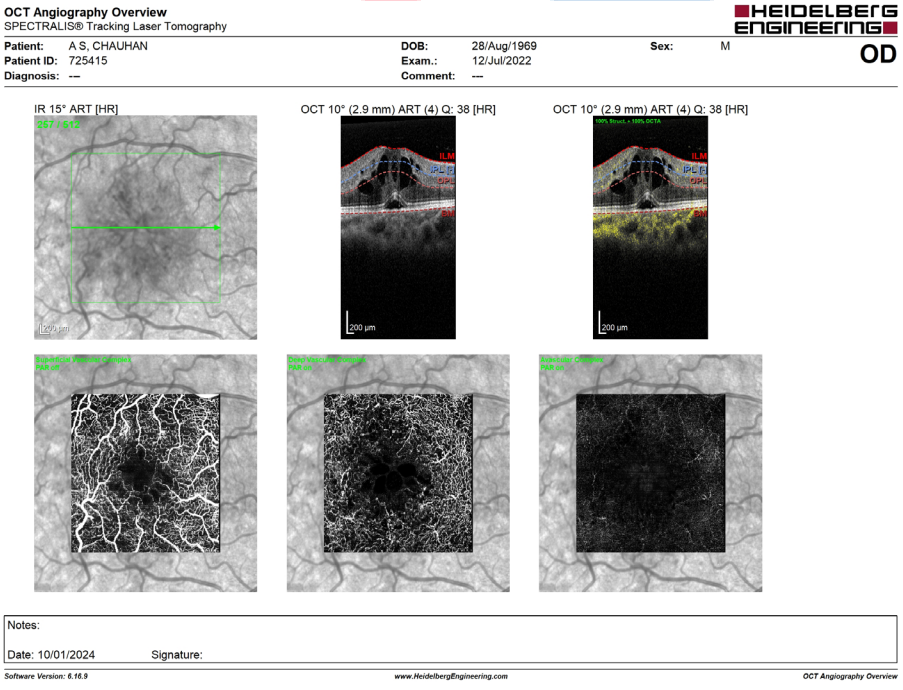

Figure: 96 This image was taken on July 12, 2022, during the first visit for OD.

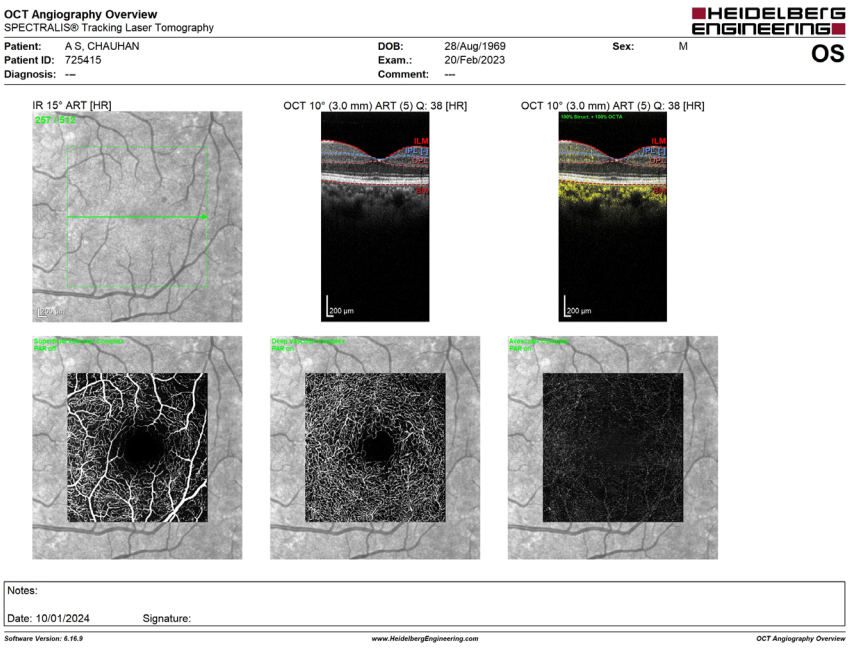

Figure: 97 This image was taken on February 20, 2023, during the second visit for OS.

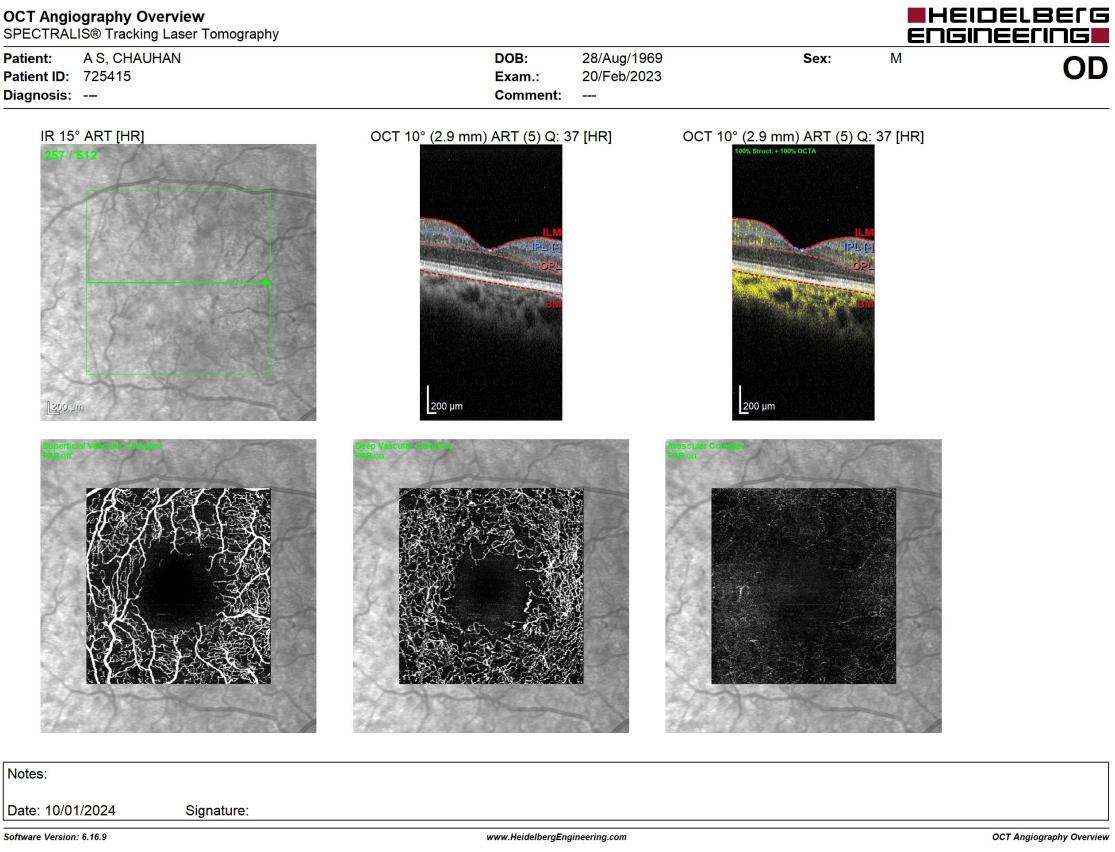

Figure: 98 This image was taken on February 20, 2023, during the second visit for OD.

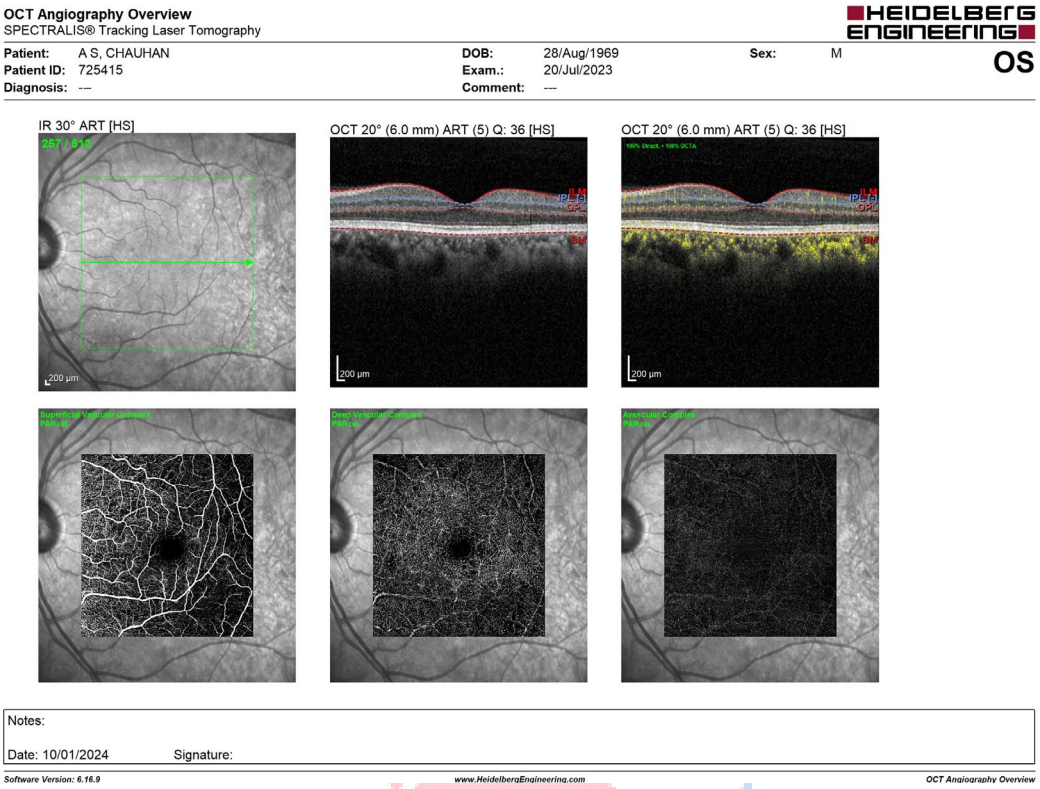

Figure: 99 This image was taken on July 20, 2023, during the second visit for OS.

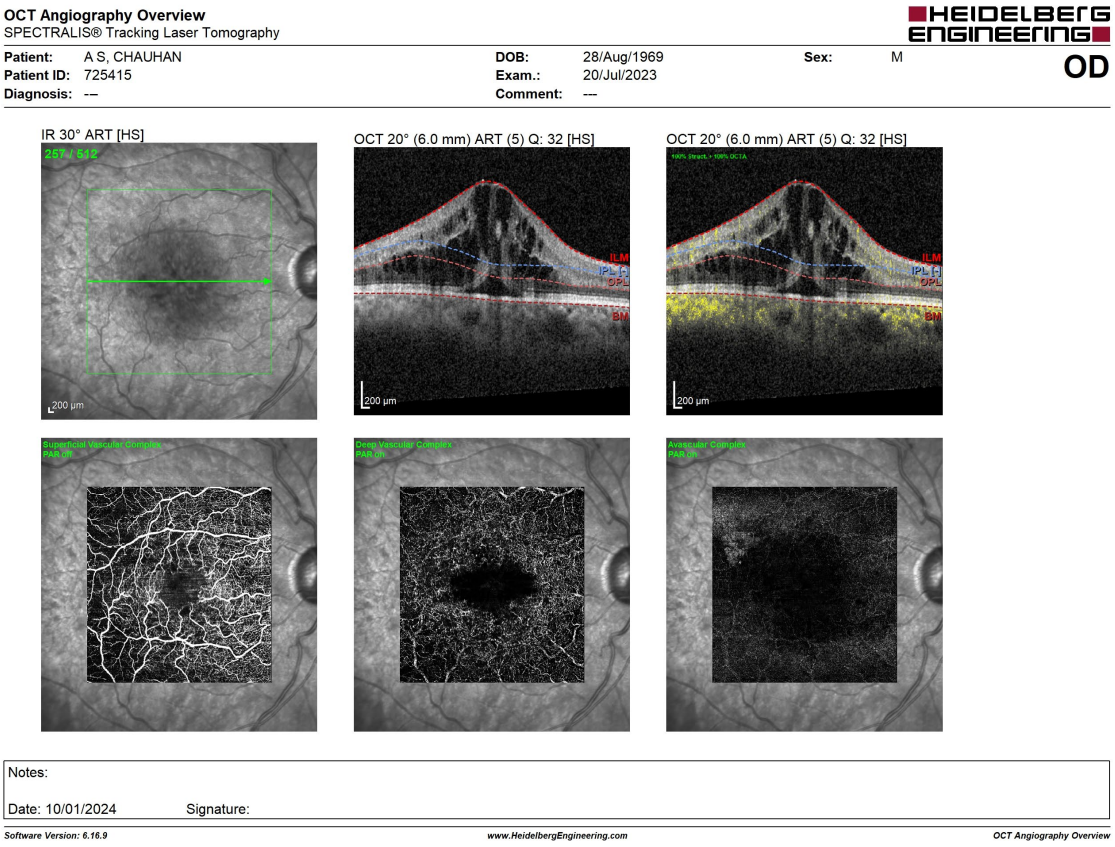

Figure: 100 This image was taken on July 20, 2023, during the second visit for OD.

The OCTA imaging method was used to diagnose this patient, and the OS was affected by the presence of CRVO. Case 3

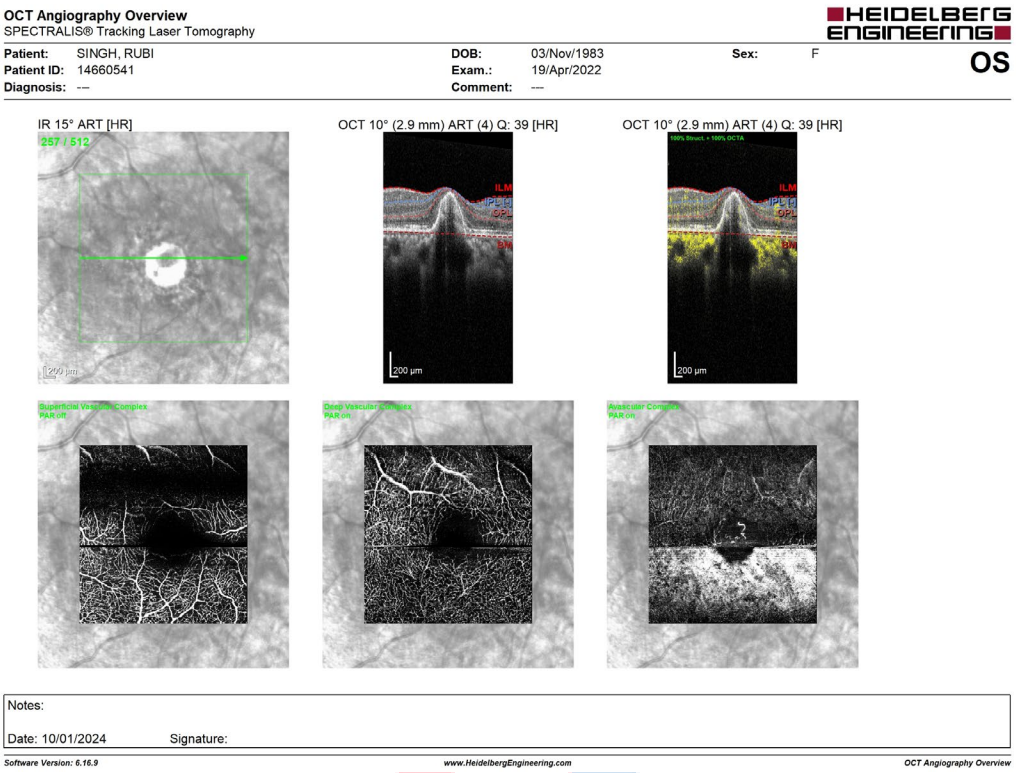

Figure: 101 This image was taken on April 19, 2022, during the first visit for OS.

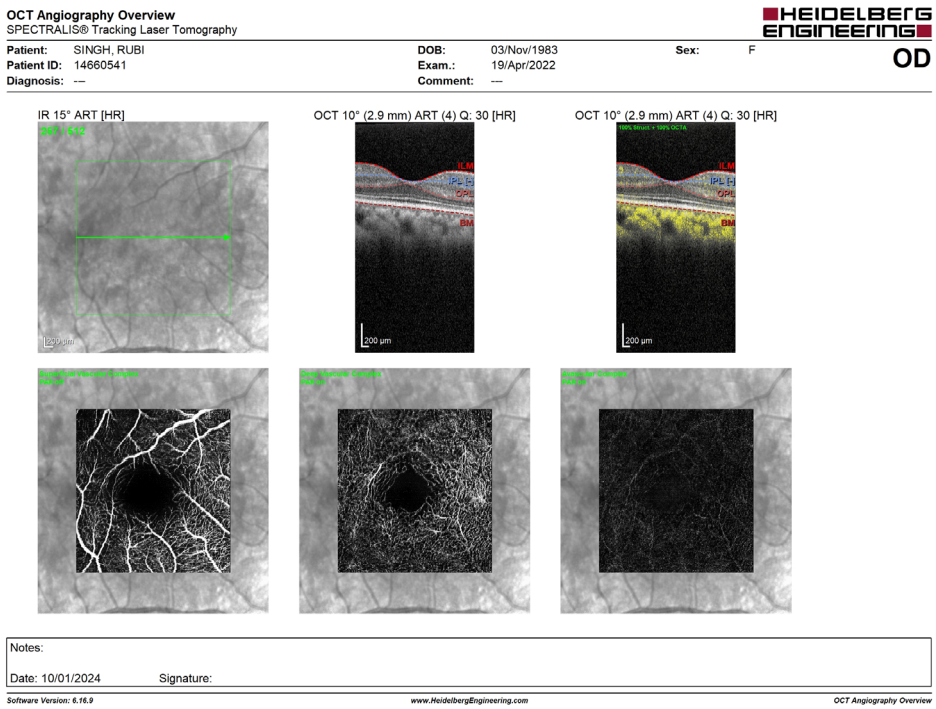

Figure: 102 This image was taken on April 19, 2022, during the first visit for OD.

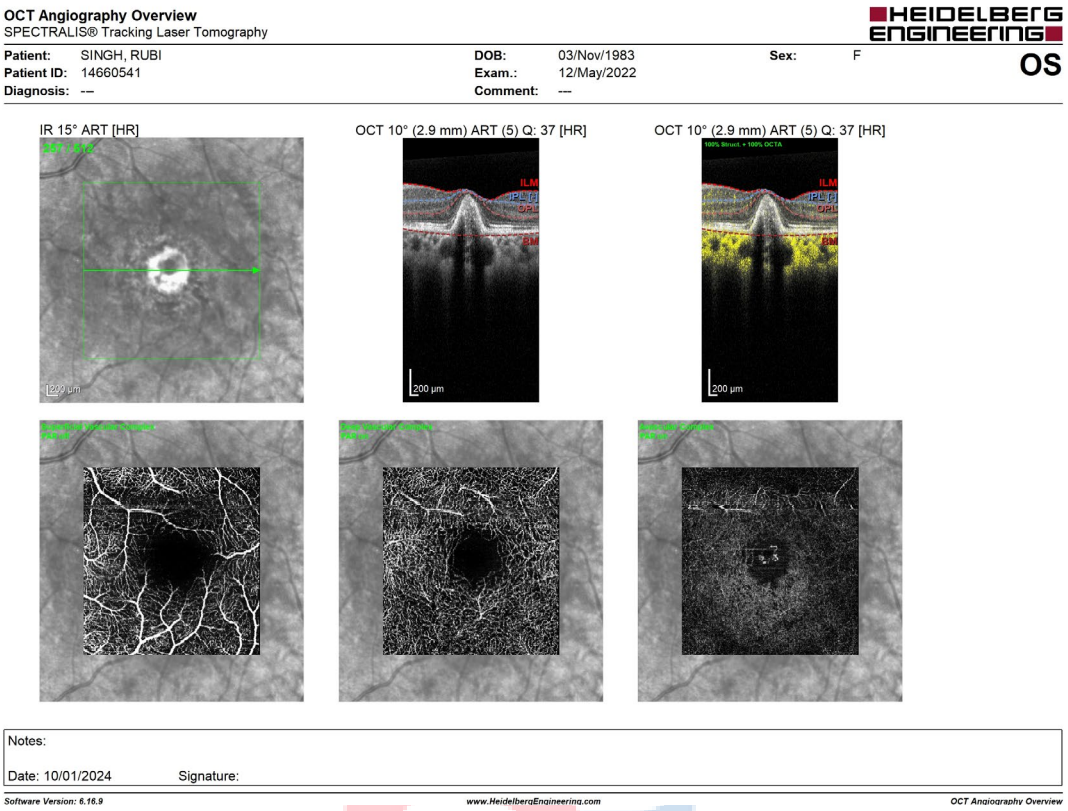

Figure: 103 This image was taken on May 12, 2022, during the second visit for OS.

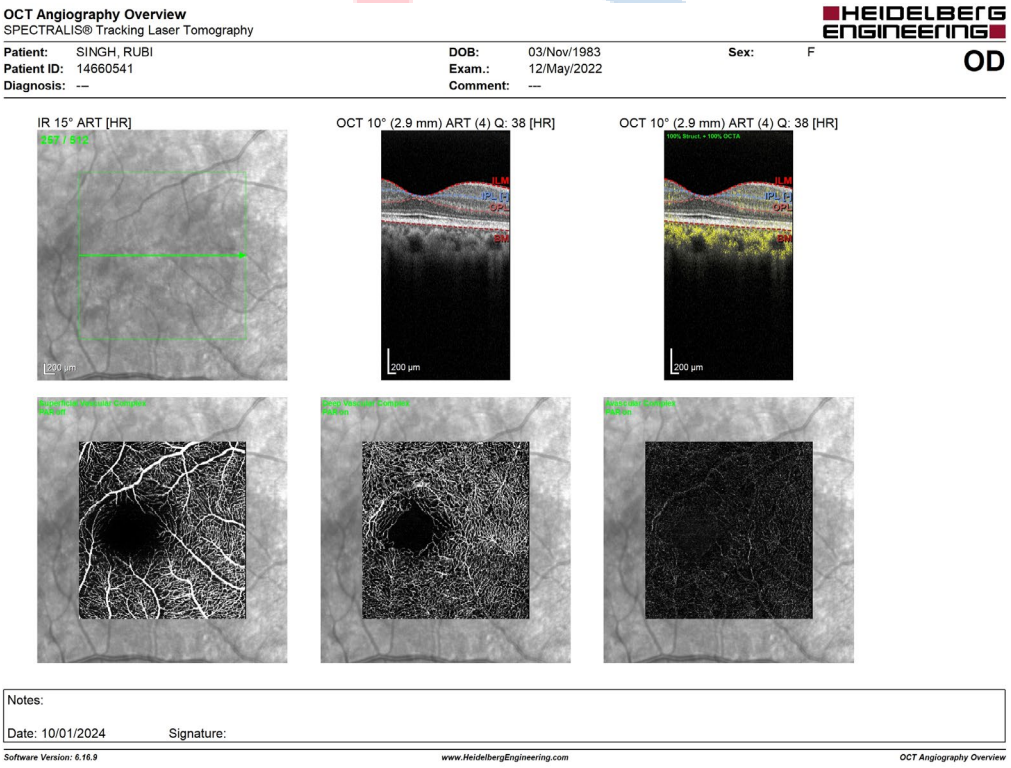

Figure: 104 This image was taken on May 12, 2022, during the second visit for OD.

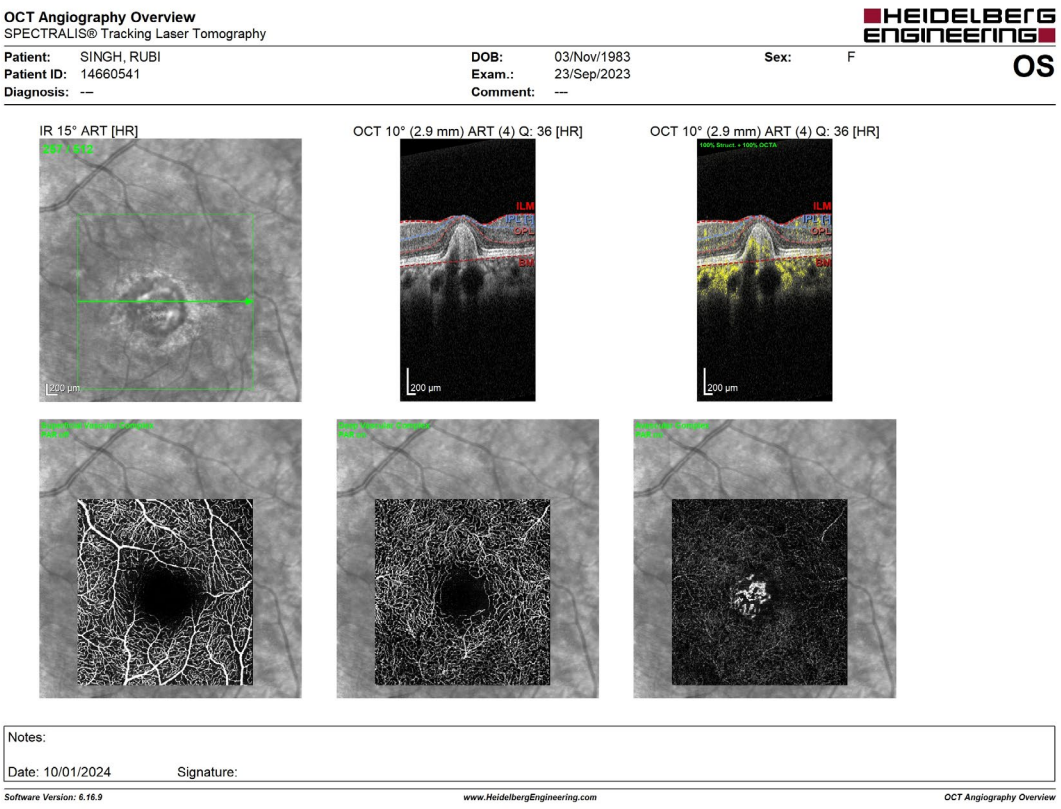

Figure: 105 This image was taken on September 23, 2022, during the third visit for OS.

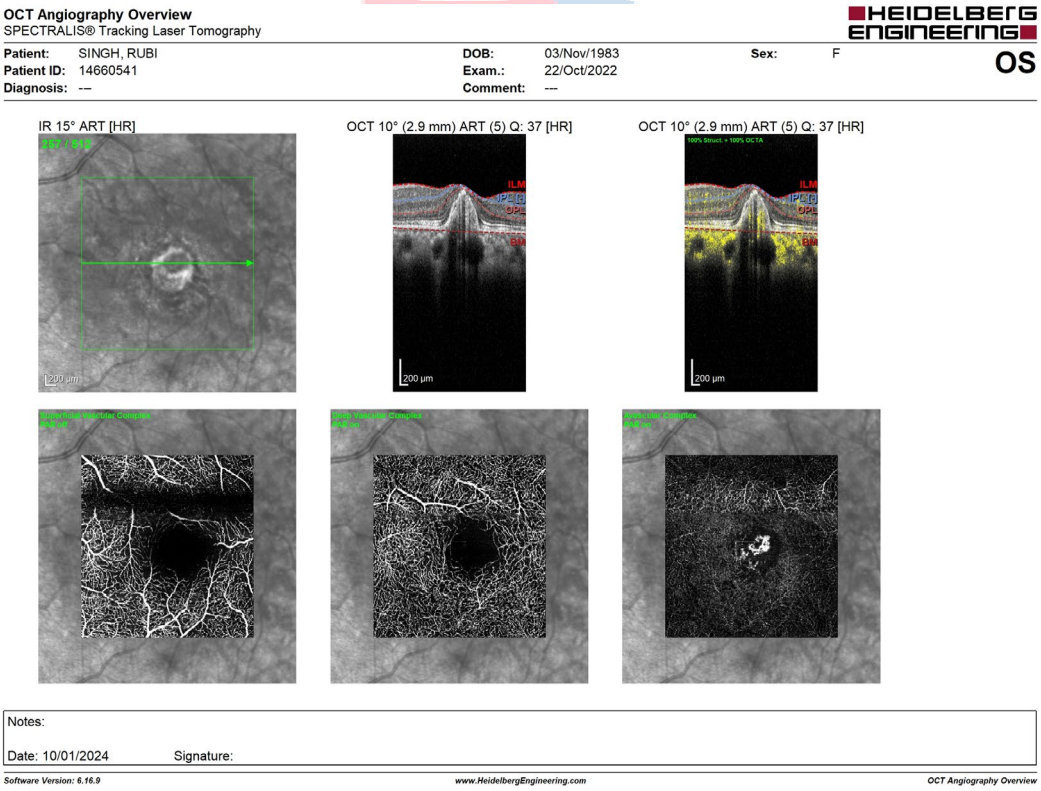

Figure: 106 This image was taken on October 22, 2022, during the third visit for OS.

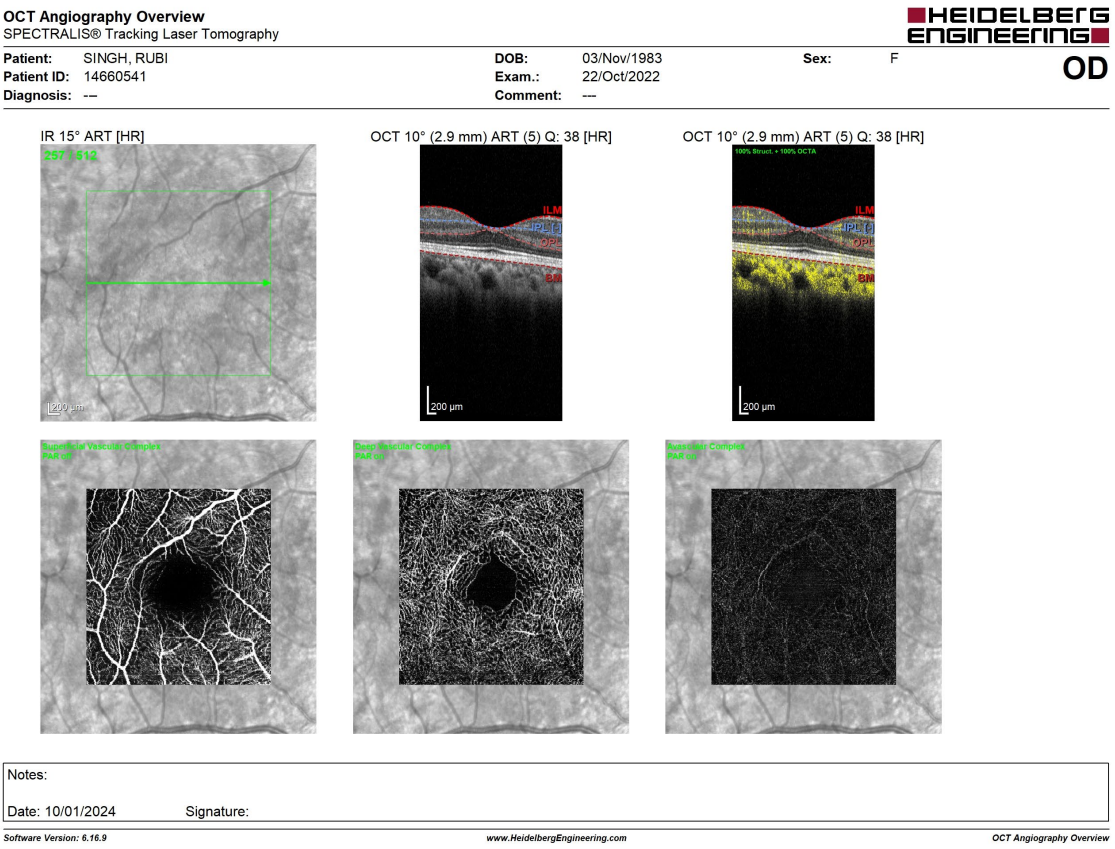

Figure: 107 This image was taken on October 22, 2022, during the third visit for OD.


DISCUSSION

DISCUSSION

Comparison of mean age group in different studies

In the present study majority of cases belonged to age group 61-70 yrs (46.1%) (118). concluded that 50-60 is the most common age group for the CRVO. Reported 50 -70 yrs as the commonest age group (114, 115).

Comparison of male to female ratio in different studies

In the present study, it was observed that 20 cases (77%) were males and 6 (23%) were females,with male to female ratio of 3.33:1.Various studies conducted by authors in (116-118)and others also revealed increased proportion in males indicating that sudden vision loss from all causes was more common in men. Unlike other studies (119), females outnumbered males in the study

Study	Male:Female ratio
Present study	3.33:1
117	11:9
116	2.33:1
118	1.69:1

Table: 20 Comparison of male to female ratio in different studies

Comparison of Macular edema

Out of the 26 patients 13 patients (50%) have swelling of the nerve fiber layer at the optic nerve head. This was similar to studies conducted by authors of (120). Studies conducted by author of (121) showed similar frequencies of macular edema (122).

Study	Macular edema	
	DME	No DME
Present study	50%	50%
120	21.87%	23.43%
121	63.42%	56.42%
122	23.68%	76.31%

Table: 21 Comparison of macular edema

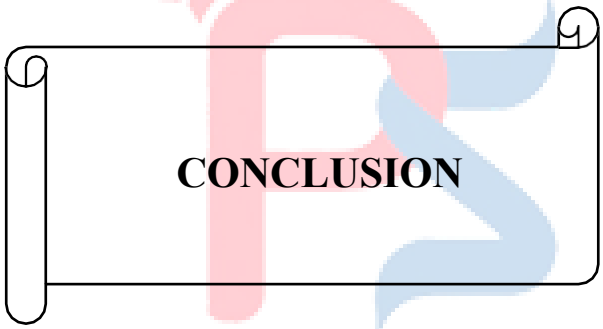
CONCLUSION

CONCLUSION

The serious and sometimes fatal illness known as central retinal vein occlusion (CRVO) mostly affects the elderly. Historically, subtypes of central retinal vein occlusion have been divided into ischemic and nonischemic groups according on the level of retinal capillary nonperfusion shown on OCTA. ME, VH, NV, and NVG are the main contributors to visual morbidity and problems associated with CRVO. Increased venous pressure in RVO results in capillaries leaking out of their regular gaps and the development of macular degeneration, which eventually results in vision loss. Moreover, the course of RVO, which is the consequence of neovascularization of the retina and iris, is determined by the degree of retinal ischemia.

When it comes to retinal imaging fundus, OCT and intravenous fluorescein angiography are two of the most often used imaging modalities. This is because they provide a plethora of knowledge on the structure and morphology of the retina.

Optical coherence tomography (OCT) is a transparent study of three-dimensional pictures used for the quick and accurate assessment of the macula in order to identify and monitor eye problemsThis OCT device may be used to measure the amount of fluid deposit in the macula layer, the volume of vitreous deposited in the retinal layer, the extent of subretinal fluid, and the detachment of the retinal pigment epithelium (RPE) in cases with CSCR. It has been shown that pathophysiologic anomalies in CSCR may be better understood with the use of high-speed, three-dimensional OCT equipment.

With the advancement of imaging technology, there has been a considerable increase in need for developing computational tools and algorithms to quantify medical pictures. If robots could understand and interpret medical images, it would be easier to analyze them. Experts may use automated picture analysis to detect conditions sooner and treat patients more swiftly and conveniently. An non-invasive, non-contact imaging method called optical coherence tomography may be used to provide high resolution cross-sectional images of living tissues. It works like an ultrasound scanner, except instead of using sound waves, it uses light rays. It is based on the theory of interference from light. The OCT system uses the time delay data to generate a depth profile of the sample by measuring the light waves that are reflected back from different sample depths. The sample structure is traversed by the beam laterally to create three-dimensional pictures.

In this research 26 patients where Male (62.86%) and (37.14%) of female are monitored to 9 months and they have 4 visits of 1^{st}, 3^{rd},6^{th} and 9^{th}months. Following parameters have been identified in patients with Central Retinal Vein Occlusion. Further through the statistical analysis with use of student's t-test the results have been performed. All patients are revealed (ME), hemorrhage at macula, IOP and RAPD. (BCVA) evaluation using standard Early Treatment Diabetic Retinopathy Study (ETDRS) charts. The patients result image from OCTA was loaded into the ImageJ software and threshold value is modified to accommodate vessel analysis and to reduce noice. Faz Longest: SCP, Faz Mean: SCP, Faz Longest: DCP, Faz Mean: DCP and Choriocapilaris Vessel density are analyzed using the software. We have concluded the findings of CRVO in the patients above 50 years.

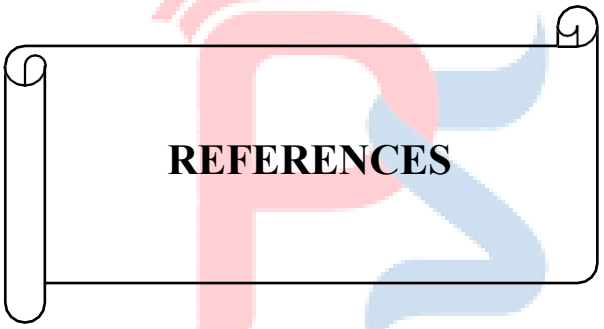

REFERENCES

REFERENCES

1. Padmasini, N. Machine learning and deep learning based strategies for diagnosis of diabetic maculopathy from sdoct retinal scans
2. Hemalakshmi, G. R. Diabetic retinal diseases detection in fundus images using intelligent models.
3. Chen, L., Yuan, M., Sun, L., Wang, Y., & Chen, Y. (2020). Evaluation of microvascular network with optical coherence tomography angiography (OCTA) in branch retinal vein occlusion (BRVO). *BMC ophthalmology*, *20*, 1-9.
4. Fan, L., Zhu, Y., & Liao, R. (2022). Evaluation of macular microvasculature and foveal avascular zone in patients with retinal vein occlusion using optical coherence tomography angiography. *International Ophthalmology*, 1-8.
5. Selvam, A., Ong, J., Bollepalli, S. C., Chhablani, J., & Vupparaboina, K. K. (2023). Artificial Intelligence in Choroid Through Optical Coherence Tomography: A Comprehensive Review. *Authorea Preprints*.
6. Iqbal, S., Khan, T. M., Naveed, K., Naqvi, S. S., & Nawaz, S. J. (2022). Recent trends and advances in fundus image analysis: A review. Computers in Biology and Medicine, 106277.
7. Dash, P., & Sigappi, A. N. (2018, July). Detection and classification of retinal diseases in spectral domain optical coherence tomography images based on SURF descriptors. In 2018 IEEE International Conference on System, Computation, Automation and Networking (ICSCA) (pp. 1-6). IEEE.
8. Oghalai, T. P., Long, R., Kim, W., Applegate, B. E., & Oghalai, J. S. (2023). Automated Segmentation of Optical Coherence Tomography Images of the Human Tympanic Membrane Using Deep Learning. Algorithms, 16(9), 445.
9. Grigoryan, E. N. (2022). Self-Organization of the Retina during Eye Development, Retinal Regeneration In Vivo, and in Retinal 3D Organoids In Vitro. *Biomedicines*, *10*(6), 1458.
10. Lakshminarayanan, V., Kheradfallah, H., Sarkar, A., & Jothi Balaji, J. (2021). Automated detection and diagnosis of diabetic retinopathy: A comprehensive survey. Journal of imaging, 7(9), 165.
11. BV, S. K. Unsupervised and supervised retinal vessels extraction methods from the fundus images.
12. Rahman, M. A., Rabbani, M., Maruf, M. H., Islam, A., & Shihavuddin, A. S. M.

(2022). Characterizing the Aging Process of the Human Eye: Tear Evaporation, Fluid Dynamics, Blood Flow, and Metabolism-Based Comparative Study. BioMed Research International, 2022.

13. Guevara-Leon, F., Grave-Capistrán, M. A., Flores-Campos, J. A., Torres-Ariza, J. L., Alcántara-Arreola, E. A., & Torres-SanMiguel, C. R. (2023). Numerical Simulation on Corneal Surface Behavior Applying Luminous Beam Levels. Applied Sciences, 13(22), 12132.
14. Ganesh, E. Earlier detection of glaucoma from aqueous humor fluid of human eye Through spintronic sensor and machine learning algorithms.
15. Limnios, I. J., Chau, Y. Q., Skabo, S. J., Surrao, D. C., & O'Neill, H. C. (2021). Efficient differentiation of human embryonic stem cells to retinal pigment epithelium under defined conditions. Stem cell research & therapy, 12, 1-14.
16. George, N. Study and Investigation on Algorithms for Segmentation of Optical Coherence Tomography OCT Images for Ophthalmic Applications.
17. Croft, M. A., Peterson, J., Smith, C., Kiland, J., Nork, T. M., Mcdonald, J. P., ... & Kaufman, P. L. (2022). Accommodative movements of the choroid in the optic nerve head region of human eyes, and their relationship to the lens. Experimental Eye Research, 222, 109124.
18. Lains, I., Wang, J. C., Cui, Y., Katz, R., Vingopoulos, F., Staurenghi, G., ... & Miller, J. B. (2021). Retinal applications of swept source optical coherence tomography (OCT) and optical coherence tomography angiography (OCTA). Progress in retinal and eye research, 84, 100951.
19. Ramesh, S. V. Longitudinal Assessment of Optic Nerve Head Progression in Glaucoma A Population Based Study.
20. Vitek, M., Rot, P., Štruc, V., & Peer, P. (2020). A comprehensive investigation into sclera biometrics: a novel dataset and performance study. Neural Computing and Applications, 32, 17941-17955.11
21. Bulloch, G., Seth, I., Sukumar, S., Chen, Y., & Zhu, Z. (2023). Scleral thinning causes, diagnosis, and management: A narrative review. Contact Lens and Anterior Eye, 101825.
22. Rana, K., Juniat, V., Patel, S., & Selva, D. (2022). Extraocular muscle enlargement. Graefe's Archive for Clinical and Experimental Ophthalmology, 260(11), 3419-3435.
23. Mahiba, C. Textural measurements and pattern recognition based diabetic retinopathy classification system of retinal images.

24. Sivamurugan, V. Some investigations on eye disease Classification using deep learning Techniques.
25. Auccahuasi, W., Flores, E., Sernaque, F., Cueva, J., Diaz, M., & Oré, E. (2020). Recognition of hard exudates using Deep Learning. Procedia Computer Science, 167, 2343-2353.
26. Garg, P., Mullick, R., Nigam, B., & Raj, P. (2020). Risk factors associated with development of senile cataract. Ophthalmology Journal, 5, 17-24.
27. Lin, Z., Wang, F. H., Wen, L., Wang, Y., Li, D., Ding, X. X., ... & Liang, Y. B. (2022). Prevalence of and risk factors for diabetic macular edema in a northeastern Chinese population. International Journal of Ophthalmology, 15(2), 320.
28. Deng, Y., Qiao, L., Du, M., Qu, C., Wan, L., Li, J., & Huang, L. (2022). Age-related macular degeneration: Epidemiology, genetics, pathophysiology, diagnosis, and targeted therapy. Genes & diseases, 9(1), 62-79.
29. Shyamsundar, B. R. Retinal Image Analysis for Screening of Diabetic Retinopathy.
30. Mahiba, C. Textural measurements and pattern recognition based diabetic retinopathy classification system of retinal images.
31. Cheong, K. X., Lee, S. Y., Ang, M., & Teo, K. Y. C. (2020). Vessel density changes on optical coherence tomography angiography after vascular endothelial growth factor inhibitor treatment for diabetic macular edema. Turkish Journal of Ophthalmology, 50(6), 343.
32. Palanisamy, G., Ponnusamy, P., & Gopi, V. P. (2023). An adaptive enhancement and fovea detection technique for color fundus image analysis. Signal, Image and Video Processing, 17(3), 831-838.
33. Yilmaz, I., Ocak, O. B., Yilmaz, B. S., Inal, A., Gokyigit, B., & Taskapili, M. (2017). Comparison of quantitative measurement of foveal avascular zone and macular vessel density in eyes of children with amblyopia and healthy controls: an optical coherence tomography angiography study. Journal of American Association for Pediatric Ophthalmology and Strabismus, 21(3), 224-228.
34. Zhang, K. Y., & Johnson, T. V. (2021). The internal limiting membrane: Roles in retinal development and implications for emerging ocular therapies. Experimental eye research, 206, 108545.
35. Datta, S., Baidya, K., Banerjee, M., Mahapatra, S., & Mukherjee, S. (2020). Retinal nerve fibre layer thinning in patients with thalassaemia, iron deficiency anaemia, and anaemia of chronic diseases. Journal of Ophthalmology, 2020, 1-7.

36. Mahmoudinezhad, G., Mohammadzadeh, V., Martinyan, J., Edalati, K., Zhou, B., Yalzadeh, D., ... & Nouri-Mahdavi, K. (2023). Comparison of Ganglion Cell Layer and Ganglion Cell/Inner Plexiform Layer Measures for Detection of Early Glaucoma. Ophthalmology Glaucoma, 6(1), 58-67.
37. Tong, J., Alonso-Caneiro, D., Kugelman, J., Phu, J., Khuu, S. K., & Kalloniatis, M. (2023). Characterisation of the normal human ganglion cell–inner plexiform layer using widefield optical coherence tomography. Ophthalmic and Physiological Optics.
38. Toulis, V., Casaroli-Marano, R., Camós-Carreras, A., Figueras-Roca, M., Sánchez-Dalmau, B., Muñoz, E., ... & do Carmo Costa, M. (2022). Altered retinal structure and function in Spinocerebellar ataxia type 3. Neurobiology of Disease, 170, 105774.
39. Parodi, M. B., Arrigo, A., Rajabian, F., Tecilazich, F., Giustina, A., Bandello, F., & Jampol, L. M. (2022). Paracentral acute middle maculopathy in central retinal vein occlusion complicating amyloid light-chain amyloidosis. Retinal Cases & Brief Reports, 16(5), 543.
40. Schmitz-Valckenberg, S., Saßmannshausen, M., Braun, M., Steffen, V., Gao, S. S., Honigberg, L., ... & Holz, F. G. (2023). Interreader Agreement and Longitudinal Progression of Incomplete/Complete Retinal Pigment Epithelium and Outer Retinal Atrophy in Age-Related Macular Degeneration. Ophthalmology Retina, 7(12), 1059-1068.
41. Lujan, B. J., Roorda, A., Croskrey, J. A., Dubis, A. M., Cooper, R. F., Bayabo, J. K., ... & Carroll, J. (2015). Directional optical coherence tomography provides accurate outer nuclear layer and Henle fiber layer measurements. Retina (Philadelphia, Pa.), 35(8), 1511.
42. O'Leary, F., & Campbell, M. (2023). The blood–retina barrier in health and disease. The FEBS Journal, 290(4), 878-891.
43. Kiser, P. D. (2022). Retinal pigment epithelium 65 kDa protein (RPE65): An update. Progress in retinal and eye research, 88, 101013.
44. Keeley, P. W., Patel, S. S., & Reese, B. E. (2023). Cell numbers, cell ratios, and developmental plasticity in the rod pathway of the mouse retina. Journal of Anatomy, 243(2), 204-222.
45. Lamb, T. D. (2016). Why rods and cones?. Eye, 30(2), 179-185.
46. Völgyi, B. (2020). Molecular biology of retinal ganglion cells. Cells, 9(11), 2483.
47. Kosta, P., Iseri, E., Loizos, K., Paknahad, J., Pfeiffer, R. L., Sigulinsky, C. L., ... & Lazzi, G. (2021). Model-based comparison of current flow in rod bipolar cells of

healthy and early-stage degenerated retina. Experimental eye research, 207, 108554.

48. Ptito, M., Bleau, M., & Bouskila, J. (2021). The retina: A window into the brain. Cells, 10(12), 3269.
49. Seilheimer, R. L., McClard, C. K., Sabharwal, J., & Wu, S. M. (2023). Modulation of narrow-field amacrine cells on light-evoked spike responses and receptive fields of retinal ganglion cells. Vision Research, 205, 108186.
50. Monjur, M., Hoque, I. T., Hashem, T., Rakib, M. A., Kim, J. E., & Ahamed, S. I. (2021). Smartphone based fundus camera for the diagnosis of retinal diseases. Smart Health, 19, 100177.
51. Wafy, M. N., Hassan, E. A., El-Maaty, A. M. A., & Abu-Seida, A. M. (2021). B-Scan biometry and color doppler ultrasound imaging of the eye in clinically normal donkeys (Equus asinus): Effect of laterality, maturity and gender. Journal of Equine Veterinary Science, 101, 103419.
52. Loo, J., Kriegel, M. F., Tuohy, M. M., Kim, K. H., Prajna, V., Woodward, M. A., & Farsiu, S. (2020). Open-source automatic segmentation of ocular structures and biomarkers of microbial keratitis on slit-lamp photography images using deep learning. IEEE journal of biomedical and health informatics, 25(1), 88-99.
53. Steinwender, G., & Wedrich, A. (2023). Slit Lamp Examination. In Cataract and Lens Surgery (pp. 69-74). Cham: Springer International Publishing.
54. Indoliya, Abhishek. Study of magnetic nanoparticles as an exogenous imaging contrast agent for magnetomotive Optical Coherence Tomography
55. Psomadakis, C. E., Marghoob, N., Bleicher, B., & Markowitz, O. (2021). Optical coherence tomography. Clinics in Dermatology, 39(4), 624-634.
56. Viedma, I. A., Alonso-Caneiro, D., Read, S. A., & Collins, M. J. (2022). Deep learning in retinal optical coherence tomography (OCT): A comprehensive survey. Neurocomputing.
57. Rank, E. A., Agneter, A., Schmoll, T., Leitgeb, R. A., & Drexler, W. (2022). Miniaturizing optical coherence tomography. Translational Biophotonics, 4(1-2), e202100007.
58. Pradhan, N. Comparative Study of Optical Coherence Tomography Findings Among Normal Versus Type II Diabetic Individuals With and Without Retinopathy.
59. Bouma, B. E., de Boer, J. F., Huang, D., Jang, I. K., Yonetsu, T., Leggett, C. L., ... & Wojtkowski, M. (2022). Optical coherence tomography. Nature Reviews Methods Primers, 2(1), 79.

60. Sharma, B. Design and Development of Fourier Domain Optical Coherence Tomography Based on Integrated Optical Components.
61. Singla, N. Quantitative Phase Imaging of Biological Samples using Optical Coherence Tomography.
62. Rao, K. D. functional extensions of optical coherence tomography for biomedical imaging applications.
63. Chouksey, S. Segmentation and Statistical Modeling of Retinal Optical Coherence Tomography Images.
64. Aumann, S., Donner, S., Fischer, J., & Müller, F. (2019). Optical coherence tomography (OCT): principle and technical realization. High resolution imaging in microscopy and ophthalmology: new frontiers in biomedical optics, 59-85.
65. Invernizzi, A., Cozzi, M., & Staurenghi, G. (2019). Optical coherence tomography and optical coherence tomography angiography in uveitis: A review. Clinical & experimental ophthalmology, 47(3), 357-371.
66. Naseripour, M., Ghasemi Falavarjani, K., Mirshahi, R., & Sedaghat, A. (2020). Optical coherence tomography angiography (OCTA) applications in ocular oncology. Eye, 34(9), 1535-1545.
67. Iovino, C., Iodice, C. M., Pisani, D., Damiano, L., Di Iorio, V., Testa, F., & Simonelli, F. (2023). Clinical Applications of Optical Coherence Tomography Angiography in Inherited Retinal Diseases: An Up-to-Date Review of the Literature. Journal of Clinical Medicine, 12(9), 3170.
68. Verma, Yogesh. Biomedical imaging using Optical Coherence Tomography
69. Nesper, P. L., Soetikno, B. T., Zhang, H. F., & Fawzi, A. A. (2017). OCT angiography and visible-light OCT in diabetic retinopathy. Vision research, 139, 191-203.
70. Alam, Z., & Poddar, R. (2022). An in-vivo depth-resolved imaging of developing zebrafish microstructure and microvasculature using swept-source optical coherence tomography angiography. Optics and Lasers in Engineering, 156, 107087.
71. Chuang, C. Y., Eggleston, M. S., & Shah, S. (2021, October). Monitoring Human Blood Flow Dynamics with Quantitative Speckle Variance Optical Coherence Tomography. In 2021 IEEE Photonics Conference (IPC) (pp. 1-2). IEEE.
72. He, B., Zhang, Y., Meng, Z., He, Z., Chen, Z., Yin, Z., ... & Xue, P. (2022). Whole Brain Micro-Vascular Imaging Using Robot Assisted Optical Coherence Tomography Angiography. IEEE Journal of Selected Topics in Quantum Electronics, 29(4:

Biophotonics), 1-9.

73. Zhang, T., Zhou, K., Rocliffe, H. R., Pellicoro, A., Cash, J. L., Wang, W., ... & Huang, Z. (2022). Windowed Eigen-Decomposition Algorithm for Motion Artifact Reduction in Optical Coherence Tomography-Based Angiography. Applied Sciences, 13(1), 378.
74. Rao, H. L., Dasari, S., Puttaiah, N. K., Pradhan, Z. S., Moghimi, S., Mansouri, K., ... & Weinreb, R. N. (2022). Optical microangiography and progressive retinal nerve fiber layer loss in primary open angle glaucoma. American Journal of Ophthalmology, 233, 171-179.
75. Chen, G., & Li, Y. (2023). Complex Correlated Phase Gradient Variance Based Optical Coherence Tomography Angiography. IEEE Photonics Journal, 15(1), 1-9.
76. Enders, C., Lang, G. E., Dreyhaupt, J., Loidl, M., Lang, G. K., & Werner, J. U. (2019). Quantity and quality of image artifacts in optical coherence tomography angiography. PloS one, 14(1), e0210505.
77. Liu, Y., Carass, A., Filippatou, A., He, Y., Solomon, S. D., Saidha, S., ... & Prince, J. L. (2019, April). Projection artifact suppression for inner retina in oct angiography. In 2019 IEEE 16th International Symposium on Biomedical Imaging (ISBI 2019) (pp. 592-596). IEEE.
78. Hormel, T. T., Hwang, T. S., Bailey, S. T., Wilson, D. J., Huang, D., & Jia, Y. (2021). Artificial intelligence in OCT angiography. Progress in Retinal and Eye Research, 85, 100965.
79. Pohlmann, D., Berlin, M., Reidl, F., Künzel, S. E., Pleyer, U., Joussen, A. M., & Winterhalter, S. (2022). Longitudinal Comparison of Constant Artifacts in Optical Coherence Tomography Angiography in Patients with Posterior Uveitis Compared to Healthy Subjects. Journal of Clinical Medicine, 11(18), 5376.
80. Kamalipour, A., Moghimi, S., Hou, H., Penteado, R. C., Oh, W. H., Proudfoot, J. A., ... & Weinreb, R. N. (2021). OCT angiography artifacts in glaucoma. Ophthalmology, 128(10), 1426-1437.
81. Anvari, P., Ashrafkhorasani, M., Habibi, A., & Falavarjani, K. G. (2021). Artifacts in optical coherence tomography angiography. Journal of Ophthalmic & Vision Research, 16(2), 271.
82. Spaide, R. F., Fujimoto, J. G., & Waheed, N. K. (2015). Image artifacts in optical coherence angiography. Retina (Philadelphia, Pa.), 35(11), 2163.
83. Rocholz, R., Corvi, F., Weichsel, J., Schmidt, S., & Staurenghi, G. (2019). OCT

angiography (OCTA) in retinal diagnostics. High resolution imaging in microscopy and ophthalmology: new frontiers in biomedical optics, 135-160.

84. Abu-Yaghi, N. E., Obiedat, A. F., AlNawaiseh, T. I., Hamad, A. M., Bani Ata, B. A., Quzli, A. A., & AlRyalat, S. A. (2022). Optical Coherence Tomography Angiography in Healthy Adult Subjects: Normative Values, Frequency, and Impact of Artifacts. BioMed Research International, 2022.
85. Lauermann, J. L., Treder, M., Heiduschka, P., Clemens, C. R., Eter, N., & Alten, F. (2017). Impact of eye-tracking technology on OCT-angiography imaging quality in age-related macular degeneration. Graefe's Archive for Clinical and Experimental Ophthalmology, 255, 1535-1542.
86. Wylęgała, A. (2018). Principles of OCTA and applications in clinical neurology. Current neurology and neuroscience reports, 18, 1-10.
87. Cole, E. D., Moult, E. M., Dang, S., Choi, W., Ploner, S. B., Lee, B., ... & Duker, J. S. (2017). The definition, rationale, and effects of thresholding in OCT angiography. Ophthalmology Retina, 1(5), 435-447.
88. Mahmoud, H., Eladawi, N., Elmogy, M., Ghazal, M., Alhalabi, M. T., Mahmoud, A. H., ... & El-Baz, A. (2020). Retinal diseases diagnosis based on optical coherence tomography angiography. In Diabetes and Fundus OCT (pp. 159-190). Elsevier.
89. Hirano, Y., Suzuki, N., Tomiyasu, T., Kurobe, R., Yasuda, Y., Esaki, Y., ... & Ogura, Y. (2021). Multimodal imaging of microvascular abnormalities in retinal vein occlusion. Journal of clinical medicine, 10(3), 405.
90. Vennila, I. Robust optimal multimodal retinal image registration algorithms for vein occlusion.
91. Hayreh, S. S., & Hayreh, S. S. (2015). Central retinal vein occlusion (pp. 621-743). Springer International Publishing.
92. Bradshaw, S. E., Gala, S., Nanavaty, M., Shah, A., Mwamburi, M., & Kefalas, P. (2016). Systematic literature review of treatments for management of complications of ischemic central retinal vein occlusion. BMC ophthalmology, 16, 1-25.
93. An, W., Zhao, Q., Yu, R., & Han, J. (2022). The role of optical coherence tomography angiography in distinguishing ischemic versus non-ischemic central retinal vein occlusion. BMC ophthalmology, 22(1), 413.
94. Hayreh, S. S. (2021). Photocoagulation for retinal vein occlusion. Progress in retinal and eye research, 85, 100964.
95. Noma, H., Yasuda, K., & Shimura, M. (2020). Cytokines and pathogenesis of central

retinal vein occlusion. Journal of clinical medicine, 9(11), 3457.

96. Berguig, J., Abdelmassih, Y., Azar, G., Lafolie, J., Alonso, A. S., Bonnin, S., ... & Mauget-Faysse, M. (2023). Central retinal vein occlusion in young population: risk factors and outcomes. Frontiers in Medicine, 10.
97. Tang, W., Liu, W., Guo, J., Zhang, L., Xu, G., Wang, K., & Chang, Q. (2022). Wide-field swept-source OCT angiography of the periarterial capillary-free zone before and after anti-VEGF therapy for branch retinal vein occlusion. Eye and Vision, 9(1), 25.
98. Pradeep T, Mehra D, Le PH. Histology, Eye. 2023 May 1. In: StatPearls [Internet]. Treasure Island (FL): StatPearls Publishing; 2024 Jan–. PMID: 31335063.
99. Bryar, P.J., Gu, D., Agron, S., Eichinger, S.E. (2019). Eye. In: Ernst, L., Ruchelli, E., Carreon, C., Huff, D. (eds) Color Atlas of Human Fetal and Neonatal Histology. Springer, Cham.
100. Blenkinsop, T. A., Salero, E., Stern, J. H., & Temple, S. (2013). The culture and maintenance of functional retinal pigment epithelial monolayers from adult human eye. Epithelial Cell Culture Protocols: Second Edition, 45-65.
101. Smith, J. R., Ashander, L. M., Ma, Y., Rochet, E., & Furtado, J. M. (2020). Model systems for studying mechanisms of ocular toxoplasmosis. Toxoplasma gondii: Methods and Protocols, 297-321.
102. Karkuzhali, S. Analysis of retinal images for diagnosis of eye diseases by feature extraction.
103. Nakamura, M., Sakamoto, M., Ueda, K., Okuda, M., Takano, F., & Yamada-Nakanishi, Y. (2023). Detection of Relative Afferent Pupillary Defect and Its Correlation with Structural and Functional Asymmetry in Patients with Glaucoma Using Hitomiru, a Novel Hand-Held Pupillometer. Journal of Clinical Medicine, 12(12), 3936.
104. Ducloyer, J. B., Bensaber, S., Khanna, R. K., Cochard, C., Lebreton, O., Le Meur, G., ... & Weber, M. (2021). Predictive values of initial semi-quantitative assessment of relative afferent pupillary defect for neovascularization in central retinal vein occlusion. Acta Ophthalmologica, 99(2), 215-220.
105. Hassanpoor, N., Abdolrahimi, V., & Niyousha, M. R. (2023). Central Retinal Vein Occlusion with Three-Retinal Quadrant Involvement: Another Focus on Optic Disc Head Vascular Anatomy Variations. Case Reports in Ophthalmological Medicine, 2023.
106. Ataş, F., & Saatci, A. O. (2022). Optociliary Shunt Vessels or Neovascularisation of

the Optic Disc: Fluorescein Angiography Versus Optical Coherence Tomography Angiography. Neuro-Ophthalmology, 46(5), 339-342.

107. Kanai, M., Sakimoto, S., Hara, C., Fukushima, Y., Sayanagi, K., Nishida, K., ... & Nishida, K. (2022). The caliber of optociliary shunt vessels is associated with macular blood flow and visual acuity in central retinal vein occlusion. Ophthalmology Science, 2(1), 100083.
108. Ullah, I., Sohail, A., Shah, M. U. F. A., Khurshid, M., Diwan, M. N., Qadir, A., & Irfan, M. (2021). Central retinal vein occlusion in patients with COVID-19 infection: a systematic review. Annals of Medicine and Surgery, 71, 102898.
109. Lee, H. E., Wang, Y., Fayed, A. E., & Fawzi, A. A. (2019). Exploring the relationship between collaterals and vessel density in retinal vein occlusions using optical coherence tomography angiography. PLoS One, 14(7), e0215790.
110. Yu, J., Jiang, C., Wang, X., Zhu, L., Gu, R., Xu, H., ... & Sun, X. (2015). Macular perfusion in healthy Chinese: an optical coherence tomography angiogram study. Investigative ophthalmology & visual science, 56(5), 3212-3217.
111. Yasuda, S., Kachi, S., Kondo, M., Ueno, S., Kaneko, H., & Terasaki, H. (2015). Significant correlation between retinal venous tortuosity and aqueous vascular endothelial growth factor concentration in eyes with central retinal vein occlusion. PLoS One, 10(7), e0134267.
112. McAllister, I. L., Gillies, M. E., Smithies, L. A., Rochtchina, E., Harper, C. A., Daniell, M. D., ... & Mitchell, P. (2010). The Central Retinal Vein Bypass Study: a trial of laser-induced chorioretinal venous anastomosis for central retinal vein occlusion. Ophthalmology, 117(5), 954-965.
113. Arrigo, A., Aragona, E., Lattanzio, R., Scalia, G., Bandello, F., & Parodi, M. B. (2021). Collateral vessel development in central and branch retinal vein occlusions are associated with worse visual and anatomic outcomes. Investigative Ophthalmology & Visual Science, 62(14), 1-1.
114. Li, Y., Hall, N. E., Pershing, S., Hyman, L., Haller, J. A., Lee, A. Y., ... & Elze, T. (2022). Age, gender, and laterality of retinal vascular occlusion: a retrospective study from the IRIS® Registry. Ophthalmology Retina, 6(2), 161-171.
115. Tang, F., Xu, F., Zhong, H., Zhao, X., Lv, M., Yang, K., ... & Chen, Q. (2019). Comparison of subfoveal choroidal thickness in eyes with CRVO and BRVO. BMC ophthalmology, 19(1), 1-7.
116. Sethukkarasi, R. (2022). A Study on Evaluating the Common Risk Factors, Systemic

Association and Clinical Profile of Central Retinal Vein Occlusion in Non-Diabetic Individuals (Doctoral dissertation, Madras Medical College, Chennai).

117. Nalcaci, S., Degirmenci, C., Akkin, C., & Mentes, J. (2019). Etiological factors in young patients with retinal vein occlusion. Pakistan Journal of Medical Sciences, 35(5), 1397.
118. Mathurkar, S., Daigavane, S., & Saldanha, C. (2022). A Comparative Study of Ganglion Cell Complex Thickness Changes in Diabetic Macular Edema and Central Retinal Vein Occlusion Macular Edema: An Optical Coherence Tomography Study. Cureus, 14(10).
119. Shin, K. U., Lee, J. Y., Han, K., & Song, S. J. (2018). Sex-specific age threshold for increased risk of retinal vein occlusion in Koreans. Thrombosis research, 167, 60-63.
120. Lee, J., Moon, B. G., Cho, A. R., & Yoon, Y. H. (2016). Optical coherence tomography angiography of DME and its association with anti-VEGF treatment response. Ophthalmology, 123(11), 2368-2375.
121. Choi, J., Kim, S. J., Kang, S. W., Son, K. Y., & Hwang, S. (2023). Local ocular factors associated with the development of diabetic macular edema: An inter-eye study. Scientific Reports, 13(1), 14868.
122. Figueras-Roca, M., Molins, B., Sala-Puigdollers, A., Matas, J., Vinagre, I., Ríos, J., & Adán, A. (2017). Peripheral blood metabolic and inflammatory factors as biomarkers to ocular findings in diabetic macular edema. PLoS One, 12(3), e0173865.
123. El-Nimri, N. W., Manalastas, P. I. C., Zangwill, L. M., Proudfoot, J. A., Bowd, C., Hou, H., ... & Weinreb, R. N. (2021). Superficial and deep macula vessel density in healthy, glaucoma suspect, and glaucoma eyes. Journal of glaucoma, 30(6), e276.
124. Lin, K. Y., Hsih, W. H., Lin, Y. B., Wen, C. Y., & Chang, T. J. (2021). Update in the epidemiology, risk factors, screening, and treatment of diabetic retinopathy. Journal of diabetes investigation, 12(8), 1322-1325.

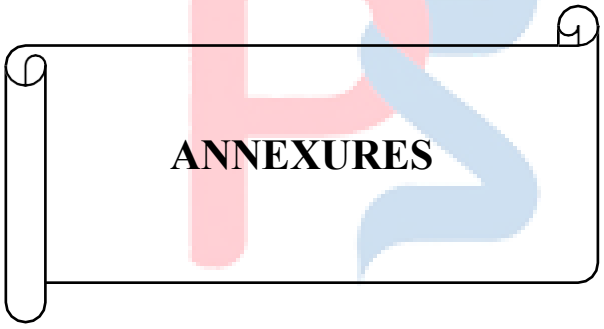
ANNEXURES

ANNEXURE I

PROFORMA

1) GENERAL INFORMATION:

Patient name: Patient id: DOB:

Exam: Age: Sex:

Co-morbidities, if any:

2) FACTORS FOR DIAGNOSING:

Laterality: BCVA:

IOP:

RAPD: Disc edema:

Hemorrhages at macula:

3) MICROSCOPY:

SCP VD:

FAZ Longest: SCP:

FAZ Mean: SCP:

DCP VD:

FAZ Longest: DCP

FAZ Mean: DCP

ANNEXURE II

MASTER CHART 1

SL.NO	AGE	AGE GROUP	GEDER	LATERALITY	BCVA	IOP	RAPD	DISC EDEMA	HEMORRHAGES
1	56	11	0	0	0.37 ± 0.28	19mmHg	1	0	1
2	72	3	0	0	0.42 ± 0.35	17mmHg	1	1	1
3	52	11	0	0	0.42 ± 0.36	18mmHg	1	1	1
4	61	12	1	0	0.42 ± 0.36	14mmHg	1	1	1
5	66	12	0	0	0.37 ± 0.28	12mmHg	1	0	1
6	63	12	1	0	0.46 ± 0.29	18mmHg	1	0	1
7	52	11	0	0	0.46 ± 0.56	18mmHg	1	1	1
8	70	12	1	0	0.37 ± 0.28	16mmHg	1	1	1

9	69	12	0	0	0.42 ± 0.35	17mmHg	1	0	1
10	68	12	0	0	0.42 ± 0.35	14mmhg	1	0	1
11	58	11	0	0	0.46 ± 0.29	21mmhg	1	0	1
12	56	11	1	0	0.46 ± 0.29	22mmHg	1	1	1
13	72	3	1	0	0.38 ± 0.28	19mmhg	1	0	1
14	54	11	0	0	0.38 ± 0.33	15mmhg	1	1	1
15	68	12	0	0	0.38 ± 0.33	14mmhg	1	0	1
16	62	12	0	0	0.42 ± 0.35	13mmhg	1	1	1
17	59	11	0	0	0.42 ± 0.35	21mmHg	1	0	1
18	54	11	0	0	0.46 ± 0.29	15mmHg	1	0	1
19	56	11	0	0	0.46 ± 0.29	14mmhg	1	0	1

20	61	12	0	0	0.37 ± 0.28	13mmhg	1	0	1
21	67	12	0	0	0.37 ± 0.28	12mmhg	1	1	1
22	66	12	0	0	0.42 ± 0.35	14mmHg	1	1	1
23	72	3	0	0	0.42 ± 0.31	16mmhg	1	0	1
24	53	11	0	0	0.35 ± 0.28	14mmhg	1	1	1
25	55	11	0	0	0.36 ± 0.28	14mmHg	1	1	1
26	64	12	1	0	0.36 ± 0.33	15mmHg	1	1	1

MASTER CHART 2

SL.NO	SCP VD	DCP VD	FAZ LONGEST: SCP	FAZ MEAN: SCP	FAZ LONGEST: DCP	FAZ MEAN: DCP	CHORIOCAPILLARIS VD	P-VALUE
1	26.975	72.858	80.455	67.284	90.2	77.862	51.268	0

2	38.431	97.41	127	108.09	128.577	118.257	37.867	0
3	24.347	94.935	77.795	72.123	74.653	69.825	78.306	0.015
4	9.241	59.03	72.993	59.481	95.047	81.625	39.216	0.76
5	26.792	91.434	82.565	72.474	91.526	81.877	58.784	0.69
6	32.103	91.906	58.523	44.985	97.755	82.03	52.505	0.01
7	24.62	91.916	74	64.332	84.971	76.084	73.969	0.92
8	36.28	95.635	104.995	86.682	128.763	120.342	53.391	0
9	30.402	95.879	90.62	80.103	136.308	125.496	41.58	0
10	19.71	60.485	64.125	56.993	102.157	96.519	61.307	0
11	26.975	72.858	80.455	67.284	90.2	77.862	51.268	0
12	38.431	97.41	127	108.09	128.577	118.257	37.867	0.06

13	24.347	94.935	77.795	72.123	74.653	69.825	78.306	0.025
14	9.241	59.03	72.993	59.481	95.047	81.625	39.216	0.61
15	26.792	91.434	82.565	72.474	91.526	81.877	58.784	0.92
16	32.103	91.906	58.523	44.985	97.755	82.03	52.505	0
17	24.62	91.916	74	64.332	84.971	76.084	73.969	0.92
18	36.28	95.635	104.995	86.682	128.763	120.342	53.391	0
19	30.402	95.879	90.62	80.103	136.308	125.496	41.58	0.13
20	19.71	60.485	64.125	56.993	102.157	96.519	61.307	0.03
21	26.975	72.858	80.455	67.284	90.2	77.862	51.268	0.24
22	38.431	97.41	127	108.09	128.577	118.257	37.867	0.6
23	24.347	94.935	77.795	72.123	74.653	69.825	78.306	0.8

24	9.241	59.03	72.993	59.481	95.047	81.625	39.216	0.3
25	26.792	91.434	82.565	72.474	91.526	81.877	58.784	0.42
26	32.103	91.906	58.523	44.985	97.755	82.03	52.505	0.53

ANNEXURE III

MASTERCHART 1

.NO	VA	P	PD	SC EDEMA	MORRHAGES
1	0.37 ± 0.28	19mmHg	1	0	1
2	0.42 ± 0.35	17mmHg	1	1	1
3	0.42 ± 0.36	18mmHg	1	1	1
4	0.42 ± 0.36	14mmHg	1	1	1
5	0.37 ± 0.28	12mmHg	1	0	1
6	0.46 ± 0.29	18mmHg	1	0	1
7	0.46 ± 0.56	18mmHg	1	1	1
8	0.37 ± 0.28	16mmHg	1	1	1

9	0.42 ± 0.35	17mmHg	1	0	1
10	0.42 ± 0.35	14mmhg	1	0	1
11	0.46 ± 0.29	21mmhg	1	0	1
12	0.46 ± 0.29	22mmHg	1	1	1
13	0.38 ± 0.28	19mmhg	1	0	1
14	0.38 ± 0.33	15mmhg	1	1	1
15	0.38 ± 0.33	14mmhg	1	0	1
16	0.42 ± 0.35	13mmhg	1	1	1
17	0.42 ± 0.35	21mmHg	1	0	1
18	0.46 ± 0.29	15mmHg	1	0	1
19	0.46 ± 0.29	14mmhg	1	0	1

20	0.37 ± 0.28	13mmhg	1	0	1
21	0.37 ± 0.28	12mmhg	1	1	1
22	0.42 ± 0.35	14mmHg	1	1	1
23	0.42 ± 0.31	16mmhg	1	0	1
24	0.35 ± 0.28	14mmhg	1	1	1
25	0.36 ± 0.28	14mmHg	1	1	1
26	0.36 ± 0.33	15mmHg	1	1	1

MASTER CHART 2

NO	P VD	P VD	Z LONGEST: SCP	Z MEAN: SCP	Z LONGEST: DCP	Z MEAN: DCP	ORIOCAPILLARIS
1	27.8	71.9	80.5	67.3	89.9	77.9	51.4

2	36.5	98.5	127.0	108.1	128.6	119.3	37.9
3	24.3	94.4	77.8	72.1	74.7	70.9	79.0
4	9.8	59.0	73.0	59.5	95.0	81.6	40.1
5	26.9	90.5	82.6	72.5	91.5	82.9	58.8
6	32.1	91.9	58.5	45.0	97.8	82.0	54.6
7	24.6	91.9	74.0	64.3	85.0	76.1	74.0
8	33.3	96.8	105.0	86.7	128.8	120.3	54.6
9	30.4	95.9	90.6	80.1	136.3	124.2	41.6
10	18.7	60.5	64.1	57.0	102.2	98.0	60.3
11	27.8	71.9	80.5	67.3	89.9	77.9	51.4
12	36.5	98.5	127.0	108.1	128.6	119.3	37.9

13	24.3	94.4	77.8	72.1	74.7	70.9	79.0
14	9.8	59.0	73.0	59.5	95.0	81.6	40.1
15	26.9	90.5	82.6	72.5	91.5	82.9	58.8
16	32.1	91.9	58.5	45.0	97.8	82.0	54.6
17	24.6	91.9	74.0	64.3	85.0	76.1	74.0
18	33.3	96.8	105.0	86.7	128.8	120.3	54.6
19	30.4	95.9	90.6	80.1	136.3	124.2	41.6
20	18.7	60.5	64.1	57.0	102.2	98.0	60.3
21	27.8	71.9	80.5	67.3	89.9	77.9	51.4
22	36.5	98.5	127.0	108.1	128.6	119.3	37.9
23	24.3	94.4	77.8	72.1	74.7	70.9	79.0

24	9.8	59.0	73.0	59.5	95.0	81.6	40.1
25	26.9	90.5	82.6	72.5	91.5	82.9	58.8
26	32.1	91.9	58.5	45.0	97.8	82.0	54.6

ANNEXURE IV

MASTER CHART 1

.NO	P VD	P VD	Z LONGEST: SCP	Z MEAN: SCP	Z LONGEST: DCP	Z MEAN: DCP	IORIOCAPILLARIS
1	24.0	72.8	80.5	67.3	89.9	77.9	51.4
2	35.7	93.5	127.0	108.1	128.6	119.3	37.9
3	22.4	94.3	77.8	72.1	74.7	70.9	34.3
4	8.7	56.7	73.0	59.5	95.0	81.6	35.4
5	27.9	90.5	82.6	72.5	91.5	82.9	33.2
6	33.1	90.9	58.5	45.0	97.8	82.0	34.6
7	24.7	90.9	74.0	64.3	85.0	76.1	32.2
8	32.3	97.0	105.0	86.7	128.8	120.3	34.4

9	30.4	97.0	90.6	80.1	136.3	124.2	41.6
10	17.7	60.4	64.1	57.0	102.2	98.0	37.3
11	24.0	72.8	80.5	67.3	89.9	77.9	36.3
12	35.7	93.5	127.0	108.1	128.6	119.3	37.9
13	22.4	94.3	77.8	72.1	74.7	70.9	38.3
14	8.7	56.7	73.0	59.5	95.0	81.6	40.1
15	27.9	90.5	82.6	72.5	91.5	82.9	32.3
16	33.1	90.9	58.5	45.0	97.8	82.0	43.3
17	24.7	90.9	74.0	64.3	85.0	76.1	32.1
18	32.3	97.0	105.0	86.7	128.8	120.3	35.1
19	30.4	97.0	90.6	80.1	136.3	124.2	33.2

20	17.7	60.4	64.1	57.0	102.2	98.0	32.2
21	24.0	72.8	80.5	67.3	89.9	77.9	31.3
22	35.7	93.5	127.0	108.1	128.6	119.3	37.9
23	22.4	94.3	77.8	72.1	74.7	70.9	31.8
24	8.7	56.7	73.0	59.5	95.0	81.6	34.2
25	27.9	90.5	82.6	72.5	91.5	82.9	34.2
26	33.1	90.9	58.5	45.0	97.8	82.0	33.6

ANNEXURE V

MASTER CHART 1

.NO	VA	P	PD	SC EDEMA	MORRHAGES
1	0.37 ± 0.28	17mmHg	1	0	1
2	0.42 ± 0.35	19mmHg	1	1	1
3	0.46 ± 0.53	17mmHg	1	1	1
4	0.46 ± 0.53	18mmHg	1	1	1
5	0.33 ± 0.33	14mmHg	1	0	1
6	0.21 ± 0.25	12mmHg	1	0	1
7	0.44 ± 0.42	18mmHg	1	1	1
8	0.37 ± 0.28	18mmHg	1	1	1

9	0.42 ± 0.35	16mmHg	1	0	1
10	0.46 ± 0.53	17mmHg	1	0	1
11	0.46 ± 0.53	14mmhg	1	0	1
12	0.33 ± 0.33	21mmhg	1	1	1
13	0.21 ± 0.25	22mmHg	1	0	1
14	0.44 ± 0.42	19mmhg	1	1	1
15	0.37 ± 0.28	15mmhg	1	0	1
16	0.42 ± 0.35	14mmhg	1	1	1
17	0.46 ± 0.53	13mmhg	1	0	1
18	0.46 ± 0.53	21mmHg	1	0	1
19	0.33 ± 0.33	15mmHg	1	0	1

20	0.21 ± 0.25	14mmhg	1	0	1
21	0.44 ± 0.42	13mmhg	1	1	1
22	0.37 ± 0.28	12mmhg	1	1	1
23	0.42 ± 0.35	14mmHg	1	0	1
24	0.46 ± 0.53	16mmhg	1	1	1
25	0.46 ± 0.53	14mmhg	1	1	1
26	0.33 ± 0.33	14mmHg	1	1	1

MASTER CHART 2

NO	P VD	P VD	Z LONGEST: SCP	Z MEAN: SCP	Z LONGEST: DCP	Z MEAN: DCP	ORIOCAPILLARIS	VALUE
1	24.0	72.8	80.5	67.3	89.9	77.9	51.4	0

2	35.7	93.5	127.0	108.1	128.6	119.3	37.9	0
3	22.4	94.3	77.8	72.1	74.7	70.9	34.3	0.015
4	8.7	56.7	73.0	59.5	95.0	81.6	35.4	0.76
5	27.9	90.5	82.6	72.5	91.5	82.9	33.2	0.69
6	33.1	90.9	58.5	45.0	97.8	82.0	34.6	0.01
7	24.7	90.9	74.0	64.3	85.0	76.1	32.2	0.92
8	32.3	97.0	105.0	86.7	128.8	120.3	34.4	0
9	30.4	97.0	90.6	80.1	136.3	124.2	41.6	0
10	17.7	60.4	64.1	57.0	102.2	98.0	37.3	0
11	24.0	72.8	80.5	67.3	89.9	77.9	36.3	0
12	35.7	93.5	127.0	108.1	128.6	119.3	37.9	0.06

13	22.4	94.3	77.8	72.1	74.7	70.9	38.3	0.025
14	8.7	56.7	73.0	59.5	95.0	81.6	40.1	0.61
15	27.9	90.5	82.6	72.5	91.5	82.9	32.3	0.92
16	33.1	90.9	58.5	45.0	97.8	82.0	43.3	0
17	24.7	90.9	74.0	64.3	85.0	76.1	32.1	0.92
18	32.3	97.0	105.0	86.7	128.8	120.3	35.1	0
19	30.4	97.0	90.6	80.1	136.3	124.2	33.2	0.13
20	17.7	60.4	64.1	57.0	102.2	98.0	32.2	0.03
21	24.0	72.8	80.5	67.3	89.9	77.9	31.3	0.24
22	35.7	93.5	127.0	108.1	128.6	119.3	37.9	0.6
23	22.4	94.3	77.8	72.1	74.7	70.9	31.8	0.8

24	8.7	56.7	73.0	59.5	95.0	81.6	34.2	0.3
25	27.9	90.5	82.6	72.5	91.5	82.9	34.2	0.42
26	33.1	90.9	58.5	45.0	97.8	82.0	51.4	0.53

KEY TO MASTER CHART

1) Age Group

S.NO	AGE GROUP
1	51-60
2	61-70
3	71-80

2) Gender

S.NO	GENDER
1	Female
2	Male

3) IMAGING

S.NO	IMAGING
1	SCP VD
2	DCP VD
3	FAZ LONGEST: SCP
4	FAZ MEAN: SCP
5	FAZ LONGEST: DCP
6	FAZ MEAN: DCP
7	CHORIOCAPILLARIS VD

8	P-VALUE